

THESIS FOR THE DEGREE OF DOCTOR OF PHILOSOPHY

Quantum optics in superconducting circuits

Generating, engineering and detecting microwave photons

SANKAR RAMAN SATHYAMOORTHY

Department of Microtechnology and Nanoscience (MC2)

Applied Quantum Physics Laboratory

CHALMERS UNIVERSITY OF TECHNOLOGY

Göteborg, Sweden 2017

Quantum optics in superconducting circuits
Generating, engineering and detecting microwave photons
SANKAR RAMAN SATHYAMOORTHY
ISBN 978-91-7597-589-4

© SANKAR RAMAN SATHYAMOORTHY, 2017

Doktorsavhandlingar vid Chalmers tekniska högskola
Ny serie nr. 4270
ISSN 0346-718X

Technical Report MC2-362
ISSN 1652-0769

Applied Quantum Physics Laboratory
Department of Microtechnology and Nanoscience (MC2)
Chalmers University of Technology
SE-412 96 Göteborg
Sweden
Telephone: +46 (0)31-772 1000

Cover:
Schematic setup of an all-optical quantum processor at microwave frequencies.
The insets show the proposals discussed in the thesis for the different components.

Printed by Chalmers Reproservice
Göteborg, Sweden 2017

Quantum optics in superconducting circuits
Generating, engineering and detecting microwave photons
Thesis for the degree of Doctor of Philosophy

SANKAR RAMAN SATHYAMOORTHY

Department of Microtechnology and Nanoscience (MC2)
Applied Quantum Physics Laboratory
Chalmers University of Technology

ABSTRACT

Quantum optics in superconducting circuits, known as circuit QED, studies the interaction of photons at microwave frequencies with artificial atoms made of Josephson junctions. Although quite young, remarkable progress has been made in this field over the past decade, especially given the interest in building a quantum computer using superconducting circuits. In this thesis based on the appended papers, we look at generation, engineering and detection of microwave photons using superconducting circuits. We do this by taking advantage of the strong coupling, on-chip tunability and huge nonlinearity available in superconducting circuits.

First, we present the strong photon-photon interaction measured experimentally, as shown in the giant cross-Kerr effect. In this work, conditional phase shift of about 20 degrees per photon was measured between two coherent fields at single photon level. Given this strong interaction, we propose and analyze a cascaded setup based on the cross-Kerr effect to detect itinerant microwave photons, a long outstanding problem with only recent experimental realizations. We show that a nondestructive detection of microwave photons is possible with few cascaded transmons. The on-chip tunability of Superconducting Quantum Interference Device (SQUID) is exploited to create a tunable superconducting resonator in the next presented experimental work. Finally, we show that by placing the atom at the end of a transmission line, microwave photons can be generated efficiently and on-demand. We also present a setup that can generate the photons in arbitrary wave packets.

Keywords: Quantum optics, superconducting circuits, circuit QED, single photon source, single photon detector, cross-Kerr effect.

ACKNOWLEDGEMENTS

A PhD program seems to be both long and short at the same time. I would like to thank all those who helped to keep up the spirits during the long times and provided ample support when time was short.

First of all, I would like to thank my supervisor Göran Johansson, for providing me with an opportunity to work in this interesting area of circuit QED. I am also thankful for all the time you spend teaching physics and being open to discussing any other topic such as career choices. I am especially grateful for all the quick support that you provide in dealing with administrative issues such as visa applications, which at times become more stressful than not having results. I should also thank Anton and Lars for providing ample guidance during the initial years of my PhD.

I am very grateful for all the discussions and support we get from our experimental colleagues in the Quantum Device Physics lab. I thank our collaborators (currently) at other universities, Ben Baragiola, Josh Combes, Bixuan Fan, Io-Chun Hoi, Mathieu Pierre, Tom Stace and Chris Wilson for all their fruitful contributions. I would also like to thank Irfan Siddiqi and his group, for hosting me at UC Berkeley and making it a memorable experience.

To everyone at Applied Quantum Physics Laboratory, thank you for making this a fun place to work. I enjoy all our discussions on physics, different cultures, languages and food. Thanks to all for the Friday fika. And those who make sure someone brings fika, good job!

Thanks to Göran, Fernando, Joel and Bala for all the comments on the thesis.

Last but not least, thanks to my parents and all my friends for their love and support. Thank you Mananyaa for working tirelessly to increase the entropy of our house. Thank you Aruna for trying to restore equilibrium every now and then.

Thanks to Stack Overflow for having answers to abstruse questions in LaTeX. Thank you coffee machine for showing the light on dark days.

LIST OF PUBLICATIONS

This thesis consists of an extended summary based on the following appended papers:

- I. Giant Cross-Kerr Effect for Propagating Microwaves Induced by an Artificial Atom,**
I.-C. Hoi, A. F. Kockum, T. Palomaki, T. M. Stace, B. Fan, L. Tornberg, S. R. Sathyamoorthy, G. Johansson, P. Delsing, and C. M. Wilson,
Physical Review Letters **111**, 053601 (2013).
- II. Quantum Nondemolition Detection of a Propagating Microwave Photon,**
S. R. Sathyamoorthy, L. Tornberg, A. F. Kockum, B. Q. Baragiola, J. Combes, C. M. Wilson, T. M. Stace, and G. Johansson,
Physical Review Letters **112**, 093601 (2014).
- III. Storage and on-demand release of microwaves using superconducting resonators with tunable coupling,**
M. Pierre, I.-M. Svensson, S. Raman Sathyamoorthy, G. Johansson, and P. Delsing,
Applied Physics Letters **104**, 232604 (2014).
- IV. Detecting itinerant single microwave photons,**
S. R. Sathyamoorthy, T. M. Stace, and G. Johansson,
Comptes Rendus Physique **17**, 756-765 (2016).
- V. Simple, robust, and on-demand generation of single and correlated photons,**
S. R. Sathyamoorthy, A. Bengtsson, S. Bens, M. Simoen, P. Delsing, and G. Johansson,
Physical Review A **93**, 063823 (2016).
- VI. Microwave field oscillation and swapping in coupled superconducting resonators,**
M. Pierre, S. R. Sathyamoorthy, I.-M. Svensson, G. Johansson, and P. Delsing,
In review (2017).

CONTENTS

Abstract	iii
Acknowledgements	v
List of publications	vii
Contents	ix
1 Introduction	1
1.1 Photon sources	3
1.2 Storage and retrieval of photons	4
1.3 Photon-photon interaction	5
1.4 Single photon detection	6
1.5 Structure of the thesis	8
2 Superconducting quantum circuits	11
2.1 Circuits as quantum systems	11
2.2 Single Cooper pair box	17
2.3 Transmission line	19
2.4 Rounding up	23
3 Open quantum systems	25
3.1 Master equation	26
3.2 Input and Output	33
3.3 Coherence functions	36
3.4 Master equation for Fock state input	38
4 Measurement	43
4.1 Photon detection	47
4.2 Homodyne detection	50
4.3 Quantum Nondemolition (QND) measurements	53
5 Connecting quantum systems	57
5.1 (S, L, H) formalism	60
5.2 Cascaded quantum systems	62
5.3 Coupled quantum systems	65
5.4 Feedback	69

6 Overview of the articles	73
6.1 Cross-Kerr Effect for propagating microwaves	73
6.2 Quantum nondemolition detection of a propagating microwave photon	75
6.3 Coupled superconducting resonators	77
6.4 Generating single photons on demand	79
7 Summary	83
References	85

List of Figures

1.1	A possible implementation of a quantum internet.	4
2.1	Schematic setup of a circuit QED experiment.	12
2.2	Circuit diagram of an LC oscillator	13
2.3	Circuit diagrams of a Josephson junction and a dc-SQUID.	15
2.4	Circuit diagram of a single Cooper Pair Box (SCB) and a transmon.	17
2.5	First three eigenenergies for a SCB for $E_J/E_C = 0.2, 2.0$ and 20.0	19
2.6	Circuit diagram of a transmission line.	20
2.7	Circuit diagram for a $\lambda/4$ resonator.	22
2.8	Circuit diagram for a $\lambda/2$ resonator.	23
3.1	Scattering of a Fock state on a qubit.	40
4.1	Probability of excitation P_{exc} of a qubit under direct photon detection, with the qubit initially in the excited state.	49
4.2	Probability of excitation P_{exc} of a qubit under direct photon detection, with the qubit initially in the plus state.	50
4.3	A schematic setup of homodyne detection.	51
4.4	Probability of excitation P_{exc} of a qubit under homodyne detection, with the qubit initially in the plus state.	52
4.5	Homodyne current j for a qubit initially in the plus state.	53
5.1	A schematic setup of two qubits cascaded.	58
5.2	The (S, L, H) products	60
5.3	Two cascaded qubits driven by a cavity output.	64
5.4	A schematic setup of two transmon qubits separated by a distance.	65
5.5	Reflection and transmission coefficient for two coupled qubits as a function of input field amplitude.	67
5.6	Reflection and transmission coefficient for two coupled qubits as a function of detuning.	67
5.7	Schematic of a two level system in front of a mirror.	69

5.8	Reflection coefficient for a qubit in front of a mirror.	70
6.1	Schematic of setup proposed in paper II for microwave photon detection.	75
6.2	Schematic setup for coupled cavities considered in papers III and VI.	77
6.3	Schematic setups proposed in paper V to generate single photons	80

*"In the beginning there was nothing.
God said, 'Let there be light!' And there was light.
There was still nothing, but you could see it a whole lot better."*

Attributed to Ellen DeGeneres

1

Introduction

The birth of quantum theory at the beginning of the 20th century revolutionized our understanding of the universe and along with Einstein's theory of relativity form the basis of our modern view on how nature works. This development of quantum mechanics now referred to as the "first quantum revolution", led to both fundamental scientific progress and several important applications. Currently, there is a huge drive to develop technologies based on quantum principles such as superposition and entanglement. This activity, termed as the "second quantum revolution" or quantum 2.0, is expected to have significant impact in computing, communications and metrology among others [1]. Research in this regard is driven by several countries and regions around the world with significant participation from industry.

While one may envision building these quantum devices top-down, a preferred approach has been to start from the mastery of individual quantum systems and build up. This can also be seen as pragmatic as the complexity of a quantum system grows exponentially with size and one would like to understand/control smaller setups before scaling up. During the initial development of quantum mechanics, control of individual quantum systems was only possible in gedanken experiments. However, with significant progress over the past several decades we

can now routinely address single quantum systems in labs around the world. For their pioneering work in this direction, Serge Haroche and David Wineland were awarded the Nobel Prize in Physics in 2012. Wineland's group traps individual ions using electric fields in ultrahigh vacuum and probes them with laser light [2]. Haroche's group takes the opposite approach, where the field at microwave frequency is trapped in a cavity and is studied by sending highly excited atoms called Rydberg atoms through the cavity [2].

The above experiments of Wineland and Haroche fall under the broad topic of quantum optics, where one studies the interaction between light and matter at the fundamental level. Specifically, the approach used in Haroche's experiments falls under the field called cavity quantum electrodynamics (cavity QED), where light-matter interactions are studied inside a cavity [3, 4]. While tremendous progress has been made in using both ions and natural atoms to build quantum devices [5], alternate approaches using solid state systems have also been developed recently. These include systems such as quantum dots, NV centers in diamond and superconducting circuits, each of which have their own pros and cons [6].

In this thesis, we will focus on superconducting circuits which has recently emerged as a promising candidate in the race to build quantum devices [7, 8]. In these devices, artificial atoms made of superconducting circuits replace real atoms and they interact with microwave photons routed through one-dimensional waveguides. Analogous to cavity QED, this area of research is known as circuit QED. As these setups are made on chip using standard microfabrication techniques, they offer a number of advantages such as tunability, scalability and mechanical stability over the traditional laser-real atom case. Due to the confinement of the field to one dimension, these systems also show large coupling between the field and the artificial atom [9]. Such advantages have enabled a plethora of experiments covering a wide range of areas such as microwave quantum optics [10], quantum information processing [7, 11, 12] and relativistic quantum mechanics [13].

In quantum information processing with superconducting circuits, one usually thinks of the artificial atoms as the quantum bits (qubits). The microwave photons are then used to manipulate and transfer information between the qubits. One can take an alternate viewpoint, where the information is always in the photons (referred to as flying qubits), and the atoms are used as photonic devices that operate on these qubits. As photons have low decoherence and can be transmitted over distance, using them as qubits is advantageous. Indeed, several proposals exist for quantum information processing using photons [14–16] including those specific to superconducting circuits [17, 18]. For such photonic quantum appli-

cations, one has to be able to generate photons on demand, manipulate them, store and retrieve them from a memory and finally detect them. In this thesis, based on the appended papers, we look at some of the solutions for achieving the above goals at microwave frequencies.

1.1 Photon sources

Photons were hypothesised by Planck as quantum packets of energy to calculate the spectrum of blackbody radiation [19]. In one of his seminal papers of 1905, Einstein used the concept of these quanta to explain the photoelectric effect [20]. This effect was already observed in the photomultiplier tubes, which we can consider as a precursor to single photon detectors. The first sources of single photons were realized in the 1970s using cascaded emission [21].

Current photon sources can be broadly put into two categories, probabilistic and deterministic [22]. The probabilistic sources include those based on parametric down-conversion and four-wave mixing. In these sources, photons from a strong pump field are converted to signal and idler photons. While this conversion process is stochastic, the emitted photon pairs are correlated such that the detection of an idler photon heralds the presence of a signal photon.

Deterministic photon sources are based on either single atomic or ensemble emitters. In a single atomic source, when a photon is needed, the atom is excited using an external drive. The atomic decay to the ground state leads to the emission of a single photon. As the atom decays in all available modes, usually one embeds the atom in a cavity to improve collection efficiency. In ensemble sources, instead of using a single atomic level, collective excitation of all the atoms in the ensemble is used to generate the desired photons.

Current research in single photon sources is pushed by applications in quantum computation and in quantum communication which include quantum key distribution and quantum repeaters [22, 23]. Other applications in combination with single photon detectors include random number generation [24].

Microwave photons have been generated using superconducting qubits coupled to transmission line resonators [25–27], including in shaped photon wave packets [28, 29]. While the use of resonators provide better collection efficiency, they also limit the bandwidth of operation. To generate photons at different frequencies, one needs tune both the qubit and cavity frequencies with good control. A cavity free setup for generating microwave photons using two transmission lines was

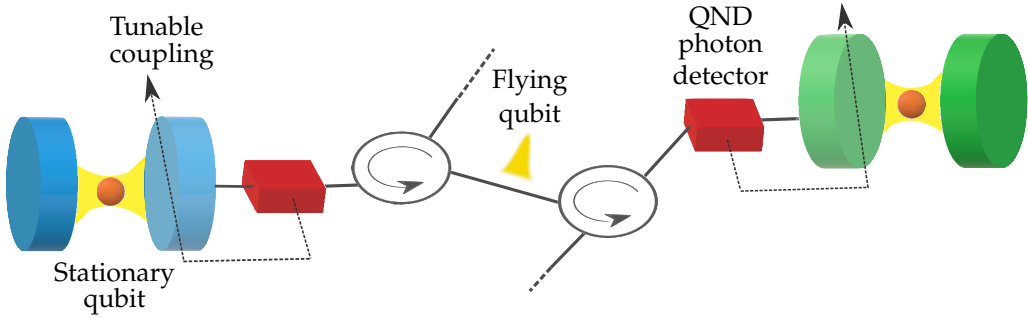


Figure 1.1: A possible implementation of a quantum internet inspired by a figure from [32]. The stationary qubits are used to process quantum information which is then sent out as photons (flying qubits). A QND photon detector detects the incoming photon and “opens or closes” a cavity to efficiently capture the incoming signal.

proposed in [30] and was experimentally realized in [31]. In paper V, we show how to generate single photons efficiently using an atom in front of a mirror.

An ideal single photon source generates indistinguishable photons on demand, with a fast repetition rate [22]. That is, the source would produce a single photon with 100% probability and have 0% probability for all other photon number states. Calculating or measuring these probabilities provides a way to determine the efficiency of the proposed setup. In paper V, we calculate these probabilities from correlation functions, which are described in chapter IV.

1.2 Storage and retrieval of photons

The setup presented in paper V and other similar schemes, can in principle generate any arbitrary superposition of 0 and 1 photons. This would be a form of photonic qubit that can be written as $\alpha |0\rangle + \beta |1\rangle$, where α and β are complex numbers with $|\alpha|^2 + |\beta|^2 = 1$. An on-demand generation of such photonic qubits could have applications in quantum communication. Assume for instance that Alice generates one such qubit and sends it to Bob. Bob then has to catch the qubit and process the information. This would form a simple transaction over a quantum network (Fig. 1.1).

The quantum internet, a distributed quantum network, is one of the long term goals of quantum information and quantum communication [32]. In this setup, analogous to the “classical internet”, individual quantum nodes are connected via

quantum channels for performing distributed quantum computing and communication. The individual nodes where the processing of information takes place are ideally made of atoms (artificial or real), while the quantum information is communicated using photons, playing the role of flying qubits. As one could imagine, a quantum memory that would store the incoming photon and retrieve it for later processing becomes an essential part of this setup. Proposals for setups that would "catch and release" [33] photons on demand exist based on atomic ensembles [34] and superconducting circuits [28, 35]. In papers III and VI, we look at one such proposal in circuit QED, where a coherent field is stored and retrieved from a tunable cavity. Apart from the use as a quantum memory, such tunable cavities can potentially be also used for generating single photon wave packets of arbitrary shapes [28, 29].

1.3 Photon-photon interaction

While photons are carriers of electromagnetic interaction, they rarely interact with each other in vacuum. While this property makes them great carriers of information, it also makes it harder to manipulate them. Effective photon-photon interactions can however be engineered using non-linear materials. One such effective interaction is the so called Kerr effect, which is the change in refractive index of a material due to an applied electric field. While a dc field can be the source of the Kerr effect, we are more interested in the ac or optical Kerr effect, where an intense beam of light changes the refractive index of the medium. The total refractive index of such a medium as seen by the intense control field is given as [36]

$$n^{(c)} = n_0^{(c)} + n_2^{(c)} I^{(c)}, \quad (1.1)$$

where $n_0^{(c)}$ is the normal (low intensity) refractive index and $I^{(c)}$ is the intensity of the incoming control field. n_2 is referred to as the second order refractive index or the non-linear Kerr index. It can be shown that this non-linear effect comes from the third order susceptibility $\chi^{(3)}$ of the medium [36]. The change of refractive index gives rise to an intensity dependent non-linear phase shift to the field over and above the one due to just n_0 . This is usually referred to as self-phase modulation (SPM). We are interested in cross-phase modulation (XPM), which is the phase shift experienced by a weak probe field due to this change caused by an intense field. Assuming that the probe is weak enough to not induce non-linearity on its own, the refractive index seen by the weaker probe

field is given by [36, 37]

$$n^{(p)} = n_0^{(p)} + n_2^{(p)} I^{(c)}. \quad (1.2)$$

This is similar to the previous case, with the non-linear term depending on the intensity of the strong field. This leads to modulation of the phase of the weaker field and is also known as the cross-Kerr effect.

Traditionally, such cross-Kerr interactions are mediated using nonlinear medium such as crystals, which are several wavelengths long and are composed of a huge number of atoms. Other setups where the Kerr nonlinearity was demonstrated include cold atoms using an EIT (electromagnetically induced transparency) scheme [38]. Whether such an interaction can be mediated by just a single atom is the question addressed in paper I. In this experimental work, two coherent fields, control and probe, are scattered off a superconducting artificial atom, the transmon. The conditional phase shift in the probe field due to the presence of the control field is measured and shown to be much higher than those obtained in the optical regime using setups such as crystal fibers [39]. Hence the title, giant cross-Kerr effect. However, it has to be noted that a single atom can only process one excitation per lifetime of the transition. So the phase change doesn't increase as one continuously increases the intensity of the control field as in the above discussion. The giant phase shift shown in paper I occurs when both the control and probe field are in the single photon regime. This is the most interesting regime for quantum optics and quantum information processing. The effect could however be further improved by cascading several of these atoms [40].

Kerr non-linearities have previously been used in several proposals for quantum information processing to make quantum gates [41–44]. There have been several studies in the literature discussing the feasibility of implementing a controlled phase gate using cross-Kerr nonlinearity [45, 46], with recent results suggesting that it is indeed possible [47]. Cross-Kerr nonlinearities have also been proposed as a way to nondestructively detect photons [37, 48–50]. We turn to this particular problem in the next subsection.

1.4 Single photon detection

Now that we have looked at generating, storing and engineering photons, let us turn our attention to detecting a single photon. Due to research and development over the past several decades, single photon detectors based on many different technologies exist in the optical regime [22, 51], and are even available commercially. Current research in this field continues to push the efficiency of

these detectors. Apart from quantum information processing and quantum communications, such single photon detectors have applications in biology, medicine, remote sensing and ranging, spectroscopy and metrology to name a few [22, 24].

Detecting a propagating single photon at microwave frequency has however been particularly challenging. This can be attributed to the fact that the energy of microwave photons are 4 to 5 orders of magnitude lower than that of optical photons. Over the past few years, several novel proposals have been put forth to address this problem [52–58] (also paper II) including a few experimental demonstrations [59–61]. A pedagogical review of some of these proposals is presented in paper IV. A itinerant single microwave photon detector has been realized recently [62] with an impedance matched lambda system. Given the popularity of superconducting circuits as a platform for quantum information processing, single microwave photon detectors would add significant flexibility to the toolbox. Apart from other applications similar to those in the optical regime, microwave photon detectors could also be useful in the search of dark matter [63, 64].

1.4.1 Quantum nondemolition detection

Traditional photon detectors such as photodiodes, are destructive. Typically they absorb the photon and convert it into an electrical signal, which is then measured (possibly after amplification). Such schemes complicate the use of photons as carriers of quantum information. For example, if the information is stored in the polarization of the photon, the detection of the photon destroys this information. A nondestructive kind of detector would allow us to process the photons, after we detect their presence (as in Fig. 1.1 for example).

Measurement back-action, the change in the state of the system due to measurement, is an inherent property of quantum mechanics. Along with the Heisenberg’s uncertainty principle, this leads to limitations in repeated measurements as follows [37]. Consider two non-commuting operators of a system, such as position x and momentum p . The uncertainty principle states that the values of these two operators cannot be simultaneously established to arbitrary precision, the lower bound in their uncertainty being $\Delta x \Delta p = \frac{1}{2} \hbar$. Any precise measurement of x , leads to a large uncertainty in p . If the system evolution depends on momentum, a second measurement of x even after a short time interval could lead to a different result [65].

Quantum nondemolition (QND) measurements were introduced in the 1970s

to circumvent the above restrictions imposed by the uncertainty principle [65–70], by using clever measurement schemes such that the uncertainty in the conjugate variable does not lead to disturbance of the measured quantity. These schemes were first devised to measure mechanical oscillators that would detect gravitational-waves, with the aim of repeating the measurements without perturbing the oscillators. The ideas were however well suited for the field of quantum optics, leading to the successful implementations of QND measurements of photon flux in the optical regime [37]. These schemes have since then been extended to microwave quantum optics, initially in cavity QED [71] and now in circuit QED [59, 72–75].

The cross-phase modulation (XPM) offered by a Kerr medium leads us to one such scheme of nondestructive photon detection [37, 48–50]. Instead of having an intense field changing the refractive index of the medium and causing a phase shift in the probe field, we would like a single photon to have such an effect. Then, by measuring the phase shift of the probe, one might infer the presence of the single photon. The single photon survives this process, making the scheme nondestructive. Given that the setup in paper I shows a giant cross-Kerr phase shift in the single photon regime, we explore if it could be used as a photon detector. We then propose a scheme using this effect in paper II and show that it overcomes the noise arising from vacuum fluctuations.

1.5 Structure of the thesis

In the next few chapters, we will briefly review the ingredients that form the basis of the appended papers. We start in chapter 2 and look at the quantum mechanical description of superconducting circuits. We will focus on how to derive the Hamiltonian of a superconducting artificial atom, the single Cooper pair box, leading towards a discussion of the transmon qubit. We will also look at transmission lines and transmission line resonators. As all of the appended papers are either experiments in circuit QED or theoretical proposals primarily aimed at experiments in circuit QED, this chapter provides a background to the physical setups used.

In chapter 3, we abstract away the physical setups used and look at the evolution of a generic quantum system coupled to an environment. We will review the derivation of the master equation that describes the evolution of such an open system. We will also look at the input-output formalism which describes how to calculate the scattered field from the atom. We will use these relations to calculate

the amplitudes and correlation functions of the output field. The theoretical part of all of the appended papers rely on the above master equations and the input-output formalism.

In chapter 4, we focus on the evolution of a quantum system under measurement. We look at the stochastic master equations describing the evolution under direct photodetection and homodyne detection. We will also add a few comments on QND measurements. Stochastic master equations are used in paper II to characterize and calculate the efficiency of the proposed microwave photon detector.

In chapter 5, we move beyond the domain of single quantum systems and look at composite setups that consists of cascaded/stacked quantum subsystems. We look at the (S,L,H) formalism that makes it easier to derive the master equation for such a composite system and apply it to a few example problems. The (S, L, H) formalism is used in paper II to derive the master equation of a chain of cascaded three level atoms. This formalism can also be used to get the master equation for an atom in front of a mirror [76], a setup that is used in paper V.

We will briefly discuss and highlight the salient points from the attached papers in chapter 6 and conclude with a summary in chapter 7.

"Resistance is futile."

The Borg
Star Trek: The Next Generation

2

Superconducting quantum circuits

The field of circuit QED is concerned with the study of light matter interaction using superconducting circuits. As already mentioned in the previous chapter, these systems are now also prime candidates for implementing quantum technologies. As this thesis falls under the domain of circuit QED, we will briefly look into the same in this chapter. Our main goal will be to understand how these macroscopic circuits can be described using quantum mechanics.

2.1 Circuits as quantum systems

While initially envisioned for mechanical systems, it has been known for a long time that electrical circuits can also be analyzed using the Lagrangian formalism [78]. In such an analysis, one chooses either charge or flux (defined below) as a generalized coordinate to calculate the energies stored in the different circuit elements, resulting in a Lagrangian of the total circuit. This, then allows us to extend the canonical quantization procedure to electrical circuits as described in references [79–81].

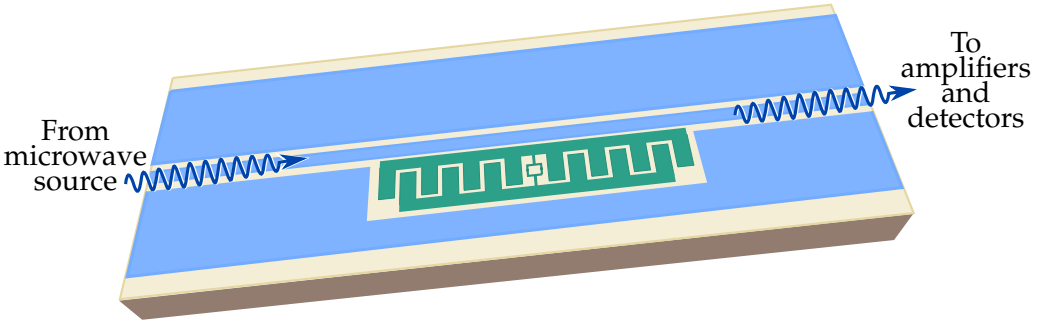


Figure 2.1: Schematic setup of a circuit QED experiment depicting the interaction of microwave photons with an artificial atom (transmon, shown in green). The microwaves are routed through a transmission line (shown in blue). Figure adapted from [77]. The circuit diagrams for a transmission line and a transmon are shown in figures 2.6 and 2.4b respectively.

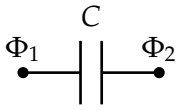
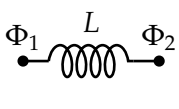
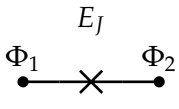
Circuit element	Symbol	Current-Voltage relation	Energy
Capacitance		$I = C\dot{V}$	$T_C = \frac{1}{2}C\dot{\Phi}^2$
Inductance		$V = L\dot{I}$	$U_L = \frac{1}{2L}\Phi^2$
Josephson element		$I = I_C \sin \phi$ $\frac{d\phi}{dt} = \frac{2e}{\hbar}V$ $\phi = 2\pi \frac{\Phi}{\Phi_0}$	$U_J = E_J \left[1 - \cos \left(2\pi \frac{\Phi}{\Phi_0} \right) \right]$

Table 2.1: Common superconducting circuit elements with the corresponding symbol, current-voltage relation and energy. The energies are written in terms of the flux drop across the circuit element $\Phi = \Phi_1 - \Phi_2$, where $\Phi_{1/2}$ are the node fluxes (defined in the text). T and U denote kinetic and potential energies respectively.

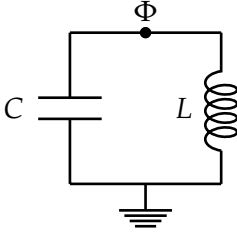


Figure 2.2: *Circuit diagram of an LC oscillator, with the bottom node grounded. Φ is the flux associated with the top node.*

For superconducting circuits, it is advantageous to work with node fluxes as the generalized coordinates (due to Josephson junctions). These are defined as the time integral of the voltages as

$$\Phi_n = \int_{-\infty}^t V_n(t') dt', \quad (2.1)$$

where V_n is the voltage at node n . Using the current-voltage relationships, we can calculate the energies stored in the element at time t as $E(t) = \int_{-\infty}^t V(t') I(t') dt'$. We list the energies of common superconducting circuit elements in table 2.1 using flux as the generalized coordinate. Analogous to classical mechanics, we denote energies that are function of the coordinate Φ itself as potential energies U , while the ones that are function of the velocity $\dot{\Phi}$ as kinetic energies T .

Using the energies of the different components, we can write down the Lagrangian of an arbitrary circuit. The simplest of such a combination is the LC oscillator (see Fig. 2.2), where we have grounded the lower node. The Lagrangian of the circuit is

$$\mathcal{L} = T_C - U_L = \frac{1}{2} C \dot{\Phi}^2 - \frac{1}{2L} \Phi^2. \quad (2.2)$$

From the Lagrangian, we can derive the Hamiltonian using the Legendre transformation. In order to do this, we need the momentum conjugate to the flux Φ given by

$$q = \frac{\partial \mathcal{L}}{\partial \dot{\Phi}} = C \dot{\Phi}, \quad (2.3)$$

which has the units of charge and in this case, corresponds to the charge on the capacitor. Now the Hamiltonian is given by,

$$\begin{aligned} H &= q \dot{\Phi} - \mathcal{L} \\ &= \frac{q^2}{2C} + \frac{\Phi^2}{2L}, \end{aligned} \quad (2.4)$$

which is analogous to the Hamiltonian of a harmonic oscillator of the form $\frac{p^2}{2m} + \frac{1}{2} m \omega^2 x$, with $m = C$ and $\omega = \sqrt{1/LC}$. So far we have considered everything

classically. To get to the quantum description, we now promote q and Φ to operators satisfying the commutation relation,

$$[\hat{\Phi}, \hat{q}] = i\hbar, \quad (2.5)$$

where we have for the first and last time explicitly included the hats to identify the operators. We can then define the ladder operators a and a^\dagger as

$$\Phi = \sqrt{\frac{\hbar}{2C\omega}}(a + a^\dagger), \quad (2.6)$$

$$q = -i\sqrt{\frac{\hbar C\omega}{2}}(a - a^\dagger), \quad (2.7)$$

which satisfy the commutation relation $[a, a^\dagger] = 1$. In terms of these operators, the Hamiltonian can be rewritten as

$$H = \hbar\omega \left(a^\dagger a + \frac{1}{2} \right). \quad (2.8)$$

The striking feature of the harmonic potential ($U \propto x^2$) is its equidistant energy spectrum, which means we cannot address individual energy transitions like for instance in a Coulomb potential ($U \propto 1/x$). Thus to mimic real atoms, we have to include a non-linearity in our circuit that would provide anharmonicity to the spectrum. In superconducting circuits, this is naturally given by Josephson junctions.

The Josephson junction is a device made of two superconductors separated by a small tunnel barrier. It is modelled as a capacitor C_J in parallel to a Josephson element characterized by its energy E_J (circuit diagram shown in Fig. 2.3a). Such junctions follow the DC and AC Josephson effects [82, 83] given by the relations

$$I(t) = I_C \sin \phi(t), \quad (2.9)$$

$$\frac{d\phi}{dt} = \frac{2e}{\hbar} V(t), \quad (2.10)$$

where ϕ is the phase difference between the order parameters of the two superconductors. The phase difference is related to the flux drop across the junction as $\phi = 2\pi\Phi/\Phi_0 = 2\pi(\Phi_1 - \Phi_2)/\Phi_0$, where $\Phi_0 = h/2e$ is the flux quantum. I_C is the critical current, i.e. the maximum supercurrent that the junction can conduct.

Combining Eq. (2.9) and Eq. (2.10), we can write (suppressing the time argument for clarity)

$$\dot{\phi} = \left(\frac{2\pi}{\Phi_0} I_C \cos \phi \right) V \equiv \frac{1}{L_J} V \quad (2.11)$$

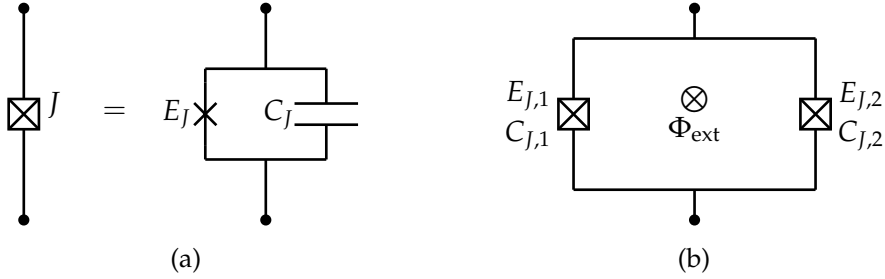


Figure 2.3: Circuit diagrams of (a) a Josephson junction and (b) a dc-SQUID. The Josephson junction is characterized by its Josephson energy E_J and capacitance C_J . The dc-SQUID consists of a superconducting loop interrupted by two Josephson junctions. An external flux through the loop Φ_{ext} can be used to tune the effective Josephson energy of the SQUID.

which shows that the Josephson junction acts as a nonlinear inductor with inductance $L_J = \left(\frac{\Phi_0}{2\pi}\right) \frac{1}{I_c \cos \phi}$. Thus in the flux basis, the Josephson junction gives a potential energy contribution to the Lagrangian as

$$U_J = \int_{-\infty}^t I(t')V(t')dt' = \frac{\hbar}{2e} I_C \int_{-\infty}^t \sin \phi(t') \frac{d\phi}{dt'} dt' = E_J(1 - \cos \phi), \quad (2.12)$$

where we have defined the Josephson energy $E_J = \frac{\hbar}{2e} I_C$. This is indeed an anharmonic potential that can be exploited to make artificial atoms. The above potential energy corresponds to that of the pure Josephson element. Adding the kinetic energy from the capacitance of the junction C_J , we can write the Lagrangian of the Josephson junction as

$$\mathcal{L} = \frac{1}{2} C_J \dot{\Phi}^2 + E_J \cos \left(\frac{2\pi}{\Phi_0} \Phi \right), \quad (2.13)$$

where we have dropped the constant term.

Placing the Josephson junctions in a loop to make a superconducting quantum interference device (SQUID), offers additional on-chip tunability. In this thesis, we will focus only on what is called a dc-SQUID, which is made of two Josephson junctions in parallel (see Fig. 2.3b). By using an external coil, one can now thread a flux Φ_{ext} through the loop containing the Josephson junctions. We will see how this allows us to realize an effective Josephson junction with a tunable Josephson energy in the following.

The condition that the superconducting order parameter must be single valued, leads to fluxoid quantization [83] which can be written in the case of the SQUID

as [84, 85]

$$\Phi_1 - \Phi_2 + \Phi_{\text{ext}} + \Phi_{\text{ind}} = n\Phi_0 \quad (2.14)$$

where Φ_{ind} is the flux induced by the circulating current in the loop and n is an integer. We will consider a small loop whose inductance is much smaller than the inductance of the Josephson junctions and neglect this term. The flux drops across the Josephson junctions are related to the phase difference across the junctions as before i.e. $\Phi_{1/2} = \frac{\Phi_0}{2\pi}\phi_{1/2}$. Without any loss of generality, we take the number of flux quanta in the loop to be 0. With this constraint, we can define

$$\Phi_1 = \Phi - \frac{1}{2}\Phi_{\text{ext}}, \quad (2.15)$$

$$\Phi_2 = \Phi + \frac{1}{2}\Phi_{\text{ext}}. \quad (2.16)$$

Considering also that the Josephson junctions are identical with $C_{J,1} = C_{J,2} = C_J/2$ and $E_{J,1} = E_{J,2} = E_J/2$, the Lagrangian of the SQUID becomes

$$\mathcal{L} = \frac{1}{2}C_{J,1}\dot{\Phi}_1^2 + \frac{1}{2}C_{J,2}\dot{\Phi}_2^2 + E_{J,1} \cos\left(\frac{2\pi}{\Phi_0}\Phi_1\right) + E_{J,2} \cos\left(\frac{2\pi}{\Phi_0}\Phi_2\right) \quad (2.17)$$

$$= \frac{1}{2}C_J\dot{\Phi}^2 + E_J(\Phi_{\text{ext}}) \cos\left(\frac{2\pi}{\Phi_0}\Phi\right), \quad (2.18)$$

where $E_J(\Phi_{\text{ext}}) = E_J \cos\left(\frac{\pi\Phi_{\text{ext}}}{\Phi_0}\right)$. To obtain the above expressions, we have also neglected the terms that only depends on Φ_{ext} . Comparing with Eq. (2.13), we see that the Lagrangian of the SQUID is analogous to that of a Josephson junction whose Josephson energy $E_J(\Phi_{\text{ext}})$ can be tuned using an external flux. As we already saw, the Josephson element acts like a nonlinear inductor with inductance $L_J = \left(\frac{\Phi_0}{2\pi}\right)^2 \frac{1}{E_J \cos\phi}$. By replacing the Josephson junction with a SQUID, we can tune this inductance using Φ_{ext} .

The tunability provided by a SQUID had been exploited in several experiments in circuit QED to either change the frequency of the artificial atoms [76] or to change the boundary conditions of a field [13]. In papers III and VI, we use a SQUID to tune the resonant frequency of the coupling cavity. We also take advantage of the tunability of the SQUID in paper V, where we propose generation of single photons in arbitrary wave packets by either changing the qubit frequency or by changing the boundary condition.

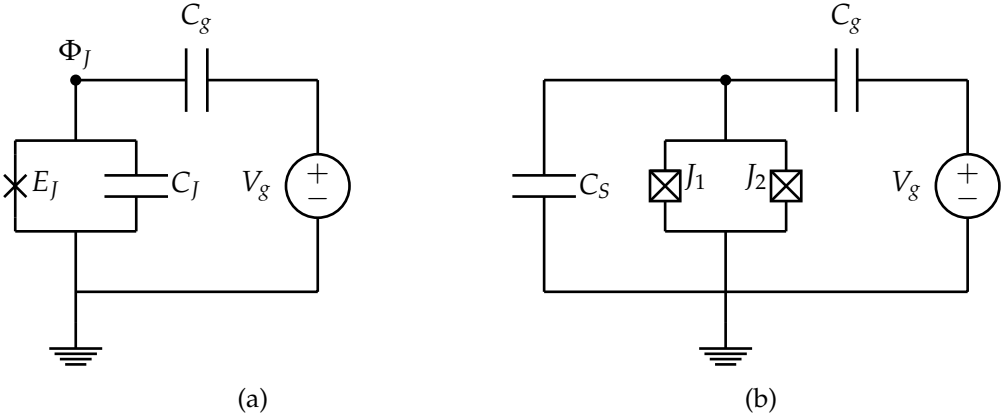


Figure 2.4: Circuit diagram of (a) single Cooper pair box (SCB) and (b) transmon, a capacitively shunted Cooper pair box. We have also replaced the Josephson junction in (b) with a SQUID to make the transmon's frequency tunable.

2.2 Single Cooper pair box

Now that we have looked at the description of some of the basic elements of superconducting circuits, let us proceed to describe how to engineer an artificial atom. In this thesis, we primarily focus on the transmon qubit [86], which is a variant of the single Cooper pair box (SCB) [87–89]. The SCB consists of a small island made of superconducting metal (such as aluminium) that is connected to a bigger metallic plate (reservoir of Cooper pairs) via a Josephson junction. The island is also capacitively coupled to a gate voltage V_g , through which the tunneling of Cooper pairs to or from the island can be controlled. Fig. 2.4a shows the circuit diagram of a SCB. From this we can write the Lagrangian of the circuit as

$$\mathcal{L} = \frac{1}{2}C_J\dot{\Phi}_J^2 + \frac{1}{2}C_g(\dot{\Phi}_J + V_g)^2 + E_J \cos\left(2\pi\frac{\Phi_J}{\Phi_0}\right), \quad (2.19)$$

where $\Phi_J = (\Phi_0/2\pi)\phi$ is once again the flux connected to the phase difference ϕ across the Josephson junction. The conjugate momentum,

$$q_J = \frac{\partial \mathcal{L}}{\partial \dot{\Phi}_J} = C_J\dot{\Phi}_J + C_g(\dot{\Phi}_J + V_g) = 2en, \quad (2.20)$$

where n is the number of Cooper pairs on the island. Using the Legendre transformation, we get the SCB Hamiltonian as

$$H = 4E_C(n - n_g)^2 - E_J \cos\left(2\pi \frac{\Phi_J}{\Phi_0}\right), \quad (2.21)$$

where $E_C \equiv e^2/2(C_g + C_J)$ is the charging energy of the island and $n_g = C_g V_g/2e$ is the number of Cooper pairs induced by the gate. We can then follow the quantization procedure and promote n and Φ_J to be operators that satisfy the commutation relation [90],

$$\left[\exp\left(i2\pi \frac{\Phi_J}{\Phi_0}\right), n\right] = -\exp\left(i2\pi \frac{\Phi_J}{\Phi_0}\right). \quad (2.22)$$

Using this commutation relation, we can show that

$$e^{\pm i2\pi \frac{\Phi_J}{\Phi_0}} |n\rangle = |n \pm 1\rangle, \quad (2.23)$$

where $|n\rangle$ represents the charge basis which are the eigenstates of the number operator such that $\hat{n} |n\rangle = n |n\rangle$. We can then write the Hamiltonian in the charge basis, by using the completeness relation (i.e. $\sum_n |n\rangle \langle n| = \mathbb{1}$) and by expanding the cosine term as sum of two exponentials as

$$H = \sum_n \left\{ 4E_C(\hat{n} - n_g)^2 |n\rangle \langle n| - \frac{1}{2}E_J \left(|n+1\rangle \langle n| + |n-1\rangle \langle n| \right) \right\}. \quad (2.24)$$

By diagonalizing the above Hamiltonian we can plot the energy levels of the SCB as a function of n_g for different values of the parameters E_C and E_J . The first three energy levels are shown in Fig. 2.5 for different values of these parameters. We see that at low ratios of E_J/E_C , the transition energies between the levels vary significantly as a function of the gate charge n_g . Any fluctuations in n_g (i.e. charge noise) leads to variations in transition frequencies that after averaging manifests itself as dephasing. As can be seen from the figure, the wiggles in the energy spectrum reduces as one increases the ratio of E_J/E_C . However, this change has a negative side-effect in reducing the anharmonicity, which is crucial to address individual transitions. Fortunately we can find values of E_J/E_C where a useful trade-off between the charge noise and anharmonicity can be achieved. The value of E_J/E_C can be modified by shunting the SCB with a large capacitor. The capacitively shunted Cooper pair box is known as a transmon [86] (schematically presented in Fig. 2.1). A simplified circuit diagram is shown in Fig. 2.4b. The insensitivity of transmons to charge noise has made them a popular superconducting qubit for implementing quantum information processing [8].

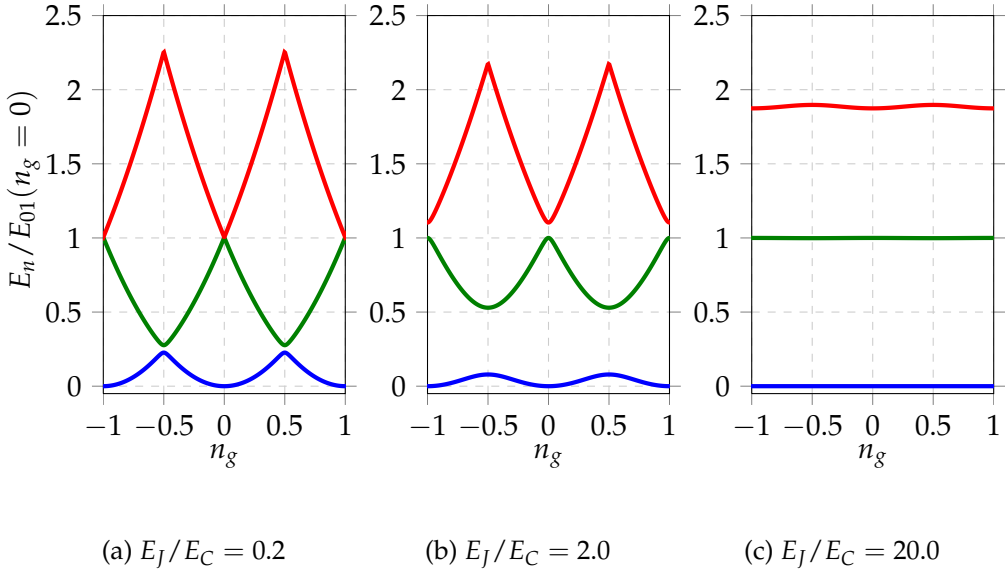


Figure 2.5: First three eigen-energies for a SCB normalized to the energy difference E_{01} at $n_g = 0$. As seen in the figures, increasing the value of E_J/E_C reduces the wiggles in the energy spectrum but also reduces the anharmonicity.

We note that, there are several other types of superconducting qubits proposed and experimentally realized [88, 91–96]. In this thesis, we will consider only the transmon and hence we will not go into the details of the rest of the qubits.

2.3 Transmission line

As mentioned previously, in circuit QED one studies the interaction of microwaves with superconducting artificial atoms such as the transmon. The microwaves are routed through a transmission line to which we turn our attention now. Microwave transmission lines consist of a central conductor separated by a dielectric to the ground plane (Fig. 2.1). They can be modeled as coupled LC oscillators as shown in Fig. 2.6, where C_0 and L_0 are the capacitance and inductance per unit length of the transmission line. By discretizing the transmission line with a small length Δx and using the node fluxes as the generalized coordinates we can write the Lagrangian of the transmission line as

$$\mathcal{L} = \sum_n \frac{1}{2} C_0 \Delta x \dot{\Phi}_n^2 - \frac{1}{2} \frac{(\Phi_n - \Phi_{n-1})^2}{L_0 \Delta x}. \quad (2.25)$$

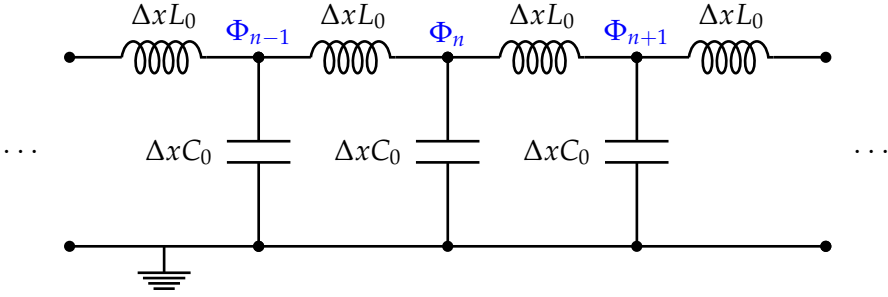


Figure 2.6: Circuit diagram of an infinite transmission line. C_0 and L_0 are the capacitance and inductance per unit length of the line. The fluxes in blue are the generalized coordinates.

The conjugate momenta,

$$q_n = \frac{\partial L}{\partial \dot{\Phi}_n} = C_0 \Delta x \dot{\Phi}_n, \quad (2.26)$$

is the charge at node n . With this, we can write down the Hamiltonian as

$$H = \sum_n \frac{1}{2} \frac{q_n^2}{C_0 \Delta x} + \frac{1}{2} \frac{(\Phi_n - \Phi_{n-1})^2}{L_0 \Delta x}, \quad (2.27)$$

which in the continuous limit gives,

$$H = \frac{1}{2} \int \left[\frac{q(x, t)^2}{C_0} + \frac{1}{L_0} \left(\frac{\partial \Phi(x, t)}{\partial x} \right)^2 \right] dx. \quad (2.28)$$

We now promote $q(x, t)$ and $\Phi(x, t)$ as the quantum mechanical field operators obeying the equal time commutation relations $[q(x, t), q(x', t)] = [\Phi(x, t), \Phi(x', t)] = 0$ and $[\Phi(x, t), q(x', t)] = i\delta(x - x')$. The flux field $\Phi(x, t)$ satisfies the massless Klein-Gordon equation

$$\frac{\partial^2 \Phi(x, t)}{\partial t^2} - v^2 \frac{\partial^2 \Phi(x, t)}{\partial x^2} = 0, \quad (2.29)$$

where $v = 1/\sqrt{L_0 C_0}$ is the propagation velocity. A general solution of the above equation

$$\Phi(x, t) = \Phi_L(kx + \omega t) + \Phi_R(-kx + \omega t) \quad (2.30)$$

consists of left and right moving parts, which can be expanded as [79, 97]

$$\Phi_R(-kx + \omega t) = \sqrt{\frac{\hbar Z_0}{4\pi}} \int_0^\infty \frac{d\omega}{\sqrt{\omega}} \left(a_R(\omega) e^{-i(-kx + \omega t)} + h.c. \right), \quad (2.31)$$

$$\Phi_L(kx + \omega t) = \sqrt{\frac{\hbar Z_0}{4\pi}} \int_0^\infty \frac{d\omega}{\sqrt{\omega}} \left(a_L(\omega) e^{-i(kx + \omega t)} + h.c. \right), \quad (2.32)$$

where $k = \omega/v$ and $Z_0 = \sqrt{L_0/C_0}$ is the characteristic impedance of the transmission line. The annihilation (a) and creation (a^\dagger) operators in the above expansion satisfy the commutation relation $[a_\alpha(\omega), a_{\alpha'}^\dagger(\omega')] = \delta(\omega - \omega') \delta_{\alpha\alpha'}$ where $\alpha = L/R$.

The Klein-Gordon field can also be expanded in terms of the wave vector k instead of the frequency as above. Using such an expansion, the Hamiltonian of the field can be shown to be of the form [85, 98]

$$H = \int_{-\infty}^{\infty} dk \hbar \omega_k \left(a_k^\dagger a_k + \frac{1}{2} [a_k, a_k^\dagger] \right) \quad (2.33)$$

where $\omega_k = v|k|$. The above Hamiltonian is that of a continuum of harmonic oscillators whose modes are defined by k , with their creation and annihilation operators satisfying the commutation relation $[a_k, a_{k'}^\dagger] = \delta(k - k')$. The transmission line acts as a bath or environment to the artificial atoms and we will model such an environment as a collection of harmonic oscillators in the following chapters.

2.3.1 Resonators

So far we have considered an infinite transmission line that supports propagating photons. We could also make cavities or resonators that support standing modes. This can be achieved by terminating a segment of transmission line either with a short to ground or an open circuit. Depending on the choice made, we get different boundary conditions resulting in different types of resonators. If both the ends of the resonator are either open (i.e.) connected to a capacitor or shorted to ground, we have a $\lambda/2$ resonator. If one end of the resonator is open and the other is grounded, we get a $\lambda/4$ resonators. Figures 2.7 and 2.8 show the circuit diagram of quarter and half wavelength resonators along with their first two modes. The boundary conditions restrict our spectrum from continuous mode to discrete multimode. The Hamiltonian becomes

$$H = \sum_m \hbar \omega_m \left(a^\dagger(\omega_m) a(\omega_m) + \frac{1}{2} \right), \quad (2.34)$$

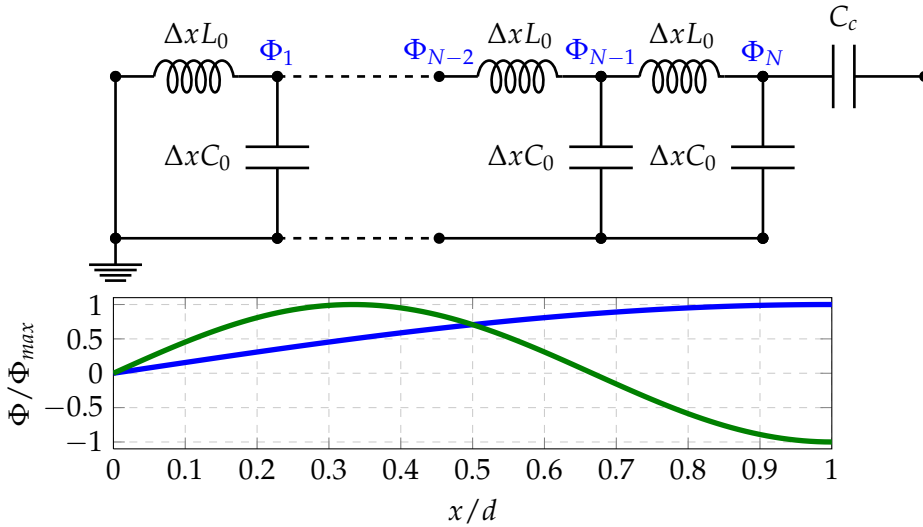


Figure 2.7: Circuit diagram for a $\lambda/4$ resonator grounded at $x = 0$. Shown below the circuit are the first two modes with normalized amplitude along the length of the cavity d .

where $\omega_m = m\pi v/d$ for $\lambda/2$ resonators and $\omega_m = (m - \frac{1}{2})\pi v/d$ for $\lambda/4$ resonators with $m \in \{1, 2, 3, \dots\}$. $v = 1/\sqrt{L_0 C_0}$ is the velocity of photons in the transmission line and d is the length of the cavity. Most often, we are only interested in the fundamental mode with $m = 1$. In this case, we get back to a single mode picture, with the Hamiltonian similar to that of an LC oscillator

$$H = \hbar\omega \left(a^\dagger a + \frac{1}{2} \right), \quad (2.35)$$

where ω is the fundamental frequency.

Resonators or cavities play an important role in the study of quantum optics, where several experiments use atoms interacting with cavity fields and the sub-field is known as cavity QED [4]. In circuit QED too resonators are routinely used, especially for reading out qubits. In paper III and VI, we look at experimental realizations of a tunable cavity. The effective cavity is made of two cavities, one of them is a $\lambda/4$ resonator called the storage cavity and the other one, called the coupling cavity is a $\lambda/2$ resonator. The $\lambda/2$ resonator has a SQUID in its center. By tuning the flux through the SQUID loop, we can tune the frequency that the cavity supports [99, 100]. It is then shown that this scheme is effectively the same as tuning the coupling of the storage cavity to the external transmission line. Such cavities with tunable coupling can be used to generate photon pulses with

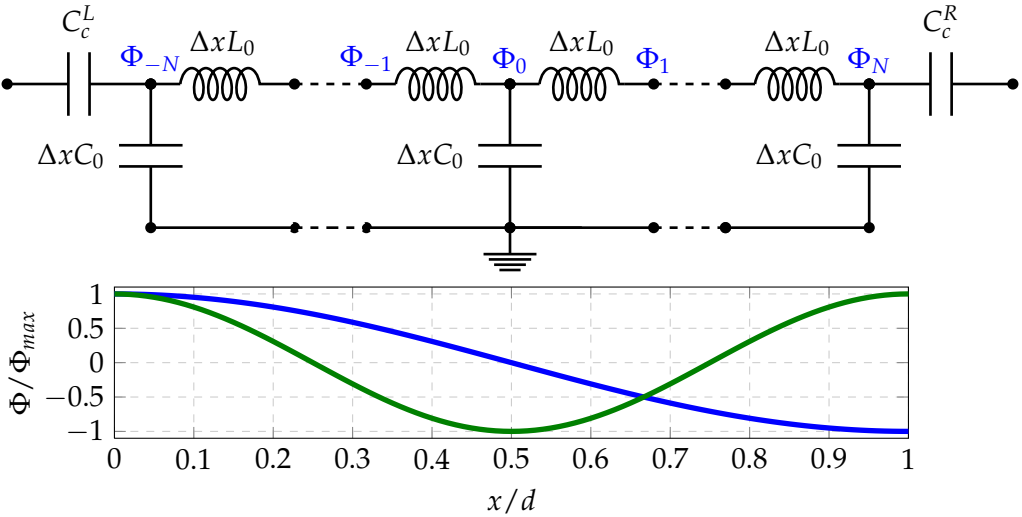


Figure 2.8: Circuit diagram for a $\lambda/2$ resonator. Shown below the circuit are the first two modes with normalized amplitude along the length of the cavity d .

different wave packets [28, 29] and to catch incoming photons of known shapes [35]. Such a tunable cavity is used in paper II as a model source of single photons enveloped in wave packets that are either Gaussian or exponentially decaying or rising.

2.4 Rounding up

Now that we have seen that using superconducting circuits, we can create artificial atoms, waveguides and resonators, it is time to motivate why not just use real atoms and optical light. While nature is rich and bountiful, it is also limited in a certain sense. Although natural atoms or ions are readily available, they have preset properties that are not widely tunable. With the advent of micro-fabrication methods and nanotechnology, there has been significant progress in tweaking these "God given" restrictions. Artificial atoms such as transmons built from bottom-up, give us access to different parameter regimes with wider in-situ tunability that are not readily available in nature. Also by confining photons to one dimension like in a transmission line we can more easily reach the strong-coupling regime which is difficult to attain in 3D space [9, 101, 102]. Apart from the traditional quantum optics related problems, these setups have been recently

used to probe for relativistic effects such as the dynamical Casimir effect [13] which is in principle impossible to attain in traditional setups with real mirrors. The downside of superconducting circuits is of course the need of cryogenics. It is also very difficult to get two superconducting qubits with exactly the same parameters. Apart from these, we also have to convert microwave photons to optical photons if we need to transmit quantum information across a network. However, the potential advantages seem to outweigh the drawbacks and circuit QED has emerged as one of the front runners for the implementation of quantum information processing [7, 8].

*The wheels on the bus go round and round,
Round and round,
Round and round,
Round and round ...*

Popular children's song that doesn't stop playing (earworm)

3

Open quantum systems

In the last chapter, we looked at how superconducting circuits with Josephson junctions can be used as qubits. These artificial atoms are manipulated by routing microwave photons through a transmission line to which the atoms are coupled. The transmission line which can be modeled as a collection of harmonic oscillators acts as an environment for the atom. We would now like to describe how such an atom coupled to an environment evolves in time. While we are specifically interested in circuit QED setups, the formalism that we will use applies to a general quantum system. These are the master equations and we will review the same in this chapter.

An isolated quantum system evolves according to the Schrödinger equation [103]

$$i\hbar \frac{\partial}{\partial t} |\psi\rangle = H |\psi\rangle, \quad (3.1)$$

where the system is described by a state vector $|\psi\rangle$ that evolves under the Hamiltonian H . The dimensions are taken care of by \hbar , a fundamental constant that we will set to 1 henceforth. While the Schrödinger equation was in itself a breakthrough of sorts, not all quantum mechanical systems can be described by a state vector. A more general formalism that allows for both pure and mixed states is

using the density matrix $\rho \equiv \sum_i p_i |\psi_i\rangle \langle \psi_i|$, where p_i is the probability for the system to be in state $|\psi_i\rangle$. From Eq. (3.1) and its conjugate bra version, we can derive the quantum Liouville or the von Neumann equation [104]

$$\dot{\rho} = -i[H, \rho]. \quad (3.2)$$

Both of these equations of motion are valid for isolated or closed systems, which means we have to take into account enough degrees of freedom (if not the whole universe) in order to use them. However, as we are interested in only a certain part of the universe that is under observation (*viz.* the system such as the artificial atom) and do not care about the rest (*viz.* the environment), we would like to get an equation of motion for the system alone. We do this by tracing out the environment's degrees of freedom from the Liouville equation. This leads us to the master equation, which describes the evolution of an open quantum system. The master equation is derived in many references including [104, 105]. We will review this derivation in the next section based on these references.

3.1 Master equation

We start with the Liouville equation rewritten as

$$\dot{\rho}_{\text{tot}} = -i[H_{\text{tot}}, \rho_{\text{tot}}] \quad (3.3)$$

with the Hamiltonian

$$H_{\text{tot}} = H_{\text{sys}} + H_{\text{bath}} + H_{\text{int}}, \quad (3.4)$$

where we have identified the internal Hamiltonian of the system H_{sys} , the bath (environment) H_{bath} and their interaction H_{int} . The interaction Hamiltonian gives the effect of the bath on the system and vice versa. It is helpful to go to the interaction picture by using the unitary transformation $U(t) = \exp\{i(H_{\text{sys}} + H_{\text{bath}})t\}$. With this transformation, Eq. (3.3) becomes,

$$\dot{\rho}^I(t) = -i[H_{\text{int}}(t), \rho^I(t)], \quad (3.5)$$

where we have defined $H_{\text{int}}(t) = U(t)H_{\text{int}}U^\dagger(t)$ and $\rho^I(t) = U(t)\rho_{\text{tot}}(t)U^\dagger(t)$. By iterating the above equation (i.e by substituting the solution back into the right hand side of the equation), we get

$$\dot{\rho}^I(t) = -i[H_{\text{int}}(t), \rho^I(0)] - \left[H_{\text{int}}(t), \int_0^t [H_{\text{int}}(t'), \rho^I(t')] dt' \right]. \quad (3.6)$$

The equations are exact up to this point. We now make some assumptions and approximations to simplify the derivation. First, we assume that the bath is very large and that the coupling between the system and the bath is weak. This means that the interaction between the system and the bath does not significantly affect the bath density matrix (Born approximation). By starting with an initial condition $\rho_{\text{tot}}(0) = \rho_{\text{sys}}(0) \otimes \rho_{\text{bath}}$, the weak coupling assumption then leads us to

$$\rho_{\text{tot}}(t) \approx \rho_{\text{sys}}(t) \otimes \rho_{\text{bath}} \quad (3.7)$$

where the system density matrix that we are after, $\rho_{\text{sys}}(t) = \text{Tr}_{\text{bath}}\{\rho_{\text{tot}}(t)\}$. By inserting this condition and tracing over the bath degrees of freedom in Eq. (3.6), we have

$$\dot{\rho}_{\text{sys}}^I(t) = - \int_0^t dt' \text{Tr}_{\text{bath}} \left\{ [H_{\text{int}}(t), [H_{\text{int}}(t'), \rho_{\text{sys}}^I(t') \otimes \rho_{\text{bath}}]] \right\} \quad (3.8)$$

where we have also assumed $\text{Tr}_{\text{bath}}\{H_{\text{int}}(t)\rho^I(0)\} = 0$.

To proceed further, we will consider the interaction Hamiltonian to be of the form $A(t)B(t)$, where A and B are the system and bath operators respectively. In the case of atoms coupled to the electromagnetic field, this is usually given by the dipole approximation which takes the form $i\sum(\sigma_{ij} + \sigma_{ji})(b_k^\dagger - b_k)$, i.e. the product of the lowering+raising operators of the atom with the creation-annihilation operators of the bath. Such an interaction gives us terms such as $\text{Tr}_{\text{bath}}\{B(t)B(t')\rho_{\text{bath}}\}$ in the above equation. These are nothing but the correlation functions of the bath which decay over a typical correlation time, say τ_{bath} . Our previous assumptions of the bath having a large number of degrees of freedom and the weak coupling means that τ_{bath} is much smaller compared to the time scales at which the system in the interaction picture evolves (say, τ_{sys}). This lets us to make the following approximations :

▷ Markov approximation: Take $\rho(t') \rightarrow \rho(t)$, as the system would not have evolved much in the time scales dictated by τ_{bath} .

▷ Substituting $t' \rightarrow t - s$, we can extend the upper limit for the time difference s to ∞ . This is also justified by the fact that $\tau_{\text{bath}} \ll \tau_{\text{sys}}$ and hence the integrand anyways goes to zero for any time $s \gg \tau_{\text{bath}}$.

With these, we have a Markovian master equation,

$$\dot{\rho}_{\text{sys}}^I(t) = - \int_0^\infty ds \text{Tr}_{\text{bath}} \left\{ [H_{\text{int}}(t), [H_{\text{int}}(t-s), \rho_{\text{sys}}^I(t) \otimes \rho_{\text{bath}}]] \right\}. \quad (3.9)$$

The above equation is valid for general systems subject to the approximations we have made (together known as the Born-Markov approximations). We are

however interested in the quantum optical master equation. In this case, the environment is the electromagnetic field which can be modeled as a collection of harmonic oscillators similar to that of the transmission line in superconducting circuits. This implies, we can write the Hamiltonians as

$$H_{\text{bath}} = \sum_k \omega_k b_k^\dagger b_k \quad (3.10)$$

and

$$H_{\text{int}} = A \otimes B = A^\dagger \otimes B^\dagger, \quad (3.11)$$

where A and B are the Hermitian system and bath operators, which in the interaction picture become $A_I(t)$ and $B_I(t)$. With this interaction Hamiltonian in Eq. (3.9), we get

$$\begin{aligned} \dot{\rho}_{\text{sys}}^I(t) = & \int_0^\infty ds \langle B_I(t)B_I(t-s) \rangle \left\{ A_I(t-s)\rho_{\text{sys}}^I(t)A_I(t) - A_I(t)A_I(t-s)\rho_{\text{sys}}^I(t) \right\} \\ & + \langle B_I(t-s)B_I(t) \rangle \left\{ A_I(t)\rho_{\text{sys}}^I(t)A_I(t-s) - \rho_{\text{sys}}^I(t)A_I(t-s)A_I(t) \right\}, \end{aligned} \quad (3.12)$$

where $\langle B_I(t)B_I(t') \rangle \equiv \text{Tr}_{\text{bath}} \{ B_I(t)B_I(t')\rho_{\text{bath}} \}$. The time evolution of the system operators can be written explicitly by expanding the operators in the energy eigenbasis of the system Hamiltonian as

$$A_I(t) = \sum_{m,n} e^{i\omega_m t} |m\rangle \langle m| A |n\rangle \langle n| e^{-i\omega_n t} = \sum_{m,n} A_{mn} |m\rangle \langle n| e^{i\omega_{mn} t} \equiv \sum_{m,n} \tilde{A}_{mn} e^{i\omega_{mn} t}, \quad (3.13)$$

where $H_{\text{sys}} |m\rangle = \omega_m |m\rangle$ and $\omega_{mn} = \omega_m - \omega_n$. We have also defined the tilde operators $\tilde{A}_{mn} = A_{mn} |m\rangle \langle n|$ to keep the notations simple in the following equations. With this form of the system operators, one can get the master equation as

$$\dot{\rho}_{\text{sys}}^I(t) = \sum_{m,n} \sum_{m',n'} \Gamma_{mn} e^{i(\omega_{m'n'} - \omega_{mn})t} \left\{ \tilde{A}_{mn}^\dagger \rho_{\text{sys}}^I(t) \tilde{A}_{m'n'} - \tilde{A}_{m'n'} \tilde{A}_{mn}^\dagger \rho_{\text{sys}}^I(t) \right\} + h.c., \quad (3.14)$$

where we have defined

$$\Gamma_{mn} = \int_0^\infty ds \langle B_I(t)B_I(t-s) \rangle e^{i\omega_{mn}s}. \quad (3.15)$$

Assuming the bath to be in its stationary state with $[H_{\text{bath}}, \rho_{\text{bath}}] = 0$, we can show that the bath correlators $\langle B_I(t)B_I(t-s) \rangle$ depend only on the time difference s and not on the time t itself [104]. Thus, we have

$$\Gamma_{mn} = \int_0^\infty ds \langle B_I(s)B_I(0) \rangle e^{i\omega_{mn}s}. \quad (3.16)$$

Now we come to the next set of approximations, that is either called the secular approximation [106] or the rotating wave approximation [104, 105]. In this, we discard the fast rotating terms in the sum (i.e.) all the terms except those that have $\omega_{mn} - \omega_{m'n'} = 0$, as they average out to zero on the time scales that we are interested in. In our case, this condition can be met for two cases: either $m = m'$ and $n = n'$ or $m = n$ and $m' = n'$. Keeping only these terms, we get,

$$\begin{aligned} \dot{\rho}_{\text{sys}}^I(t) = & \sum_{m,n} \Gamma_{mn} \left\{ \tilde{A}_{mn}^\dagger \rho_{\text{sys}}^I(t) \tilde{A}_{mn} - \tilde{A}_{mn} \tilde{A}_{mn}^\dagger \rho_{\text{sys}}^I(t) \right\} \\ & + \sum_{m,n} \Gamma_{mm} \left\{ \tilde{A}_{mm}^\dagger \rho_{\text{sys}}^I(t) \tilde{A}_{nn} - \tilde{A}_{nn} \tilde{A}_{mm}^\dagger \rho_{\text{sys}}^I(t) \right\} + h.c. \end{aligned} \quad (3.17)$$

Substituting $\Gamma_{mn} = \frac{1}{2}\gamma_{mn} + iS_{mn}$ and noting that Γ_{mm} is independent of the energy levels (as $\omega_{mm} = 0$), we get

$$\begin{aligned} \dot{\rho}_{\text{sys}}^I(t) = & \sum_{mn} \left(\gamma_{mn} \left(\tilde{A}_{mn}^\dagger \rho_{\text{sys}}^I(t) \tilde{A}_{mn} - \frac{1}{2} \left\{ \tilde{A}_{mn} \tilde{A}_{mn}^\dagger, \rho_{\text{sys}}^I(t) \right\} \right) \right. \\ & - iS_{mn} \left[\tilde{A}_{mn} \tilde{A}_{mn}^\dagger, \rho_{\text{sys}}^I(t) \right] \\ & + \gamma_{mm} \left(\tilde{A}_{mm}^\dagger \rho_{\text{sys}}^I(t) \tilde{A}_{nn} - \frac{1}{2} \left\{ \tilde{A}_{nn} \tilde{A}_{mm}^\dagger, \rho_{\text{sys}}^I(t) \right\} \right) \\ & \left. - iS_{mm} \left[\tilde{A}_{nn} \tilde{A}_{mm}^\dagger, \rho_{\text{sys}}^I(t) \right] \right). \end{aligned} \quad (3.18)$$

The above can be written more succinctly by defining a Hamiltonian

$$\begin{aligned} H_{LS} & \equiv \sum_{mn} (S_{mn} \tilde{A}_{mn} \tilde{A}_{mn}^\dagger + S_{mm} \tilde{A}_{nn} \tilde{A}_{mm}^\dagger) \\ & = \sum_{mn} S_{mn} |A_{mn}|^2 |m\rangle \langle m| + \sum_m S_{mm} |A_{mm}|^2 |m\rangle \langle m| \end{aligned} \quad (3.19)$$

and a dissipation super-operator

$$\begin{aligned} \mathcal{D}\rho_{\text{sys}}^I(t) & \equiv \sum_{mn} \gamma_{mn} \left(\tilde{A}_{mn}^\dagger \rho_{\text{sys}}^I(t) \tilde{A}_{mn} - \frac{1}{2} \left\{ \tilde{A}_{mn} \tilde{A}_{mn}^\dagger, \rho_{\text{sys}}^I(t) \right\} \right) \\ & + \sum_{mn} \gamma_{mm} \left(\tilde{A}_{mm}^\dagger \rho_{\text{sys}}^I(t) \tilde{A}_{nn} - \frac{1}{2} \left\{ \tilde{A}_{nn} \tilde{A}_{mm}^\dagger, \rho_{\text{sys}}^I(t) \right\} \right). \end{aligned} \quad (3.20)$$

The master equation then becomes

$$\dot{\rho}_{\text{sys}}^I(t) = -i[H_{LS}, \rho_{\text{sys}}^I(t)] + \mathcal{D}\rho_{\text{sys}}^I(t). \quad (3.21)$$

The Hamiltonian H_{LS} leads to a renormalization of the system eigenfrequencies and is usually referred to as Lamb shift. As it commutes with H_{sys} , it can be added to the same but it is usually neglected as it only leads to a small shift of eigenenergies. Going back to the system's frame from the interaction picture, we get

$$\dot{\rho}_{\text{sys}}(t) = -i[H_{\text{sys}}, \rho_{\text{sys}}(t)] + \mathcal{D}\rho_{\text{sys}}(t), \quad (3.22)$$

where the first term is the same as that from the Liouville equation for the system alone. The second term leads to an irreversible decay of the initial state of the system and hence the name dissipator. By explicitly writing the frequencies involved in the γ terms, we see that

$$\gamma_{mn} = \Gamma_{mn} + \Gamma_{mn}^* = \int_{-\infty}^{\infty} \langle B_I^\dagger(s) B_I(0) \rangle e^{i\omega_{mn}s} \quad (3.23)$$

and

$$\gamma_{mm} = \int_{-\infty}^{\infty} \langle B_I^\dagger(s) B_I(0) \rangle e^{i0s} \quad (3.24)$$

are nothing but the power spectral density of the bath at the frequencies ω_{mn} and 0 respectively (Wiener-Khinchin theorem) [107].

It is instructive to look at the master equation for a two-level system (2LS) in a thermal bath as this is the most relevant case for this thesis. As the name suggests, we have only two levels which we label the ground state $|0\rangle \equiv (1 \ 0)^T$ and the excited state $|1\rangle \equiv (0 \ 1)^T$. If this is an atomic system such as a transmon, the higher transitions are neglected assuming they are well separated in frequency from the lower transition and also assuming that we will not drive the system strongly as that would lead to excitation of the higher levels. Thus we have an effective two-level system which can be mapped to a spin- $\frac{1}{2}$ particle in a magnetic field and we can write our system operators using the Pauli matrices. The system Hamiltonian $H_{\text{sys}} = -\frac{\Delta}{2}\sigma_z$, where $\Delta = \omega_1 - \omega_0$ is the transition frequency between the ground and excited state. The interaction Hamiltonian can be written as

$$H_{\text{int}}(t) = iA_I(t) \sum_k g_k \left[b_k(t) - b_k^\dagger(t) \right], \quad (3.25)$$

where g_k is the coupling between the k^{th} mode of the bath and the system. For a thermal bath in equilibrium at temperature T , we have the average number of photons in mode k as (Planck distribution)

$$N(\omega_k) = \frac{1}{\exp(\beta\omega_k) - 1} \quad (3.26)$$

where $\beta = 1/k_B T$. With this we have,

$$\langle B_I^\dagger(s) B_I(0) \rangle = \sum_k g_k^2 \left(N(\omega_k) e^{i\omega_k s} + [1 + N(\omega_k)] e^{-i\omega_k s} \right). \quad (3.27)$$

Going to the continuum limit by replacing \sum_k in the above with $\int d\omega J(\omega)$, where $J(\omega)$ is the density of states, it can be shown that

$$\gamma_{mn} = 2\text{Real}[\Gamma_{mn}] = \gamma_0 \begin{cases} 1 + N(\omega_{mn}) & \text{for } \omega_{mn} > 0 \\ N(\omega_{mn}) & \text{for } \omega_{mn} < 0 \end{cases} \quad (3.28)$$

where $\gamma_0 = 2\pi J(|\omega_{mn}|)g(|\omega_{mn}|)^2$ is the rate of spontaneous decay. To get to the above result, we have used the formula

$$\int_0^\infty ds e^{i\omega s} = \pi\delta(\omega) - i\mathcal{P}\frac{1}{\omega}, \quad (3.29)$$

where \mathcal{P} is the Cauchy principal value.

The coupling of the bath to the system can be categorized into longitudinal (along the direction of quantization) and transverse (perpendicular to the direction of quantization). They lead to different kinds of decoherence of the system as we will see below.

- Transverse coupling

Assuming the coupling of the bath to the qubit is along the x-direction, we have the system part of the interaction Hamiltonian as $A_I(t) = \sigma_x(t) = \sigma_+ e^{i\Delta t} + \sigma_- e^{-i\Delta t}$ where $\sigma_- = |0\rangle\langle 1|$ and $\sigma_+ = \sigma_-^\dagger$. This means only the off-diagonal elements are non-zero and we have $\tilde{A}_{mn} = (1 - \delta_{mn}) |m\rangle\langle n|$ where $m, n \in \{0, 1\}$. Combining this along with Eq. (3.20) and Eq. (3.28), we get

$$\mathcal{D}\rho = \gamma_0(N+1) \left(\sigma_- \rho \sigma_+ - \frac{1}{2} \{ \sigma_+ \sigma_-, \rho \} \right) + \gamma_0 N \left(\sigma_+ \rho \sigma_- - \frac{1}{2} \{ \sigma_- \sigma_+, \rho \} \right), \quad (3.30)$$

where $N \equiv N(\omega_{mn})$, the average number of thermal photons in the bath with frequency equal to the transition frequency $\omega_{mn} = \Delta$. At $T = 0$, we have no thermal photons in the bath on average i.e. $N = 0$ and this further reduces the dissipator to a form that we write as

$$\mathcal{D} \left[\sqrt{\Gamma} \sigma_- \right] \rho \equiv \Gamma \left(\sigma_- \rho \sigma_+ - \frac{1}{2} \{ \sigma_+ \sigma_-, \rho \} \right). \quad (3.31)$$

The dissipators that we will use in the following sections and in the appended papers are of this kind, as we will assume to work at 0 K. We have changed

the notation of the relaxation rates to $\Gamma = \gamma_0$ to be consistent with the attached papers.

- Longitudinal coupling

For the coupling along the quantization axis, we have $A_I(t) = \sigma_z(t) = |0\rangle\langle 0| e^{i\omega_{00}t} - |1\rangle\langle 1| e^{i\omega_{11}t}$, where $\omega_{00} = \omega_{11} = 0$. We now only have the diagonal terms in the dissipator with $\tilde{A}_{mn} = (-1)^m \delta_{mn} |m\rangle\langle n|$ where $m, n \in \{0, 1\}$. Defining the pure dephasing rates $2\Gamma_\phi = \gamma_{00} + \gamma_{11}$, we once again rewrite the dissipator in the form

$$\begin{aligned} \mathcal{D} \left[\sqrt{\frac{\Gamma_\phi}{2}} \sigma_z \right] \rho &= \frac{\Gamma_\phi}{2} \left(\sigma_z \rho \sigma_z - \frac{1}{2} \{ \sigma_z \sigma_z, \rho \} \right) \\ &= \frac{\Gamma_\phi}{2} (\sigma_z \rho \sigma_z - \rho). \end{aligned} \quad (3.32)$$

In general the master equation of the two level system coupled to a thermal bath at 0 K can be written as,

$$\dot{\rho} = -i \left[-\frac{\Delta}{2} \sigma_z, \rho \right] + \mathcal{D}[L] \rho + \mathcal{D}[L_\phi] \rho, \quad (3.33)$$

where we have defined the so called Lindblad operators $L = \sqrt{\Gamma} \sigma_-$ and $L_\phi = \sqrt{\frac{\Gamma_\phi}{2}} \sigma_z$. The first term on the RHS gives a Liouvillian evolution of the system under its own Hamiltonian. The second term leads not only to the decay of excited state population (relaxation) but also to decay of the off-diagonal elements of the density matrix (dephasing). The third term affects only the off-diagonal elements (and hence the rate is called pure dephasing). We can see this from the solution of the above master equation which starting from a density matrix $\rho(0)$ at $t = 0$, is given as

$$\rho(t) = \begin{pmatrix} 1 - \rho_{11}(0) e^{-\Gamma t} & \rho_{01}(0) e^{i\Delta t} e^{-\gamma t} \\ \rho_{10}(0) e^{-i\Delta t} e^{-\gamma t} & \rho_{11}(0) e^{-\Gamma t} \end{pmatrix}, \quad (3.34)$$

where $\gamma = \Gamma/2 + \Gamma_\phi$ is called the total decoherence rate. At this point we note that in the appended papers, we use a shorthand notation for the master equation by defining a Liouvillian superoperator \mathcal{L} such that

$$\dot{\rho} = \mathcal{L} \rho. \quad (3.35)$$

3.2 Input and Output

The master equation presented in the previous section describes the evolution of an open quantum system such as a transmon coupled to a transmission line. To learn about the properties of the transmon or to manipulate the qubit, we scatter microwave photons on it and measure the output radiation. Alternatively, we might also be interested in the effect of the transmon on the microwave photons. For all of these reasons, we use the input-output theory that gives the relationship between the incoming and the scattered field. We will review the derivation of this relation based on the reference [108].

We once again begin with the total Hamiltonian of our system coupled to a bath as

$$H = H_{\text{sys}} + H_{\text{bath}} + H_{\text{int}} \quad (3.36)$$

$$H_{\text{bath}} = \int_0^\infty d\omega \omega b_\omega^\dagger b_\omega \quad (3.37)$$

$$H_{\text{int}} = i \int_0^\infty d\omega g(\omega) \left(b_\omega^\dagger a - a^\dagger b_\omega \right) \quad (3.38)$$

where a is a system operator and $g(\omega)$ is the coupling strength between the bath and the system. The bath operators obey the usual commutation relation $[b_\omega, b_{\omega'}^\dagger] = \delta(\omega - \omega')$. The interaction Hamiltonian is written after the rotating wave approximation (RWA), which is valid in the weak coupling regimes that we consider. As a next step, we extend the lower limits in the integrals of H_{bath} and H_{int} to $-\infty$. This approximation is valid if the operators a are off-diagonal in the eigenbasis of H_{sys} and evolve as $a(t) = a \exp(i\omega_s t)$. Then the terms in the integrals that are far off-resonance from ω_s are negligibly small. In this thesis, we assume that we have interactions of the above type. For example, for a qubit coupled to a transmission line with $H_{\text{sys}} = -\frac{1}{2}\omega_{qb}\sigma_z$, we consider only the dipole coupling to the transmission line. This means the interaction term involves only the off-diagonal $\sigma_x = \sigma_- + \sigma_+$ operator as mentioned in the previous section. We also assume that the coupling is slowly varying around the system frequency ω_s . This lets us to approximate $g(\omega) = \sqrt{\Gamma/2\pi}$.

With these we have the Hamiltonians as

$$H_{\text{bath}} = \int_{-\infty}^\infty d\omega \omega b_\omega^\dagger b_\omega, \quad (3.39)$$

$$H_{\text{int}} = i\sqrt{\frac{\Gamma}{2\pi}} \int_{-\infty}^\infty d\omega \left(b_\omega^\dagger a - a^\dagger b_\omega \right). \quad (3.40)$$

Using these Hamiltonians, we can write down the Heisenberg's equations of motion

$$\dot{b}_\omega = -i\omega b_\omega + \sqrt{\frac{\Gamma}{2\pi}} a, \quad (3.41)$$

$$\dot{X} = i[H_{\text{sys}}, X] - \sqrt{\frac{\Gamma}{2\pi}} \int_{-\infty}^{\infty} d\omega \left(b_\omega^\dagger [a, X] - [a^\dagger, X] b_\omega \right), \quad (3.42)$$

where X is an arbitrary system operator. Solving Eq. (3.41) with initial condition at $t_0 < t$, we get

$$b_\omega(t) = e^{-i\omega(t-t_0)} b_\omega(t_0) + \sqrt{\frac{\Gamma}{2\pi}} \int_{t_0}^t dt' e^{i\omega(t'-t)} a(t'), \quad (3.43)$$

where $b_\omega(t_0)$ is the state of the field at t_0 . Substituting the solution in Eq. (3.42) and defining

$$b_{\text{in}}(t) = \frac{1}{\sqrt{2\pi}} \int_{-\infty}^{\infty} d\omega e^{-i\omega(t-t_0)} b_\omega(t_0) \quad (3.44)$$

we get

$$\begin{aligned} \dot{X}(t) = & i[H_{\text{sys}}, X(t)] - \left(\sqrt{\Gamma} b_{\text{in}}^\dagger(t) + \frac{\Gamma}{2} a^\dagger(t) \right) [a(t), X(t)] \\ & + \left(\sqrt{\Gamma} b_{\text{in}}(t) + \frac{\Gamma}{2} a(t) \right) [a^\dagger(t), X(t)]. \end{aligned} \quad (3.45)$$

The above equation is known as the quantum Langevin equation. We interpret $b_{\text{in}}(t)$ as the input field that interacts with our system at time t . From the commutation relation of the bath operators, we see that $[b_{\text{in}}(t), b_{\text{in}}^\dagger(t')] = \delta(t - t')$.

Solving Eq. (3.41) with a final condition at a later time $t_1 > t$, we get

$$b_\omega(t) = e^{-i\omega(t-t_1)} b_\omega(t_1) - \sqrt{\frac{\Gamma}{2\pi}} \int_t^{t_1} dt' e^{i\omega(t'-t)} a(t'), \quad (3.46)$$

where $b_\omega(t_1)$ is the state of the field at t_1 . Defining the output field as

$$b_{\text{out}}(t) = \frac{1}{\sqrt{2\pi}} \int_{-\infty}^{\infty} d\omega e^{-i\omega(t-t_1)} b_\omega(t_1) \quad (3.47)$$

and substituting the above solution in Eq. (3.42), we get

$$\begin{aligned} \dot{X}(t) = & i[H_{\text{sys}}, X(t)] - \left(\sqrt{\Gamma} b_{\text{out}}^\dagger(t) - \frac{\Gamma}{2} a^\dagger(t) \right) [a(t), X(t)] \\ & + \left(\sqrt{\Gamma} b_{\text{out}}(t) - \frac{\Gamma}{2} a(t) \right) [a^\dagger(t), X(t)]. \end{aligned} \quad (3.48)$$

We interpret $b_{\text{out}}(t)$ as the output field that leaves the system at time t . Comparing Eq. (3.45) and Eq. (3.48), we have

$$b_{\text{out}}(t) = b_{\text{in}}(t) + \sqrt{\Gamma}a(t), \quad (3.49)$$

which gives us the relation between the input and output. By solving the system dynamics for $a(t)$ and by specifying an input field, we can calculate the output field. For a qubit that is driven by a coherent field, we can write the coherent output field as

$$\alpha_{\text{out}}(t) = \alpha_{\text{in}}(t) + \sqrt{\Gamma} \langle \sigma_-(t) \rangle, \quad (3.50)$$

where $\alpha_{\text{in/out}}(t) = \langle b_{\text{in/out}}(t) \rangle$ is the complex amplitude of the coherent input/output fields and $\langle \sigma_-(t) \rangle = \text{Tr}[\sigma_- \rho_{\text{sys}}(t)]$. In this case, we have assumed that the atom is connected to the bath or environment through a single port. This situation corresponds to having an atom in front of a mirror. In superconducting circuits, this means we have an artificial atom at the end of a semi-infinite transmission line. The above input-output relations can be extended to the situation where we have a system coupled to an open 1-D transmission line as

$$b_{\text{out}}^L(t) = b_{\text{in}}^L(t) + \sqrt{\frac{\Gamma}{2}}a(t), \quad (3.51)$$

$$b_{\text{out}}^R(t) = b_{\text{in}}^R(t) + \sqrt{\frac{\Gamma}{2}}a(t), \quad (3.52)$$

where $b_{\text{in/out}}^{L/R}$ are the left and right moving input/output fields. We have kept the total decay rate of the system at Γ . Driving a two-level atom only from the left with a coherent field of amplitude α_{in} , now gives the coherent outputs as

$$\alpha_{\text{out}}^L(t) = \alpha_{\text{in}}(t) + \sqrt{\frac{\Gamma}{2}} \langle \sigma_-(t) \rangle, \quad (3.53)$$

$$\alpha_{\text{out}}^R(t) = \sqrt{\frac{\Gamma}{2}} \langle \sigma_-(t) \rangle. \quad (3.54)$$

In this case, $\alpha_{\text{out}}^L(t)$ is the transmitted field and $\alpha_{\text{out}}^R(t)$ is the reflected field. Most often, we are interested in the steady-state or the stationary outputs. In this case, one can drop the time arguments in the above equations and the atomic term becomes $\langle \sigma_- \rangle_{\text{ss}} = \text{Tr}[\sigma_- \rho_{\text{ss}}]$, where ρ_{ss} is the steady state solution of the master equation. In such a situation, we can define the reflection and transmission coefficients as $r = \alpha_{\text{out}}^R / \alpha_{\text{in}}$ and $t = \alpha_{\text{out}}^L / \alpha_{\text{in}} = 1 + r$.

3.3 Coherence functions

As the input-output relations give us the total output field, we can also calculate coherence functions of the output field. Also known as correlation functions, they tell us about the statistics of the outgoing radiation.

The first order correlation function of the output field is defined as

$$G^{(1)}(t_1, t_2) = \langle b_{\text{out}}^\dagger(t_1)b_{\text{out}}(t_2) \rangle, \quad (3.55)$$

which is usually given normalized as

$$g^{(1)}(t_1, t_2) = \frac{\langle b_{\text{out}}^\dagger(t_1)b_{\text{out}}(t_2) \rangle}{\sqrt{\langle b_{\text{out}}^\dagger(t_1)b_{\text{out}}(t_1) \rangle \langle b_{\text{out}}^\dagger(t_2)b_{\text{out}}(t_2) \rangle}}. \quad (3.56)$$

In the case of stationary fields, the above correlation depends only on the time difference $t_1 - t_2 = \tau$ as

$$g^{(1)}(\tau) = \frac{\langle b_{\text{out}}^\dagger(t)b_{\text{out}}(t+\tau) \rangle}{\langle b_{\text{out}}^\dagger(t)b_{\text{out}}(t) \rangle}. \quad (3.57)$$

These correlation functions can be calculated using [105]

$$\langle b_{\text{out}}^\dagger(t_1)b_{\text{out}}(t_2) \rangle = \text{Tr} \left[b_{\text{out}}^\dagger P(t_1, t_2) \{ b_{\text{out}} \rho(t_2) \} \right] \text{ for } t_1 > t_2, \quad (3.58)$$

$$\langle b_{\text{out}}^\dagger(t_1)b_{\text{out}}(t_2) \rangle = \text{Tr} \left[b_{\text{out}} P(t_2, t_1) \{ \rho(t_2) b_{\text{out}}^\dagger \} \right] \text{ for } t_2 > t_1, \quad (3.59)$$

where the propagator $P(t, t')$ evolves everything on its right from time t' to t . As we require this to be true for the density matrix as well, we have $\rho(t) = P(t, t')\rho(t')$. Differentiating this with respect to t , and using the master equation $\dot{\rho}(t) = \mathcal{L}(t)\rho(t)$, we end up with a differential equation for the propagator $\dot{P}(t, t') = \mathcal{L}(t)P(t, t')$ with the initial condition $P(t', t') = 1$ [30]. From the solution of this differential equation, we can calculate the correlation function as above.

The first order correlation function is an amplitude-amplitude correlation function and can be measured using a Mach–Zehnder interferometer [109]. The normalized first order correlation, also known as degree of first order coherence, has values such that $0 \leq |g^{(1)}(t_1, t_2)| \leq 1$. The value of 1 corresponds to a fully first-order coherent light and the value 0 means that the radiation is incoherent. Both quantum and classical fields satisfy these limits.

A more interesting quantity is the second order correlation function, which is an intensity-intensity correlation that is measured using a Hanbury Brown and Twiss interferometer [109]. It is defined as

$$G^{(2)}(t_1, t_2) = \langle b_{\text{out}}^\dagger(t_2)b_{\text{out}}^\dagger(t_1)b_{\text{out}}(t_1)b_{\text{out}}(t_2) \rangle, \quad (3.60)$$

and is normalized as

$$g^{(2)}(t_1, t_2) = \frac{\langle b_{\text{out}}^\dagger(t_2)b_{\text{out}}^\dagger(t_1)b_{\text{out}}(t_1)b_{\text{out}}(t_2) \rangle}{\langle b_{\text{out}}^\dagger(t_1)b_{\text{out}}(t_1) \rangle \langle b_{\text{out}}^\dagger(t_2)b_{\text{out}}(t_2) \rangle}. \quad (3.61)$$

In the case of stationary fields, the above correlation once again depends only on the time difference $t_1 - t_2 = \tau$ as

$$g^{(2)}(\tau) = \frac{\langle b_{\text{out}}^\dagger(t)b_{\text{out}}^\dagger(t+\tau)b_{\text{out}}(t+\tau)b_{\text{out}}(t) \rangle}{\langle b_{\text{out}}^\dagger(t)b_{\text{out}}(t) \rangle^2}. \quad (3.62)$$

The numerator can be calculated as [105],

$$\langle b_{\text{out}}^\dagger(t_2)b_{\text{out}}^\dagger(t_1)b_{\text{out}}(t_1)b_{\text{out}}(t_2) \rangle = \text{Tr} \left[b_{\text{out}}^\dagger b_{\text{out}} P(t_1, t_2) \{ b_{\text{out}} \rho(t_2) b_{\text{out}}^\dagger \} \right]. \quad (3.63)$$

The second order correlation function is used to determine if the radiation is "nonclassical". Using a classical theory, the lower limit for $g^{(2)}(0)$ is 1 and $g^{(2)}(\tau) \leq g^{(2)}(0)$. However, in the quantum version both of these conditions can be violated and we can have $0 \leq g^{(2)}(0) \leq 1$. Any output radiation that leads to $g^{(2)}(0) < 1$ is said to have sub-Poissonian statistics and radiations with $g^{(2)}(\tau) > g^{(2)}(0)$ are called antibunched [110].

The $g^{(2)}(\tau)$ can be thought of as the conditional probability for detecting a photon at time τ if a photon was detected at time t . The output field from an ideal single photon source has $g^{(2)}(0) = 0$. However $g^{(2)}(0) = 0$ alone may not be a full measure of the efficiency of a single photon source as it only means that there are no more than 1 photon at the same time in the output. Consider for example a qubit coupled to an open transmission line driven by a coherent field α_{in} from the left. The reflected field (as in Eq. (3.54) but without the average) has $g^{(2)}(0) = 0$. However, as shown in [30], the probability to have a single photon in the reflected field by exciting the qubit with a π -pulse has a maximum of 50%. This is because the qubit can equally radiate in the left and right moving fields and does this with 50 % probability. Thus, to calculate the full efficiency of the source we have to calculate the probability distribution for the number of photons in the output field, which can be done also using the correlation functions.

Moving from the first and second order coherence functions, we define a general m^{th} order correlation function as

$$\begin{aligned} G^{(m)}(t_1, t_2, \dots, t_m) &= \left\langle b_{\text{out}}^\dagger(t_1) b_{\text{out}}^\dagger(t_2) \dots b_{\text{out}}^\dagger(t_m) b_{\text{out}}(t_m) \dots b_{\text{out}}(t_2) b_{\text{out}}(t_1) \right\rangle \\ &= \text{Tr} \left[b_{\text{out}} P(t_m, t_{m-1}) \left\{ \dots P(t_3, t_2) \left\{ b_{\text{out}} P(t_2, t_1) \left\{ b_{\text{out}} \rho(t_1) b_{\text{out}}^\dagger \right\} b_{\text{out}}^\dagger \right\} \dots \right\} b_{\text{out}}^\dagger \right], \end{aligned} \quad (3.64)$$

where the propagators act on the braces immediately on their right. From the m^{th} order correlation function, we can calculate photon m -tuples and the probability to have m photons in the output as outlined in reference [30].

3.4 Master equation for Fock state input

As mentioned in the introduction, recent progress in quantum optics and quantum information depend on manipulation of single photons. Such a single photon state in a continuous mode is given by [109]

$$|1_\xi\rangle = \int d\omega \tilde{\xi}(\omega) b^\dagger(\omega) |0\rangle, \quad (3.65)$$

where $\tilde{\xi}(\omega)$ is the spectral density function (SDF) or the wave packet in frequency space. The Fourier transform of the SDF gives a wave packet in the time domain $\xi(t)$, which satisfies the normalization condition $\int dt |\xi(t)|^2 = 1$. We can then define a photon wave packet creation operator

$$a_\xi^\dagger = \int dt \bar{\xi}(t) a^\dagger(t) \quad (3.66)$$

such that $|1_\xi\rangle = a_\xi^\dagger |0\rangle$. Any arbitrary number state $|N_\xi\rangle$ can be created by applying the operator N times on the vacuum state and taking care of the normalization.

We would like to describe the evolution of a system driven by such a single photon Fock state. The absorption of the single photon by the system leaves the field in an entirely different state as opposed to the case for a coherent field. As the single photon starts interacting with the system, it also gets entangled with the same. Unlike in the derivation of the master equation, one has to keep track of all of the system-field correlations [111]. To address this issue, one can take two approaches. In the first one, we can include the source of the photons

(usually a cavity) in our picture, and use the Markovian master equations. The other approach is to derive master equations explicitly considering Fock state inputs. The second approach previously calculated by different authors for specific scenarios [112–114], was unified and extended to a general situation in reference [115]. We will briefly describe the formalism here and refer to the original paper for more details.

Consider a system interacting with a input field in state $|N_{\xi}\rangle$. As before, we assume that initially at time $t = 0$, the system and the field are uncorrelated and can be represented as a product state

$$\rho(0) = \rho_{\text{sys}} \otimes |N_{\xi}\rangle \langle N_{\xi}|. \quad (3.67)$$

The evolution of the system is then given by the time evolution of the asymmetric reduced density matrices defined as

$$\rho_{m,n}(t) \equiv \text{Tr}_{\text{field}} \left[U(t) (\rho_{\text{sys}} \otimes |m_{\xi}\rangle \langle n_{\xi}|) U^{\dagger}(t) \right], \quad (3.68)$$

where m, n label the Fock subspaces that run from 0 to N . The time evolution of the total state is given by the unitary operator $U(t)$. The master equation for these reduced density matrices is then shown to be

$$\dot{\rho}_{m,n} = -i[H, \rho_{m,n}] + \mathcal{D}[L] \rho_{m,n} + \sqrt{m} \tilde{\zeta}(t) [\rho_{m-1,n}, L^{\dagger}] + \sqrt{n} \tilde{\zeta}^*(t) [L, \rho_{m,n-1}], \quad (3.69)$$

with the initial condition $\rho_{m,n}(0) = \rho_{\text{sys}}(0) \delta_{mn}$. The first term in the above equation gives the evolution of the system under the Hamiltonian H . The second term leads to dissipation due to the presence of the environment. These two terms are very similar to that of the master equation derived in the previous sections. The last two terms describe the coupling of the single photon to the system and contribute whenever $\tilde{\zeta}(t) \neq 0$ (i.e.) when the N -photon wave packet starts interacting with the system. As can be seen from the equation, these coupling terms however involve the reduced density matrix of lower-levels. Thus we have to solve a (thankfully finite) set of $(N+1)^2$ master equations, that couple downwards from $\rho_{N,N}$ to $\rho_{0,0}$. Using the fact that the total density matrix has to be Hermitian, which leads us to the conclusion $\rho_{n,m} = \rho_{m,n}^{\dagger}$, we can reduce the number of equations to be solved to $\frac{1}{2}(N+1)(N+2)$.

It is also interesting to look at the output field quantities - the mean photon flux and the integrated photon flux. Here too we get a system of coupled equations. The mean photon flux is given by

$$f_{\text{out}}(t) = E_{m,n}[L^{\dagger}L] + \sqrt{m} \tilde{\zeta}^*(t) E_{m-1,n}[L] + \sqrt{n} \tilde{\zeta}(t) E_{m,n-1}[L^{\dagger}] + \sqrt{mn} |\tilde{\zeta}(t)|^2, \quad (3.70)$$

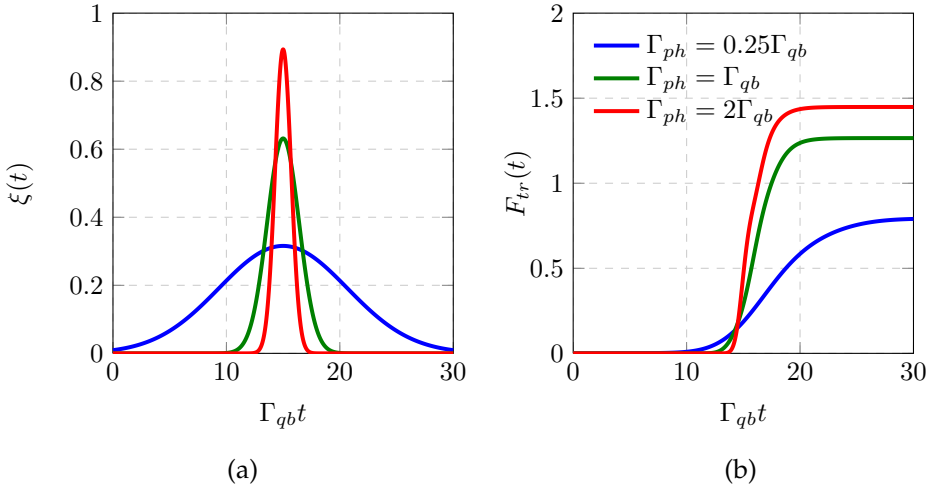


Figure 3.1: (a) Gaussian wave packets of different width given by Γ_{ph} . (b) Integrated photon flux (F_{tr}) in the transmitted field for these different wave packets.

where $E_{m,n}[O] \equiv \text{Tr}[\rho_{m,n}^\dagger O]$. The integrated flux output till time t is $F(t) = \int_0^t f_{\text{out}}(t') dt'$.

3.4.1 Example: Scattering of a two photon wave packet on a two level system

As an example, let us consider scattering a two photon state on a two level system coupled to an open transmission line. The Fock state is enclosed in a Gaussian wave packet given by

$$\xi(t) = \left(\frac{\Gamma_{ph}^2}{2\pi} \right)^{1/4} \exp \left(- \frac{\Gamma_{ph}^2 (t - T_{ph})^2}{4} \right), \quad (3.71)$$

where Γ_{ph} is the width of the wave packet and T_{ph} is the time of arrival of the peak of the wave packet at the two level system. The Fock state master equations in this case are

$$\begin{aligned} \dot{\rho}_{m,n} = & -i \left[-\frac{\Delta}{2} \sigma_z, \rho_{m,n} \right] + \Gamma_{qb} \mathcal{D}[\sigma_-] \rho_{m,n} \\ & + \sqrt{m} \sqrt{\frac{\Gamma_{qb}}{2}} \xi(t) [\rho_{m-1,n}, \sigma_+] + \sqrt{n} \sqrt{\frac{\Gamma_{qb}}{2}} \xi(t) [\sigma_-, \rho_{m,n-1}], \end{aligned} \quad (3.72)$$

where Δ is the energy difference between the ground and excited state of the qubit, Γ_{qb} is the coupling rate of the qubit to the transmission line. The indices $m, n \in \{0, 1, 2\}$. We numerically solve these coupled equations for three different widths of the wave packet and show the result in Fig. 3.1. The first panel shows the input photon wave packets with $T_{ph} = 15$. The second panel shows the integrated flux in the transmitted field. As can be seen from the figure, a wider pulse in time is mostly reflected by the qubit. As the wave packets become sharper in time, they become broader in frequency and are not close to resonance of the transition. Also as the pulse contains more than 1 photon, the qubit gets saturated quickly. So we see most of the field getting transmitted.

எப்பொருள் எத்தன்மைத் தாயினும் அப்பொருள்
மெய்ப்பொருள் காண்பது அறிவு.

திருக்குறள் - 355

(possibly written between 4th to 1st BCE [116])

*In everything of every kind whatsoever,
Wisdom perceives Truth in that thing.*

Thirukkural - 355

(English Translation - Himalayan Academy [117])

4

Measurement

In the previous chapter, we studied the evolution of a quantum system in the presence of an environment. In this regard, we started from a unitary evolution given by the quantum Liouville equation. A quantum system can also undergo a different kind of evolution - the one under measurement. Consider a quantum state $|\psi\rangle$, say that of a quantum harmonic oscillator. We would like to measure the number of excitations in the oscillator. As per the postulates of quantum mechanics, such an observable is represented by a Hermitian operator, say N , with eigenstates $|n\rangle$ which form a complete orthonormal basis in the system Hilbert space¹. In this basis, we can expand $|\psi\rangle$ to $\sum_n c_n |n\rangle$, where $c_n = \langle n|\psi\rangle$. As introduced in the elementary quantum mechanics courses, the effect of a measurement is to "collapse" the above state into an eigenstate of the corresponding measurement operator, N in our example. Suppose the measurement result is n , then the state after measurement is $|\psi'\rangle = |n\rangle = \frac{1}{c_n} |n\rangle \langle n|\psi\rangle$. Starting with a density matrix ρ , which can now also include mixed states, the state after the measurement is

$$\rho' = \frac{\Pi_n \rho \Pi_n}{\text{Tr}(\Pi_n \rho \Pi_n)}, \quad (4.1)$$

¹We assume a non-degenerate spectrum for simplicity.

where $\Pi_n = |n\rangle\langle n|$ is known as the projection operator. The above collapse model is known as the von Neumann projection postulate [104]. We note that the projectors obey $\Pi_{n'}^\dagger \Pi_n = \delta_{nn'} \Pi_n$ and $\sum_n \Pi_n^\dagger \Pi_n = \mathbb{1}$.

As introduced above, measurements cause instantaneous non-unitary evolution of the system. In experiments however, measurements take time during which the system can also evolve according to some unitary dynamics. In some cases, for example to do feedback, a continuous monitoring of the system is required. We would also like to have the back action of the measurement on the system as small as possible. All of this is possible by coupling a second quantum system, called probe to our original system of interest and then performing a measurement on the probe [118]. In circuit QED and other setups, the state of a qubit is read by scattering photons on the qubit and then measuring the photons, which act as the probe system. The aim of paper II is to build a photon detector, i.e to measure the state of the control field to see if it contains either 0 or 1 photon. To achieve this, we use a coherent field as a probe and measure the scattered field continuously using a homodyne detector. The interaction between the control and probe fields is mediated by a three-level atom. For this, we require a description of continuous measurement of probe quantum systems. We will look at this problem in this chapter.

Before starting with the full development of master equations under measurement, we will look at a simple example to explain a few salient points. Let us take a qubit in state $|\psi\rangle = \alpha|0\rangle + \beta|1\rangle$ as our system, with $|\alpha|^2 + |\beta|^2 = 1$. The simplest probe is another qubit which we initialize in the state $|0\rangle$. The system and probe now evolve by some unitary dynamics. We take as an example the unitary operator [119],

$$U_{CNOT}(\theta) = \exp(-i\theta U_{CNOT}) = \cos\theta \mathbb{1} - i \sin\theta U_{CNOT} \quad (4.2)$$

where $U_{CNOT} = |0\rangle\langle 0| \otimes \mathbb{1} + |1\rangle\langle 1| \otimes \sigma_x$. U_{CNOT} is the CNOT gate that flips the state of the probe qubit if the system qubit is in state $|1\rangle$. After the interaction, we have the total state of the system and probe as

$$|\psi\rangle_{\text{tot}} = \cos\theta (\alpha|00\rangle + \beta|10\rangle) - i \sin\theta (\alpha|00\rangle + \beta|11\rangle). \quad (4.3)$$

Having $\theta = \pi/2$, gives a fully entangled state (neglecting the global phase) $|\psi\rangle_{\text{tot}} = \alpha|00\rangle + \beta|11\rangle$. In such a case, measuring the probe (in the σ_z basis) as $|0\rangle$ or $|1\rangle$ fully projects the system to the corresponding state. Such a measurement is then termed as a "strong" measurement and we have full information about the state of the system after measurement. Instead let us suppose $\theta \ll 1$. Expanding

the state in Eq. (4.3) for small θ , we have

$$|\psi\rangle_{\text{tot}} \approx \frac{1}{\sqrt{1+\theta^2}} [\alpha(1-i\theta)|00\rangle + \beta|10\rangle - i\theta\beta|11\rangle]. \quad (4.4)$$

Measuring the probe in the σ_z basis now give the following outcomes. If we measure the probe to be in state $|0\rangle$, the system is in state

$$|\psi'\rangle_0 = \frac{\alpha(1-i\theta)|0\rangle + \beta|1\rangle}{\sqrt{|\alpha(1-i\theta)|^2 + |\beta|^2}}. \quad (4.5)$$

This measurement result occurs with probability $p_0 = (|\alpha(1-i\theta)|^2 + |\beta|^2)/(1+\theta^2)$ (close to 1). Instead if we measure the probe to be in state $|1\rangle$, the system is in state

$$|\psi'\rangle_1 = |1\rangle. \quad (4.6)$$

The above result occurs with probability $p_1 = |\beta|^2\theta^2/(1+\theta^2)$. Thus in this case we see that, while most of the time there is very little information gained about the system (i.e. when we measure the probe to be in state $|0\rangle$), every now and then there is a "jump" with a small probability during which the system collapses to state $|1\rangle$.

Instead if we choose to measure the probe in the σ_x basis, we get the following states for the system qubit

$$|\psi'\rangle_+ = \alpha|0\rangle + \beta|1\rangle \quad (4.7)$$

$$|\psi'\rangle_- = \alpha|0\rangle + \beta e^{2i\phi}|1\rangle, \quad \phi = \arctan(\theta) \quad (4.8)$$

for the measurement results $+/-$, which occur with equal probabilities. This measurement however does not give any information about the state of the system, but gives a phase kick to the system depending on the results. The above kind of measurements where the information gain about the system and corresponding backaction is small are known as weak measurements [119]. In the above examples, θ can be thought of as the parameter that quantifies the strength of the measurement. It could be a function of parameters such as the strength of the coupling between the system and the probe and the time period during which the system and the probe were coupled.

Moving from these examples, let us proceed to describe these indirect measurements in general, following references [104] and [120]. Consider that we would like to measure a quantum system in the state ρ_{sys} . We couple a probe in the

initial state $|\psi\rangle$ to the system and let them evolve under a unitary U for time t . The total state at time t is

$$\rho_{\text{tot}}(t) = U(t) (\rho_{\text{sys}}(0) \otimes |\psi\rangle \langle \psi|) U^\dagger(t), \quad (4.9)$$

where $\rho_{\text{sys}}(0)$ is the initial state of the system and we use the shorthand $U(t)$ for $U(t, 0)$. We then perform a projective measurement on the probe. Assume that we find that the probe is in state $|i\rangle$. The system is then in the state

$$\begin{aligned} \rho_{\text{sys},i}(t) &= \frac{1}{p_i} \langle i| U(t) (\rho_{\text{sys}}(0) \otimes |\psi\rangle_p \langle \psi|_p) U^\dagger(t) |i\rangle \\ &\equiv \frac{1}{p_i} \Omega_i(t) \rho_{\text{sys}}(0) \Omega_i^\dagger(t) \end{aligned} \quad (4.10)$$

where we have defined the measurement operators $\Omega_i(t) = \langle i| U(t) |\psi\rangle$ and the probabilities $p_i = \langle \Omega_i^\dagger(t) \Omega_i(t) \rangle = \text{Tr}[\Omega_i(t) \rho_{\text{sys}}(0) \Omega_i^\dagger(t)]$. As opposed to projection operators, we can see from the definition that $\Omega_i^\dagger \Omega_j \neq \delta_{ij} \Omega_i$. However, we still have $\sum_i \Omega_i^\dagger \Omega_i = \mathbb{1}$, which ensures that the probabilities sum to 1. If we ignore the measurement results, we get the unconditional system state [118]

$$\rho_{\text{sys}}^{uc} = \sum_i \Omega_i(t) \rho_{\text{sys}}(0) \Omega_i^\dagger(t) \quad (4.11)$$

which is usually a mixed state. This state would be the same as the one obeying the unconditional master equations similar to those described in the previous chapter. Thus, we have a connection between open quantum systems and measurement.

Our aim now is to get a differential equation for the state of the system while we continuously measure the probe. This can be derived using Eq. (4.10) for short time scales dt as

$$\rho_{\text{sys},i}(t + dt) = \frac{1}{p_i} \Omega_i(dt) \rho_{\text{sys}}(t) \Omega_i^\dagger(dt). \quad (4.12)$$

Due to the probabilistic nature of the measurement (and the corresponding back action), this differential equation will be stochastic in nature. As one can imagine, the equations also depend on the type of measurement that is performed. In the microwave domain, and thus also in the appended papers, the measurement of choice and necessity is the homodyne detection. A homodyne detector is usually modeled using two photodetectors as will be shown in the following section (Fig. 4.3). Thus, we will start with the problem of getting a stochastic master equation for a system under photodetection and then proceed to homodyne detection. In either of these cases we will only outline the derivation and refer the reader to other sources for detailed calculations.

4.1 Photon detection

Let us start with a physical model similar to those considered in the previous chapter - a qubit coupled to a bath of harmonic oscillators. We then follow references [104, 120] to derive a stochastic master equation. The Hamiltonian of the total system is

$$H = H_{\text{sys}} + H_{\text{bath}} + H_{\text{int}}, \quad (4.13)$$

where we have

$$H_{\text{sys}} = \frac{1}{2} \omega_{\text{qb}} \sigma_z, \quad (4.14)$$

$$H_{\text{bath}} = \sum_k \omega_k b_k^\dagger b_k, \quad (4.15)$$

$$H_{\text{int}} = \sum_k g_k (b_k + b_k^\dagger) \sigma_x + H_{\text{drive}}, \quad (4.16)$$

where g_k is the coupling strength of the qubit to the mode k . The Hamiltonian H_{drive} contains other qubit only terms such as a Rabi drive of the form $\Omega_R \sigma_x$. Going to the rotating frame with $R = \exp(i \sum_k \omega_k b_k^\dagger b_k t - \frac{1}{2} i \omega_{\text{qb}} \sigma_z t)$, we have the total Hamiltonian after neglecting the fast rotating terms (rotating wave approximation) as

$$\tilde{H} = \sigma_+ B(t) + \sigma_- B^\dagger(t) + \tilde{H}_{\text{drive}}, \quad (4.17)$$

where we have defined $B(t) = \sum_k g_k b_k e^{-i(\omega_k - \omega_{\text{qb}})t}$ for brevity. Considering small time step dt , the unitary operator to second order is

$$U(dt) \equiv U(t+dt, t) \approx 1 - i \int_t^{t+dt} dt_1 \tilde{H}(t_1) - \int_t^{t+dt} dt_1 \int_t^{t_1} dt_2 \tilde{H}(t_1) \tilde{H}(t_2). \quad (4.18)$$

Measuring the bath in the Fock basis gives the following measurement operators

$$\Omega_0(dt) = \langle 0 | U(t+dt, t) | 0 \rangle = 1 - i \tilde{H}_{\text{drive}} dt - g_0 \sigma_+ \sigma_- \quad (4.19)$$

$$\Omega_{1,k}(dt) = \langle 1_k | U(t+dt, t) | 0 \rangle = f_k \sigma_- \quad (4.20)$$

with the corresponding probabilities $p_i = \langle \Omega_i^\dagger \Omega_i \rangle$. The operator $\Omega_{1,k}$ corresponds to measuring a photon in mode k while Ω_0 corresponds to the measurement result of not detecting any photon in any of the modes k . The parameters f_k and g_0 are the integrals defined as

$$g_0 = \int_t^{t+dt} dt_1 \int_t^{t_1} dt_2 \sum_k g_k^2 e^{-i(\omega_k - \omega_{\text{qb}})(t_1 - t_2)}, \quad (4.21)$$

$$f_k = -i \int_t^{t+dt} dt_1 g_k e^{i(\omega_k - \omega_{\text{qb}})t_1}. \quad (4.22)$$

From $\rho_{1,k}(t+dt, t) = \Omega_{1,k}\rho(t)\Omega_{1,k}^\dagger / \langle \Omega_{1,k}\Omega_{1,k}^\dagger \rangle$, we see that the normalized conditioned state for photon detection doesn't depend on f_k . Thus we can treat detection in any mode k as equivalent for the dynamics of the system. A photon detection in any mode k happens with the probability, $p_1 = \sum_k \langle \Omega_{1,k}\Omega_{1,k}^\dagger \rangle = \sum_k |f_k|^2 \langle \sigma_+\sigma_- \rangle$. Furthermore, it can be shown that $\sum_k |f_k|^2 = \Gamma dt$ and $g_0 = \frac{1}{2}\Gamma dt$, where Γ is the decay rate of the qubit [104, 120]. Using all of these, the qubit states conditioned on the measurement results can be written as

$$\begin{aligned} \rho_0(t+dt) &= \frac{1}{p_0}\Omega_0\rho(t)\Omega_0^\dagger \\ &= \frac{1}{p_0}\left(\rho(t) - i[\tilde{H}_{\text{drive}}, \rho(t)]dt - \frac{1}{2}\Gamma\{\sigma_+\sigma_-, \rho(t)\}dt\right) \\ &= \rho(t) - i[\tilde{H}_{\text{drive}}, \rho(t)]dt - \frac{1}{2}\Gamma\{\sigma_+\sigma_-, \rho(t)\}dt + \Gamma\langle\sigma_+\sigma_-\rangle\rho(t)dt, \end{aligned} \quad (4.23)$$

$$\begin{aligned} \rho_1(t+dt) &= \frac{1}{p_1}\Omega_1\rho(t)\Omega_1^\dagger \\ &= \frac{\sigma_-\rho(t)\sigma_+}{\langle\sigma_+\sigma_-\rangle}, \end{aligned} \quad (4.24)$$

where we have only kept the terms to first order in dt . The above equations can be combined into a single master equation by defining a measurement record $N(t)$ that counts the number of photons detected over time. The corresponding increment $dN(t) = N(t+dt) - N(t)$ has the properties $dN^2(t) = dN(t)$ (i.e. we detect only 0 or 1 photons in the time interval dt) and $E[dN(t)] = \Gamma\langle\sigma_+\sigma_-\rangle dt$, where $E[\cdot]$ is the classical average. With this the evolution of the qubit can be written as

$$d\rho = -i[\tilde{H}_{\text{drive}}, \rho]dt - \frac{1}{2}\Gamma\{\sigma_+\sigma_-, \rho\}dt + \Gamma\langle\sigma_+\sigma_-\rangle\rho dt + \left(\frac{\sigma_-\rho\sigma_+}{\langle\sigma_+\sigma_-\rangle} - \rho\right)dN(t). \quad (4.25)$$

This is the stochastic master equation (SME) that we were after. The solution of the above equation is called a quantum trajectory, which gives the path taken by the system under measurement [118]. Averaging over several trajectories (ideally infinitely many) gives back the evolution described by the unconditional master equation similar to the ones discussed in the previous chapter. In deriving the above SME, we assumed that all the photons in the bath were detected. In case of

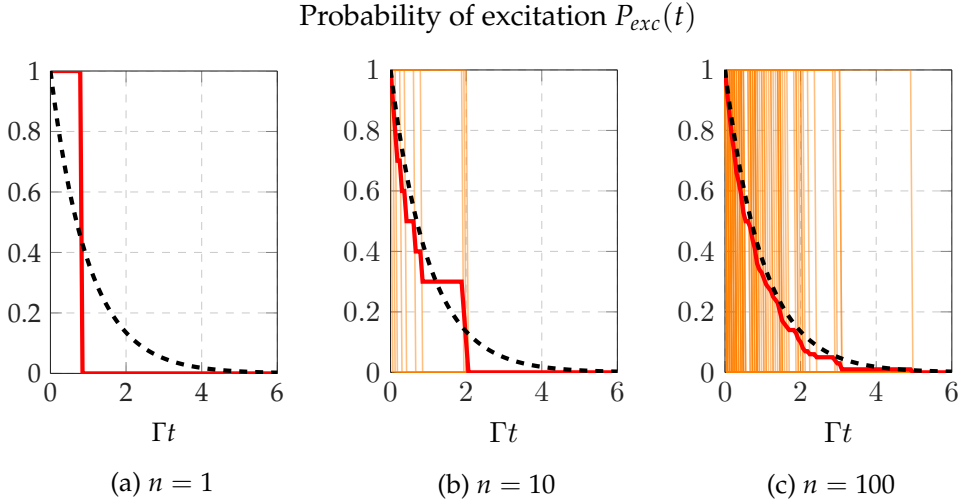


Figure 4.1: Probability of excitation P_{exc} of a qubit under direct photon detection as a function of time, for n trajectories. The qubit is initially in the excited state. The solid red lines are the averages over n trajectories $E_n[P_{exc}]$. The dashed lines correspond to the average evolution from the unconditional master equation. We see from the individual trajectories (orange traces) that the qubit stays in the excited state until a jump takes it to the ground state.

inefficient detection, the SME is modified to be [118]

$$\begin{aligned}
 d\rho = & -i[\tilde{H}_{\text{drive}}, \rho]dt - \frac{1}{2}\eta\Gamma\{\sigma_+\sigma_-, \rho\}dt + \eta\Gamma\langle\sigma_+\sigma_-\rangle\rho dt + (1-\eta)\Gamma\mathcal{D}[\sigma_-]\rho dt \\
 & + \left(\frac{\sigma_-\rho\sigma_+}{\langle\sigma_+\sigma_-\rangle} - \rho \right) dN(t)
 \end{aligned} \tag{4.26}$$

with $E[dN(t)] = \eta\Gamma\langle\sigma_+\sigma_-\rangle dt$ and $0 \leq \eta \leq 1$ is the detection efficiency. In figures 4.1 and 4.2, we show simulation results based on the above SME for a qubit initially in state $|1\rangle$ and state $\frac{1}{\sqrt{2}}(|0\rangle + |1\rangle)$. The simulations were performed using QuTip [121]. While the unconditional dynamics look similar in both the cases (exponential decay), we can see qualitative differences in the individual trajectories. In the case where we know that the atom is in the excited state with 100% probability, a change in the quantum state does not happen unless there is a photodetection. However, if we have a superposition of $|0\rangle$ and $|1\rangle$ and don't detect a photon for a long time, this would imply that the qubit was more likely to have been in the ground state. Thus, not detecting a photon is also a signal and the state of the qubit is updated based on this measurement result [122].

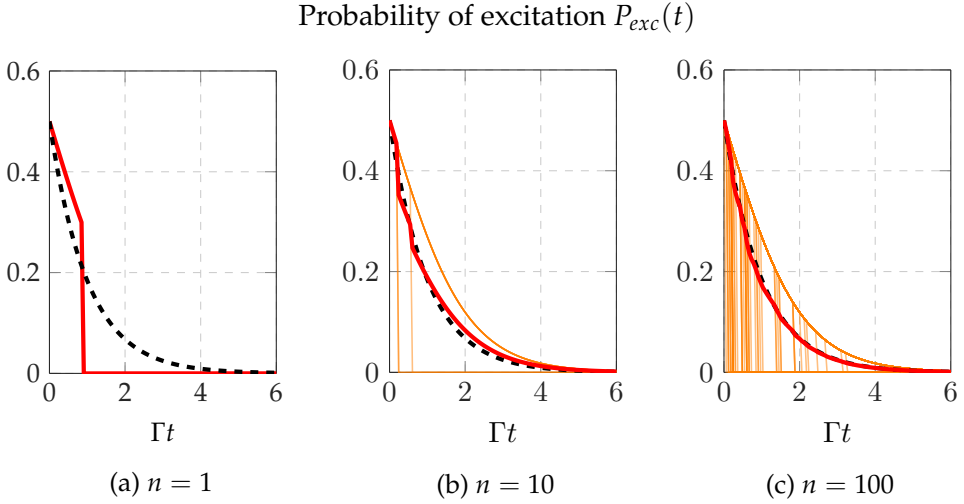


Figure 4.2: Probability of excitation P_{exc} of a qubit under direct photon detection as a function of time, for n trajectories.. The qubit is initially in an equal superposition of ground and excited state. The solid red lines are the averages over n trajectories $E_n[P_{exc}]$. The dashed lines are the average evolution from the unconditional master equation. We see from the individual trajectories (orange traces) that even in the absence of any jump the state of the qubit decays.

4.2 Homodyne detection

Now that we have looked at the evolution of a qubit under photon detection, let us move towards homodyne detection. A schematic setup for the same is shown in Fig. 4.3. In this setup, the output field from the system, a is mixed with a strong coherent field β (in mode b) from a local oscillator (LO) using a beam splitter. We will consider a 50:50 beam splitter (balanced homodyne detection) including a $\pi/2$ phase shift for the reflected field. The output fields from such a beam splitter is given by

$$\begin{pmatrix} c \\ d \end{pmatrix} = \frac{1}{\sqrt{2}} \begin{pmatrix} 1 & i \\ i & 1 \end{pmatrix} \begin{pmatrix} a \\ b \end{pmatrix}. \quad (4.27)$$

Detectors D_1 and D_2 , measure the photocurrent in the fields output from the beam splitter, c and d . The difference in the measured photocurrents gives the homodyne current $j(t)$.

As in the previous section, we start with the Hamiltonian in the rotating frame

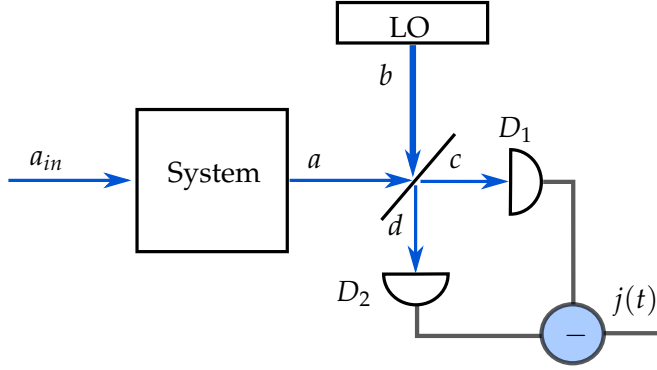


Figure 4.3: A schematic setup of homodyne detection. We are interested in measuring the output from the system, a . This field is mixed with a very (ideally infinitely) strong coherent field β from the local oscillator at a beam splitter. The output fields from the beam splitter are measured by the photodetectors D_1 and D_2 . The difference in the measured photocurrents gives the homodyne current $j(t)$.

that now includes the local oscillator field as

$$\tilde{H} = \sigma_- A^\dagger(t) + \sigma_+ A(t) + \beta B^\dagger(t) + \beta^* B(t) + \tilde{H}_{\text{drive}}, \quad (4.28)$$

where we have defined $A(t) = \sum_k g_k a_k e^{-i(\omega_k - \omega_{\text{qb}})t}$ and $B(t) = \sum_k g_k b_k e^{-i(\omega_k - \omega_{\text{qb}})t}$ similar to previous section. From the second order perturbation theory, we can write the unitary operator $U(t + dt, t)$ also as before.

The detectors D_1 and D_2 lead to three measurement outcomes - no photon detected (corresponding to Ω_0) and a single photon detected in either of the detector (corresponding to $\Omega_{1,c/d}$). The detectors measure modes c and d which are linear combinations of the modes a and b according to the beam splitter equation above. Defining two measurement records $N_{1/2}(t)$ for the two detectors along with their corresponding increments, one can arrive at an SME for the evolution of the qubit state. Taking the limit $|\beta| \rightarrow \infty$, the SME for homodyne detection can be shown to be of the form [118, 120]

$$d\rho = -i[\tilde{H}_{\text{drive}}, \rho]dt + \Gamma \mathcal{D}[\sigma_-] \rho dt + \sqrt{\eta \Gamma} \mathcal{M}[\sigma_-] \rho dW(t), \quad (4.29)$$

where $dW(t)$ is a Wiener increment with $E[dW(t)] = 0$ and $E[dW(t)^2] = dt$. The measurement super-operator $\mathcal{M}[c] \rho \equiv (e^{i\phi} c \rho + e^{-i\phi} \rho c^\dagger) - \langle e^{i\phi} c + e^{-i\phi} c^\dagger \rangle \rho$ and $0 \leq \eta \leq 1$ is the measurement efficiency. In this limit, the homodyne current becomes

$$j(t)dt = \sqrt{\eta \Gamma} \langle \sigma_- e^{-i\phi} + \sigma_+ e^{i\phi} \rangle dt + dW(t). \quad (4.30)$$

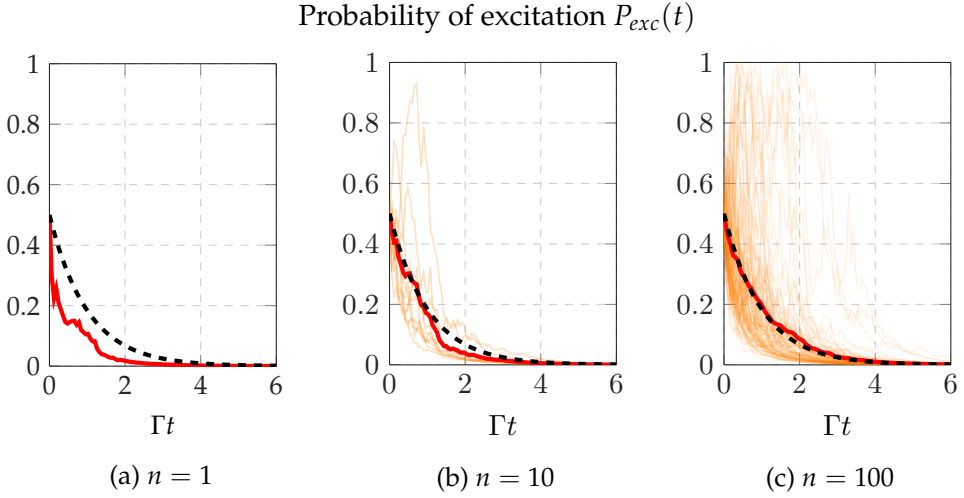


Figure 4.4: Probability of excitation P_{exc} of a qubit under homodyne detection as a function of time, for n trajectories. The qubit is initially in an equal superposition of ground and excited state. The solid red lines are the averages over n trajectories $E_n[P_{exc}]$. The dashed lines are the average evolution from the unconditional master equation. Individual trajectories are in orange.

The phase angle ϕ defines the quadrature of measurement. In particular, for the above case, $\phi = 0$ (usually called the in-phase component) gives information about σ_x and $\phi = \pi/2$ (known as the quadrature) is proportional to σ_y of the qubit. From the above properties of the Wiener increment we see that taking the classical expectation value of the whole equation just gives us back the master equation as expected.

To compare with the results from direct photon detection, we show the trajectories from homodyne detection in figures 4.4 and 4.5. The simulations were performed using QuTip [121]. We take the qubit to be initially in an equal superposition of $|0\rangle$ and $|1\rangle$. There is no external driving of the qubit and we will also assume no pure dephasing. As compared to direct photon detection, we see no jumps in the evolution and the state of the system follows a diffusive trajectory [123]. We could also see what the measurement record itself would look like by plotting the homodyne current. The results are shown for in-phase measurement ($\phi = 0$). So, we are just measuring the projection on the x-axis of the Bloch sphere as $j(t)dt = \sqrt{\Gamma} \langle \sigma_- + \sigma_+ \rangle dt + dW(t)$. As we can see from the figure, while the individual measurements just look like noise, a clear pattern emerges after averaging over several runs.

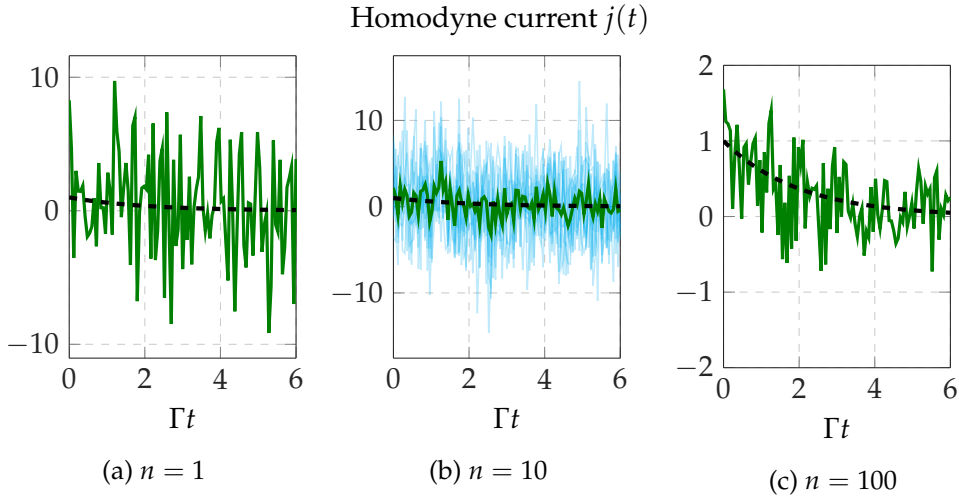


Figure 4.5: Homodyne current j for n trajectories as a function of time. The qubit is initially in an equal superposition of ground and excited state. The solid green lines are the averages over n trajectories $E_n[j]$. The dashed lines are the average evolution from the unconditional master equation. Individual trajectories are in cyan, which we don't show in (c) for clarity. We have taken $\phi = 0$, which corresponds to measuring σ_x in this case.

In the absence of a photon detector at microwave frequencies, homodyne detectors have been the go-to measurement setup for superconducting circuits. The setup however is different from the above (due to the absence of photo-detectors) which is just a theoretical model. In circuit QED experiments, the signal to be measured is mixed with a local oscillator signal and amplified using linear amplifiers. These amplified signals are then down-converted to a DC signal and measured as a voltage [124, 125]. Such detectors have been used in the experiments of papers I, III and VI. In paper II, we use homodyne detectors as part of the proposal to do single photon detection at microwave frequencies. Stochastic master equations such as the above one play an important role in the analysis of the proposed setup.

4.3 Quantum Nondemolition (QND) measurements

Quantum measurements as introduced in the first quantum mechanics courses and textbooks are not only ideal projective measurements, they are also ideal QND measurements. Take the typical example of a Stern-Gerlach measurement.

A stream of spin- $\frac{1}{2}$ particles is measured in one of the Pauli basis, say σ_z . The measurement projects the spin into the state $|\uparrow\rangle$ or $|\downarrow\rangle$. If we then have a second measurement device also measuring the projection along the z-axis, the measurement result is expected to be exactly same as the previous result (100% correlated). This is possible under the following considerations. The first is that the measurable does not change in between the two measurements. In other words, the observable (say A) being measured is a constant of motion under free evolution i.e. $[H_{\text{sys}}, A] = 0$. The second assumption is that the interaction between the system and the measurement apparatus does not modify the observable. If we once again consider that the measurement is done using a probe system, this assumption implies that the interaction Hamiltonian between the probe and system commutes with the observable i.e. $[H_{\text{int}}, A] = 0$. The above condition that the observable commutes with the total Hamiltonian is sufficient but not necessary. A more general condition that is necessary and sufficient is to demand $[A, U(t, 0)]|\psi\rangle = 0$, where the unitary operator $U(t, 0)$ gives the total evolution of the system and the probe which is in the initial state $|\psi\rangle$ [104].

Let us look at a typical system in quantum optics - a two level atom coupled to a single mode cavity. The dynamics of such a system after the rotating wave approximation (RWA) is given by the Jaynes-Cummings Hamiltonian [126]

$$H = \frac{1}{2}\omega_{\text{qb}}\sigma_z + \omega_{\text{cav}}\left(a^\dagger a + \frac{1}{2}\right) + g(a\sigma_+ + a^\dagger\sigma_-) \quad (4.31)$$

where $\omega_{\text{qb}/\text{cav}}$ is the frequency of the qubit/cavity and g is the coupling strength between them. As we can see $[H, \sigma_z] \neq 0$ due to the form of the interaction Hamiltonian. Thus if we perform a measurement in the σ_z eigenbasis of the qubit (to determine the excitation probability), a second measurement might not give the same result. To use such a setup for qubit readouts, we have to choose the parameter regime where the energy exchange between the qubit and the cavity is suppressed. This is the dispersive limit with $|\Delta| = |\omega_{\text{qb}} - \omega_{\text{cav}}| \gg g$. Choosing this parameter regime and applying the unitary transformation

$$U = \exp\left[\frac{g}{\Delta}\left(a\sigma_+ - a^\dagger\sigma_-\right)\right] \quad (4.32)$$

we end up with the dispersive Hamiltonian

$$H_{\text{disp}} \approx \frac{1}{2}(\omega_{\text{qb}} + \chi)\sigma_z + \omega_{\text{cav}}a^\dagger a + \chi\sigma_z a^\dagger a \quad (4.33)$$

where $\chi = g^2/\Delta$ and we have kept terms only up to second order in g/Δ . Now we see that $[H_{\text{disp}}, \sigma_z] = 0$ and we can have a QND measurement of the qubit

population. The above Hamiltonian can be rewritten as $\frac{1}{2}(\omega_{\text{qb}} + \chi)\sigma_z + (\omega_{\text{cav}} + \chi\sigma_z)a^\dagger a$, where the cavity frequency now depends on σ_z of the qubit. If we are in the strong dispersive regime with $\chi > \kappa$, the bandwidth of the cavity, we can measure this change in frequency from a reflection measurement.

It has to be noted however that there is still a "collapse" of the wavefunction even in a QND measurement. In the words of Braginsky and Khalili [49],

The origin of the term "quantum nondemolition" translates from the intention to emphasize the following basic property: if, before a measurement, an object is not in one of the eigenstates of the measured value, the QND measurement destroys this state but does not demolish it. For example, if an oscillator is initially in the coherent quantum state, the QND measurement of energy will destroy this state and create N-state, although this measurement does not include demolition, as in classical photodetectors.

For instance in the above example, if the qubit is not in the eigenstate of σ_z , the above dispersive measurement will project it to either state $|0\rangle$ or $|1\rangle$. The QND nature of the measurement then guarantees that we get the same result on repeating the measurement. This can also be used for instance to reset the qubit to the ground state before starting an experiment as it might be excited due to thermal fluctuations.

As mentioned in the above quote, usual photon detectors such as photomultiplier tubes are destructive in nature. They absorb the photon and generate an electrical signal which is measured. To have a non-destructive or QND photon detection, we require the interaction Hamiltonian to commute with the number operator. One such Hamiltonian is the Kerr Hamiltonian written as $H_{\text{int}} = gn_c n_p$, where $n_{c/p}$ is the number operator for control/probe fields. Measuring the change in the probe field due to the presence/absence of a photon in the control field leads to a photon detector. In paper I, we look at a system where such a kind of interaction is effectively mediated. Using this effect, we propose in paper II, a setup to nondestructively detect microwave photons.

I have yet to see any problem, however complicated, which, when you looked at it the right way, did not become still more complicated.

Attributed to Poul Anderson

5

Connecting quantum systems

Over the past decade the coherence times of superconducting qubits have been exponentially increasing [7], mimicking the well known Moore's law. The "long" coherence times that is shown by current transmon qubits has placed them as a qubit of choice for building scalable quantum computers [8]. Many groups around the world are actively pushing towards setups with several transmon type qubits (for example see [127–131]). This implies that we need to develop tools and formalisms to describe such complex quantum systems. Apart from applications in quantum computation, such formalisms would also be useful in other quantum devices where we have more than one quantum subsystem.

Let us start by looking at a typical example where the output of one quantum system becomes the input of the next system. Such a setup, known as a cascaded quantum system, was first looked at in references [132, 133]. While the master equation is derived starting from a Hamiltonian in [132], we will here briefly review the approach taken in [105]. We look at an example setup shown in Fig. 5.1, where we have two qubits connected to an unidirectional field. This can be implemented in circuit QED by placing a transmon at the end of a transmission line and by using circulators. As shown in the figure, the output field from qubit 1 drives the qubit 2 after a time τ .

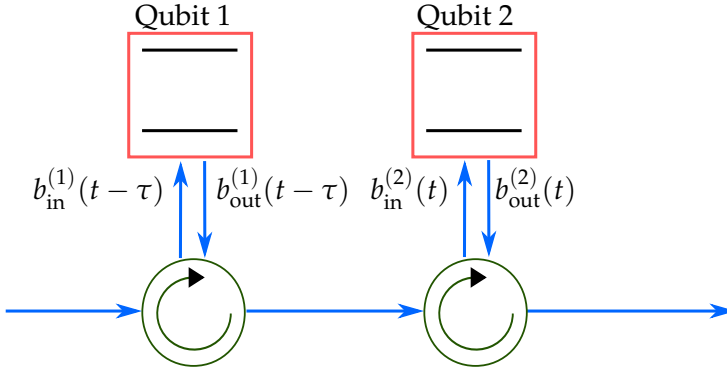


Figure 5.1: A schematic setup of two qubits cascaded.

Writing out the input-output relation (Eq. (3.49)) for the qubits, we have

$$b_{\text{out}}^{(1)}(t) = b_{\text{in}}^{(1)}(t) + L^{(1)}(t) \quad (5.1)$$

$$b_{\text{out}}^{(2)}(t) = b_{\text{in}}^{(2)}(t) + L^{(2)}(t) = b_{\text{in}}^{(1)}(t - \tau) + L^{(1)}(t - \tau) + L^{(2)}(t) \quad (5.2)$$

where we have defined $L^{(1/2)} = \sqrt{\Gamma_{1/2}}\sigma_-^{(1/2)}$. Considering two system operators X_1 and X_2 belonging to qubits 1 and 2 respectively, we can write the quantum Langevin equations (Eq. (3.45))

$$\begin{aligned} \dot{X}_i(t) = & i[H_{\text{sys}}^{(i)}, X_i(t)] - \left(\sqrt{\Gamma_i} b_{\text{in}}^{(i)\dagger}(t) + \frac{\Gamma_i}{2} \sigma_+^{(i)}(t) \right) [\sigma_-^{(i)}(t), X_i(t)] \\ & + \left(\sqrt{\Gamma_i} b_{\text{in}}^{(i)}(t) + \frac{\Gamma_i}{2} \sigma_-^{(i)}(t) \right) [\sigma_+^{(i)}(t), X_i(t)], \end{aligned} \quad (5.3)$$

for $i = 1, 2$. Now considering an operator X belonging to either of the two qubits, we can combine the two equations above as

$$\begin{aligned} \dot{X}(t) = & i[H_{\text{sys}}, X(t)] - \left(\sqrt{\Gamma_1} b_{\text{in}}^\dagger(t) + \frac{\Gamma_1}{2} \sigma_+^{(1)}(t) \right) [\sigma_-^{(1)}(t), X(t)] \\ & + \left(\sqrt{\Gamma_1} b_{\text{in}}(t) + \frac{\Gamma_1}{2} \sigma_-^{(1)}(t) \right) [\sigma_+^{(1)}(t), X(t)] \\ & - \left(\sqrt{\Gamma_2} b_{\text{in}}^\dagger(t - \tau) + \sqrt{\Gamma_1 \Gamma_2} \sigma_+^{(1)}(t - \tau) + \frac{\Gamma_2}{2} \sigma_+^{(2)}(t) \right) [\sigma_-^{(2)}(t), X(t)] \\ & + \left(\sqrt{\Gamma_2} b_{\text{in}}(t - \tau) + \sqrt{\Gamma_1 \Gamma_2} \sigma_-^{(1)}(t - \tau) + \frac{\Gamma_2}{2} \sigma_-^{(2)}(t) \right) [\sigma_+^{(2)}(t), X(t)], \end{aligned} \quad (5.4)$$

where $H_{\text{sys}} = H_{\text{sys}}^{(1)} + H_{\text{sys}}^{(2)}$. To get to the above result, we have used $b_{\text{in}}^{(2)}(t) = b_{\text{in}}^{(1)}(t - \tau) + L^{(1)}(t - \tau)$ and have replaced $b_{\text{in}}^{(1)}$ with just b_{in} . The above equation

contains operators at two times t and $t - \tau$ which makes it difficult to solve. In the case of unidirectional flow, such as the example we are considering here, we can redefine the operators of the second system to take care of this time difference [105]. In this chapter, we will however make an approximation and take $\tau \rightarrow 0$ even in the case of bidirectional flow including the case of feedback. This means we assume the propagation time between the different subsystems is negligible compared to the evolution of the subsystems. This approximation is also related to the fact that we have made the weak coupling approximation while deriving the Langevin equations and the input-output equations[134]. With this approximation, we have

$$\begin{aligned} \dot{X}(t) = & i[H_{\text{sys}}, X(t)] - \left(\sqrt{\Gamma_1} b_{\text{in}}^\dagger(t) + \frac{\Gamma_1}{2} \sigma_+^{(1)}(t) \right) [\sigma_-^{(1)}(t), X(t)] \\ & + \left(\sqrt{\Gamma_1} b_{\text{in}}(t) + \frac{\Gamma_1}{2} \sigma_-^{(1)}(t) \right) [\sigma_+^{(1)}(t), X(t)] \\ & - \left(\sqrt{\Gamma_2} b_{\text{in}}^\dagger(t) + \sqrt{\Gamma_1 \Gamma_2} \sigma_+^{(1)}(t) + \frac{\Gamma_2}{2} \sigma_+^{(2)}(t) \right) [\sigma_-^{(2)}(t), X(t)] \\ & + \left(\sqrt{\Gamma_2} b_{\text{in}}(t) + \sqrt{\Gamma_1 \Gamma_2} \sigma_-^{(1)}(t) + \frac{\Gamma_2}{2} \sigma_-^{(2)}(t) \right) [\sigma_+^{(2)}(t), X(t)]. \end{aligned} \quad (5.5)$$

The output from the total system in this approximation is then $b_{\text{out}}(t) = b_{\text{in}}(t) + L^{(1)}(t) + L^{(2)}(t)$, which implies that the effective coupling of the system is $L^{(1)} + L^{(2)}$. Rewriting the above equation as,

$$\begin{aligned} \dot{X}(t) = & i[H_{\text{sys}} + \frac{i}{2} (L^{(1)\dagger} L^{(2)} - L^{(2)\dagger} L^{(1)})], X(t) \\ & - \left(b_{\text{in}}^\dagger(t) + \frac{1}{2} (L^{(1)\dagger} + L^{(2)\dagger}) \right) [L^{(1)} + L^{(2)}, X(t)] \\ & + \left(b_{\text{in}}(t) + \frac{1}{2} (L^{(1)} + L^{(2)}) \right) [L^{(1)\dagger} + L^{(2)\dagger}, X(t)] \end{aligned} \quad (5.6)$$

and comparing with the quantum Langevin equation for a single system (Eq. (3.45)), we can see that the total system acts with an effective Hamiltonian and coupling operator given as

$$H_{\text{eff}} = H_{\text{sys}}^{(1)} + H_{\text{sys}}^{(2)} + \frac{i}{2} (L^{(1)\dagger} L^{(2)} - L^{(2)\dagger} L^{(1)}) \quad (5.7)$$

$$L_{\text{eff}} = L^{(1)} + L^{(2)}. \quad (5.8)$$

By using the fact that $\text{Tr}[\dot{X}\rho] = \text{Tr}[X\dot{\rho}]$, one can write down the master equation for the total system of two qubits. Considering that the bath is in vacuum the

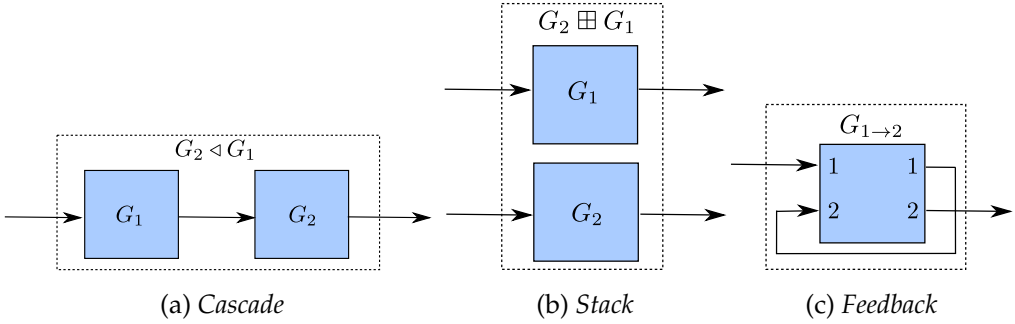


Figure 5.2: Connecting quantum systems - The series product, the concatenation product and the feedback.

master equation can be shown to be [132]

$$\dot{\rho} = -i[H_{\text{sys}}, \rho] + \mathcal{D} [L^{(1)}] \rho + \mathcal{D} [L^{(2)}] \rho - [L^{(2)\dagger}, L^{(1)}\rho] - [\rho L^{(1)\dagger}, L^{(2)}] \quad (5.9)$$

which is the same as

$$\dot{\rho} = -i[H_{\text{eff}}, \rho] + \mathcal{D} [L_{\text{eff}}] \rho. \quad (5.10)$$

While it is possible to extend the above method, one can imagine that it becomes tedious if we have a complex network with many subsystems and several connections. A modular approach that makes the derivation of the master equations easier has been proposed in [135, 136] and is known as the (S, L, H) formalism. We will look at an introduction to this formalism and apply it to a few systems of interest in this chapter. For more details, we refer to a recent review [134] that provides a good pedagogical overview and discusses the history and applications of the formalism.

5.1 (S, L, H) formalism

In this formalism, each subsystem is described by a triplet $G \equiv (S, L, H)$, where S is the scattering matrix, L is the vector of coupling operators of the subsystem and H is the Hamiltonian of the subsystem. Some examples of the (S, L, H) triplets are given in table 5.1. Once the triplets are identified for each of the subsystem, the total triplet for the composite system can be written using the following products (also see Fig. 5.2). The series product \triangleleft of the triplets describes feeding the output

<i>System</i>	(S, L, H) triplet
50:50 beam splitter	$G_{BS} = \left(\frac{1}{\sqrt{2}} \begin{bmatrix} 1 & i \\ i & 1 \end{bmatrix}, \begin{bmatrix} 0 \\ 0 \end{bmatrix}, 0 \right)$
Phase shifter	$G_{\phi} = (e^{i\phi}, 0, 0)$
Qubit with one input and output port (Atom in front of a mirror)	$G_{qb} = \left(\mathbb{1}, \sqrt{\Gamma} \sigma_-, -\frac{1}{2} \omega_{qb} \sigma_z \right)$
Qubit connected to an open transmission line	$G_{qb} = \left(\mathbb{1}, \begin{bmatrix} \sqrt{\Gamma/2} \sigma_- \\ \sqrt{\Gamma/2} \sigma_- \end{bmatrix}, -\frac{1}{2} \omega_{qb} \sigma_z \right)$

Table 5.1: Examples of some (S, L, H) triplets.

from one subsystem into another

$$G_2 \triangleleft G_1 = \left(S_2 S_1, S_2 L_1 + L_2, H_1 + H_2 + \frac{1}{2i} (L_2^\dagger S_2 L_1 - L_1^\dagger S_2^\dagger L_2) \right). \quad (5.11)$$

The concatenation product \boxplus is used for composing subsystems into a system with stacked channels

$$G_2 \boxplus G_1 = \left(\begin{bmatrix} S_2 & 0 \\ 0 & S_1 \end{bmatrix}, \begin{bmatrix} L_2 \\ L_1 \end{bmatrix}, H_2 + H_1 \right). \quad (5.12)$$

Lastly, we have feedback, written as $[(S, L, H)]_{k \rightarrow l} = (\tilde{S}, \tilde{L}, \tilde{H})$, where the output from the k^{th} port of the system is fed back as the input through the l^{th} port of the same system. The triplet is given by [137]

$$\tilde{S} = S_{\setminus [k]} + \begin{pmatrix} S_{1,l} \\ \vdots \\ S_{k-1,l} \\ S_{k+1,l} \\ \vdots \\ S_{n,l} \end{pmatrix} (1 - S_{k,l})^{-1} (S_{k,1} \dots S_{k,l-1} S_{k,l+1} \dots S_{k,n}),$$

$$\begin{aligned}\tilde{L} &= L_{[\not{k}]} + \begin{pmatrix} S_{1,l} \\ \vdots \\ S_{k-1,l} \\ S_{k+1,l} \\ \vdots \\ S_{n,l} \end{pmatrix} (1 - S_{k,l})^{-1} L_k, \\ \tilde{H} &= H + \frac{1}{2i} \left(\left(\sum_{j=1}^n L_j^\dagger S_{j,l} \right) (1 - S_{k,l})^{-1} L_k - \text{h.c.} \right),\end{aligned}\quad (5.13)$$

where $S_{[\not{k}]}$ and $L_{[\not{k}]}$ are the original scattering matrix and coupling vector with row k and column l removed.

Using the above defined products, we can write down the (S, L, H) triplet for the whole system

$$G_{\text{tot}} = \left(S_{\text{tot}}, \begin{bmatrix} L_1 \\ \vdots \\ L_n \end{bmatrix}, H_{\text{tot}} \right), \quad (5.14)$$

from which we can extract the corresponding master equation as

$$\dot{\rho} = -i [H_{\text{tot}}, \rho] + \sum_{i=1}^n \mathcal{D}[L_i] \rho, \quad (5.15)$$

where the dissipation super-operator is given by $\mathcal{D}[c] \rho = c \rho c^\dagger - \frac{1}{2} c^\dagger c \rho - \frac{1}{2} \rho c^\dagger c$ as in previous chapters. The output from the i^{th} channel is just given by L_i . At this point, we once again note that the above rules work in the Markov limit and assume that the propagation time between the different subsystems is negligible [134]. Systems that involve appreciable time delays between subsystems and in the feedback loop are considered using other approaches, for example [138, 139].

5.2 Cascaded quantum systems

As a first example, let us relook at the cascaded setup in Fig. 5.1. We will derive the master equation now via the (S, L, H) formalism considering no input fields. The total (S, L, H) triplet in this case, assuming that no phase is gained by the

field in between the two qubits, is

$$\begin{aligned} G_{\text{tot}}^{\text{qb}} &= G_{\text{qb}}^{(2)} \triangleleft G_{\text{qb}}^{(1)} \\ &= \left(\mathbb{1}, L^{(1)} + L^{(2)}, H_{\text{tot}} \right) \end{aligned} \quad (5.16)$$

where the total Hamiltonian is

$$H_{\text{tot}}^{\text{qb}} = H_{\text{qb}}^{(1)} + H_{\text{qb}}^{(2)} + \frac{1}{2i} \left(L^{(2)\dagger} L^{(1)} - L^{(1)\dagger} L^{(2)} \right) \quad (5.17)$$

with $H_{\text{qb}}^{(i)} = -\frac{1}{2}\omega_{\text{qb}}\sigma_z^{(i)}$ and the Lindblad operator $L^{(i)} = \sqrt{\Gamma_i}\sigma_-^{(i)}$. The master equation from G_{tot} is

$$\dot{\rho} = -i[H_{\text{tot}}^{\text{qb}}, \rho] + \mathcal{D} \left[L^{(1)} + L^{(2)} \right] \rho, \quad (5.18)$$

which can be rewritten as

$$\dot{\rho} = -i[H_{\text{qb}}^{(1)} + H_{\text{qb}}^{(2)}, \rho] + \mathcal{D} \left[L^{(1)} \right] \rho + \mathcal{D} \left[L^{(2)} \right] \rho - \mathcal{C} \left[L^{(1)}, L^{(2)} \right] \rho, \quad (5.19)$$

where we have defined a coupling super-operator

$$\mathcal{C} [c_1, c_2] \rho \equiv \left[c_2^\dagger, c_1 \rho \right] + \left[\rho c_1^\dagger, c_2 \right]. \quad (5.20)$$

The above equations are the same as in Eq. (5.9). Now we will extend the system to the case where the chain of qubits is driven by a cavity output from the left. The (S, L, H) triple for a tunable cavity is given as

$$G_{\text{cav}} = \left(\mathbb{1}, L_{\text{cav}} = \sqrt{\kappa(t)}a, H_{\text{cav}} = \omega_{\text{cav}}a^\dagger a \right). \quad (5.21)$$

The total (S, L, H) is now

$$\begin{aligned} G_{\text{tot}} &= G_{\text{qb}}^{(2)} \triangleleft G_{\text{qb}}^{(1)} \triangleleft G_{\text{cav}} \\ &= \left(\mathbb{1}, L_{\text{cav}} + L^{(1)} + L^{(2)}, H_{\text{tot}} \right), \end{aligned} \quad (5.22)$$

where the total Hamiltonian

$$\begin{aligned} H_{\text{tot}} &= H_{\text{cav}} + H_{\text{qb}}^{(1)} + H_{\text{qb}}^{(2)} + \frac{1}{2i} \left(L^{(2)\dagger} L^{(1)} - L^{(1)\dagger} L^{(2)} \right) \\ &\quad + \frac{1}{2i} \left(L_{\text{cav}} (L^{(1)\dagger} + L^{(2)\dagger}) - (L^{(1)} + L^{(2)}) L_{\text{cav}}^\dagger \right). \end{aligned} \quad (5.23)$$

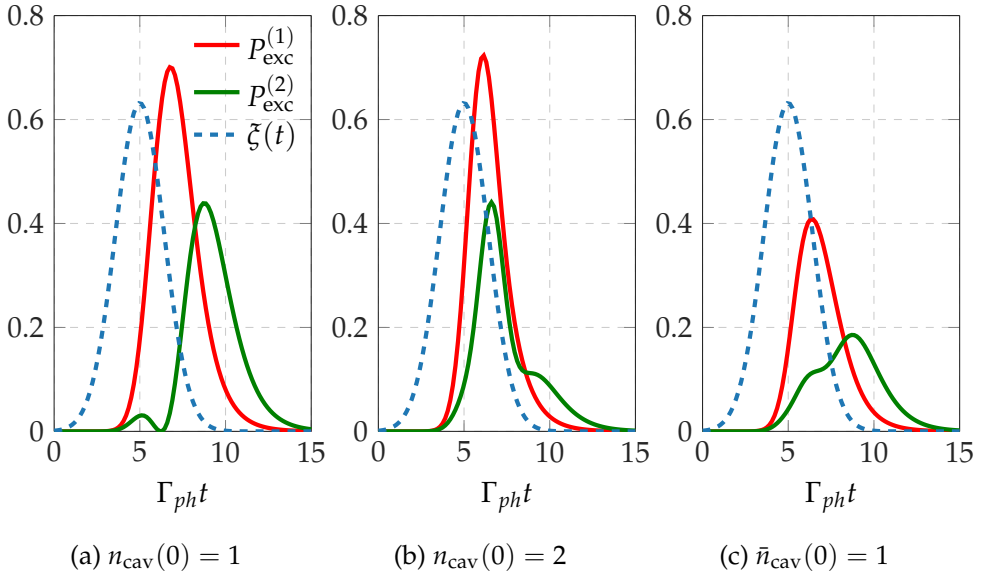


Figure 5.3: Probability of excitation of two cascaded qubits driven by a cavity output. The initial cavity state contains (a) 1 photon, (b) 2 photons and (c) a coherent state with an average of 1 photon. The coupling rates are such that $\Gamma_1 = \Gamma_{ph}$ and $\Gamma_2 = 2\Gamma_1$. Both the qubits are on resonance with the incoming field. The photon shape $\zeta(t)$ is plotted for reference.

Writing the master equation from the above (S, L, H) triple and expanding the dissipator terms, we end up with

$$\begin{aligned} \dot{\rho} = & -i[H_{\text{eff}}, \rho] + \mathcal{D}[L_{\text{cav}}]\rho + \mathcal{D}[L^{(1)}]\rho + \mathcal{D}[L^{(2)}]\rho \\ & - \mathcal{C}[L^{(1)}, L^{(2)}]\rho - \mathcal{C}[L_{\text{cav}}, L^{(1)} + L^{(2)}]\rho, \end{aligned} \quad (5.24)$$

where $H_{\text{eff}} = H_{\text{cav}} + H_{\text{tr}}^{(1)} + H_{\text{tr}}^{(2)}$.

We will consider the cases where we start the cavity in a Fock state with one or two photons and a coherent state. We tune the coupling of the cavity such that the output photon is in a Gaussian wave packet (Eq. (3.71)) [114]. We numerically solve the master equation and show the results in Fig. 5.3. The first two panels (a) and (b) show the probability of excitation of the two qubits when we start with $n_{\text{cav}} = 1$ and $n_{\text{cav}} = 2$ Fock states in the cavity. For the $n_{\text{cav}} = 1$ case, we see that the second qubit gets excited appreciably by the field that is coming from the relaxation of the first qubit as expected. In contrast, for the $n_{\text{cav}} = 2$ case, both the

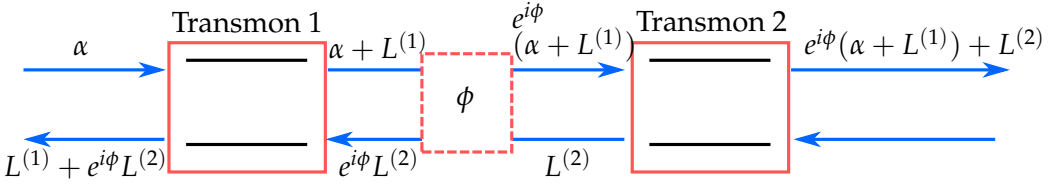


Figure 5.4: A schematic setup of two transmon qubits separated by a distance. We send in a coherent signal of amplitude α from the left and look at the transmitted and reflected part.

qubits get excited almost simultaneously. This can be attributed to the saturation of the first qubit and so the rest of the field is transmitted to the second qubit which then gets excited. In the third panel (c), we see the excitation of the qubits when the cavity is loaded with a coherent field with average number of photons $\bar{n}_{\text{cav}} = 1$. As the coherent state has a Poisson distribution of photon numbers, we see that the second qubit gets excited appreciably at the same time as the first qubit, compared to the case with only a single photon in the cavity.

5.3 Coupled quantum systems

Now, let us look at the scenario where we have two transmons coupled to an open transmission line. We consider only the two lowest levels of the transmons i.e. essentially qubits. The distance between the two transmons is modeled as a phase gained by the field. However as mentioned before, we have assumed that the traveling time of the field between the two qubits is negligible, i.e. it is much smaller than the time of evolution of the system. The setup is driven from the left by a coherent field of strength α . A schematic setup is shown in the Fig. 5.4.

As each transmon can both reflect and transmit the incoming fields, it is convenient to write the right going and left going parts of the equations separately and then stack them using the concatenation product. In this case, the (S, L, H) triplets of the individual transmons can be written as,

$$G_{\text{tr}}^{(i)} = G_{\text{Ltr}}^{(i)} \boxplus G_{\text{Rtr}}^{(i)} \quad (5.25)$$

where

$$\begin{aligned} G_{\text{Rtr}}^{(i)} &= \left(1, L^{(i)}, H_{\text{tr}}^{(i)} \right), \\ G_{\text{Ltr}}^{(i)} &= \left(1, L^{(i)}, 0 \right), \end{aligned} \quad (5.26)$$

with $L^{(i)} = \sqrt{\Gamma_i/2} \sigma_-^{(i)}$ as before. The Hamiltonian of the individual transmons in the frame rotating with the frequency of the incoming drive ω_d is given by $H_{\text{tr}}^{(i)} = -(\Delta^{(i)}/2) \sigma_z^{(i)}$, where $\Delta^{(i)} = \omega_{01}^{(i)} - \omega_d$ is the detuning of the i -th qubit and σ_z is the third Pauli matrix. The incoming signal in its own rotating frame is represented by the triplet

$$G_\alpha = (1, \alpha, 0) \quad (5.27)$$

and the phase gained between the qubits by

$$G_\phi = (e^{i\phi}, 0, 0). \quad (5.28)$$

With these, we can write the total triplet for the above setup using the series and concatenation products as,

$$\begin{aligned} G_{\text{tot}} &= \left(G_{\text{Rtr}}^{(2)} \triangleleft G_\phi \triangleleft G_{\text{Rtr}}^{(1)} \triangleleft G_\alpha \right) \boxplus \left(G_{\text{Ltr}}^{(1)} \triangleleft G_\phi \triangleleft G_{\text{Ltr}}^{(2)} \right) \\ &= \left(\begin{bmatrix} e^{i\phi} & 0 \\ 0 & e^{i\phi} \end{bmatrix}, \begin{bmatrix} e^{i\phi} (\alpha + L^{(1)}) + L^{(2)} \\ L^{(1)} + e^{i\phi} L^{(2)} \end{bmatrix}, H_{\text{tot}} \right) \end{aligned} \quad (5.29)$$

where

$$\begin{aligned} H_{\text{tot}} &= H_{\text{tr}}^{(1)} + H_{\text{tr}}^{(2)} + \frac{1}{2i} \left(L^{(1)\dagger} \alpha - \alpha^* L^{(1)} \right) + \frac{1}{2i} \left(e^{i\phi} L^{(2)\dagger} \alpha - e^{-i\phi} \alpha^* L^{(2)} \right) \\ &\quad + \sin \phi \left(L^{(1)\dagger} L^{(2)} + L^{(2)\dagger} L^{(1)} \right). \end{aligned} \quad (5.30)$$

The first two terms in the above Hamiltonian are that of the bare qubits, while the next two give the interaction of the field with the qubits. The last term is usually referred to as exchange interaction that is mediated by virtual photons. The master equation can be written from the total (S, L, H) triplet as

$$\dot{\rho} = -i[H_{\text{tot}}, \rho] + \mathcal{D} \left[e^{i\phi} (\alpha + L^{(1)}) + L^{(2)} \right] \rho + \mathcal{D} \left[L^{(1)} + e^{i\phi} L^{(2)} \right] \rho. \quad (5.31)$$

Such a master equation was also derived in [140] for N -atoms with M levels using a different formalism. As a special case, they also look at two qubits separated by an arbitrary distance. To compare our results with the above reference, we rewrite the above master equation by expanding the dissipation super-operators as

$$\dot{\rho} = -i[H_{\text{eff}}, \rho] + \sum_{i,j=1}^2 Y_{i,j} \left(\sigma_-^{(i)} \rho \sigma_-^{(j)\dagger} - \frac{1}{2} \left\{ \sigma_-^{(j)\dagger} \sigma_-^{(i)}, \rho \right\} \right), \quad (5.32)$$

introducing the matrix

$$Y \equiv \begin{pmatrix} \Gamma_1 & \cos \phi \sqrt{\Gamma_1 \Gamma_2} \\ \cos \phi \sqrt{\Gamma_1 \Gamma_2} & \Gamma_2 \end{pmatrix} \quad (5.33)$$

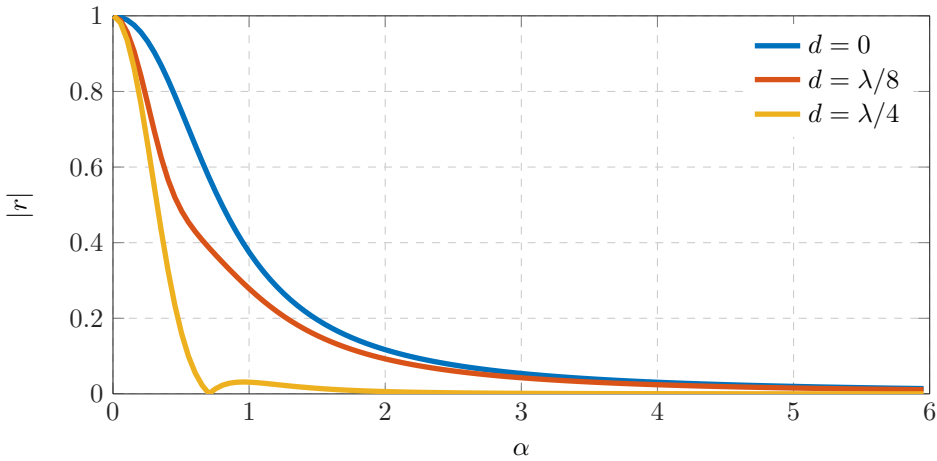


Figure 5.5: Absolute value of the reflection coefficient for the setup in Fig. 5.4 for different distances between the qubits. Both the qubits are on resonance with the incoming coherent field and also have the same coupling rates (Γ) to the transmission line.

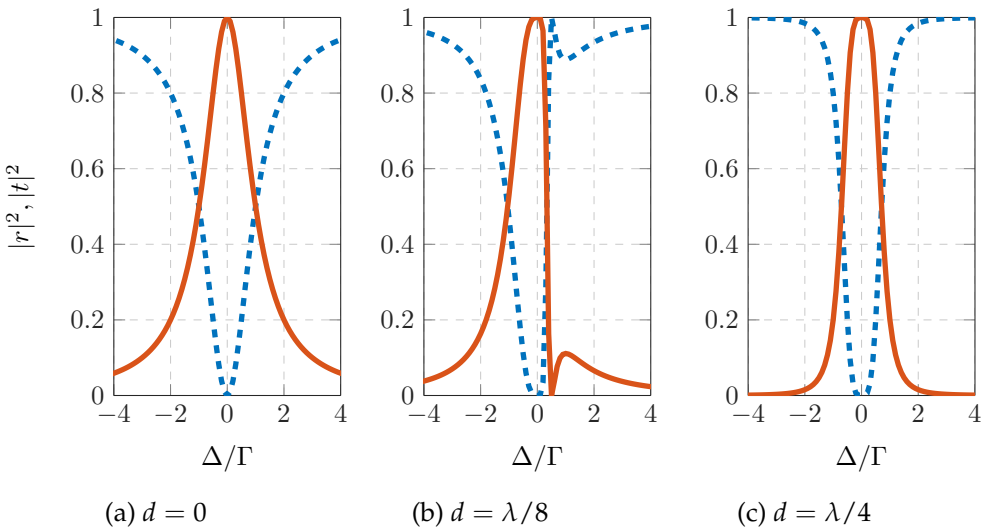


Figure 5.6: Reflection (solid lines) and transmission (dashed lines) coefficient as a function of qubit detuning $\Delta^{(1)} = \Delta^{(2)} = \Delta$ at low input power. Both the qubits have the same coupling rates (Γ) to the transmission line. Plots (a) and (c) agree with the results shown in [140] for the case of $d = \lambda$ and $d = 3\lambda/4$ respectively.

and the effective Hamiltonian

$$H_{\text{eff}} = H_{\text{tr}}^{(1)} + H_{\text{tr}}^{(2)} - \frac{1}{2i} \left(\alpha^* L^{(1)} - \alpha L^{(1)\dagger} \right) - \frac{1}{2i} \left(\alpha^* e^{-i\phi} L^{(2)} - \alpha e^{i\phi} L^{(2)\dagger} \right). \quad (5.34)$$

The master equation can be written in diagonal form, by diagonalizing the Y matrix. By this procedure, we get the coupling rate of the dressed states (labeled B and D following [140]) as

$$\Gamma_{B/D} = \frac{\Gamma_1 + \Gamma_2}{2} \pm \frac{1}{2} \sqrt{(\Gamma_1)^2 + (\Gamma_2)^2 + 2 \cos 2\phi \Gamma_1 \Gamma_2} \quad (5.35)$$

and the dressed lowering operators given by

$$\sigma_-^\mu = \frac{(\Gamma_\mu - \Gamma_2) \sigma_-^{(1)} + \cos \phi \sqrt{\Gamma_1 \Gamma_2} \sigma_-^{(2)}}{\sqrt{(\Gamma_\mu - \Gamma_2)^2 + \Gamma_1 \Gamma_2 \cos^2 \phi}} \quad (5.36)$$

where $\mu = B/D$. Using these, we can write the master equation as

$$\dot{\rho} = -i[H_{\text{eff}}, \rho] + \mathcal{D}[L_B] \rho + \mathcal{D}[L_D] \rho, \quad (5.37)$$

where $L_{\mu=B/D} = \sqrt{\Gamma_\mu} \sigma_-^\mu$. From the steady state solution of the above equation, we can get the coherently transmitted and reflected fields at steady state as

$$\alpha_{\text{tr}} = \left\langle e^{i\phi} \left(\alpha + L^{(1)} \right) + L^{(2)} \right\rangle_{ss}, \quad (5.38)$$

$$\alpha_{\text{ref}} = \left\langle L^{(1)} + e^{i\phi} L^{(2)} \right\rangle_{ss}. \quad (5.39)$$

From these, the reflection ($r = \alpha_{\text{ref}}/\alpha$) and transmission coefficients ($t = \alpha_{\text{tr}}/\alpha$) can be calculated. We plot $|r|$ for three different values of distance between the qubits $d = \phi\lambda/2\pi$ in Fig. 5.5. As can be seen from the figure, at low power ($\alpha \ll 1$) almost all of the field is reflected by the qubits. As the power is increased, the qubits get saturated and more and more of the incoming field gets transmitted. Thus the reflection coefficient goes to 0 at higher powers. We also plot the $|r|^2$ and $|t|^2$ as a function of the detuning Δ in Fig. 5.6 at low input power. In this regime, we have fully coherent scattering with $|r|^2 + |t|^2 = 1$. We can compare the results in subplots (a) and (c) to the results shown in [140] for the case of $d = \lambda$ and $d = 3\lambda/4$ respectively. We also show the results for an intermediate distance of $d = \lambda/8$.

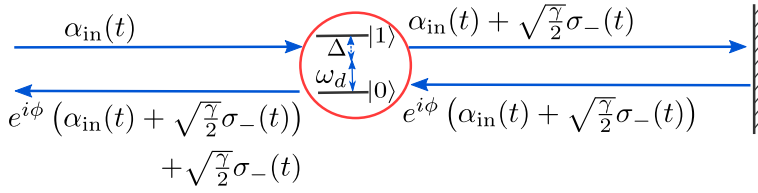


Figure 5.7: Schematic of a two level system in front of a mirror.

5.4 Feedback

At the beginning of this chapter, we looked at the case of having qubits coupled unidirectionally. One key requirement in that case was to have only one input-output port. In superconducting circuits, we can achieve this by placing the qubit (transmon) at the end of a transmission line which can either be open or shorted to ground. This boundary condition acts as a mirror for the field. In this section, we explicitly look at the master equation for a two level system that is in front of a mirror. A schematic is shown in Fig. 5.7, where the distance between the qubit and the mirror is once again modeled as a phase gained by the field. The field reflected from the mirror is fed back to the qubit and we can use the feedback operation of the (S, L, H) formalism to derive the master equation as in [76]. In this case, the triplet for the qubit-mirror without any drive is given by

$$G = (\tilde{S}, \tilde{L}, \tilde{H}) = [(G_\phi \boxplus I) \triangleleft G_{tr}]_{1 \rightarrow 2} \quad (5.40)$$

where the triplets G_{tr} and G_ϕ are same as in Eq. (5.25) and Eq. (5.28) respectively. We have to concatenate an identity triple $I = (1, 0, 0)$ to keep the dimensions intact. Using the feedback rules given in Eq. (5.13), we get

$$\tilde{S} = e^{i\phi}, \quad (5.41)$$

$$\tilde{L} = (1 + e^{i\phi})L, \quad (5.42)$$

$$\tilde{H} = H_{tr} + \sin \phi L^\dagger L, \quad (5.43)$$

where $H_{tr} = -(\omega_0/2)\sigma_z$ and $L = \left(\sqrt{\gamma/2}\right)\sigma_-$. With this triplet, we can now include the drive which could be either a coherent state or a Fock state. In this example, we will assume a coherent input specified by a triplet G_α as in Eq. (5.27). The total triplet is then

$$G_{tot} = (\tilde{S}, \tilde{L}, \tilde{H}) \triangleleft G_\alpha \quad (5.44)$$

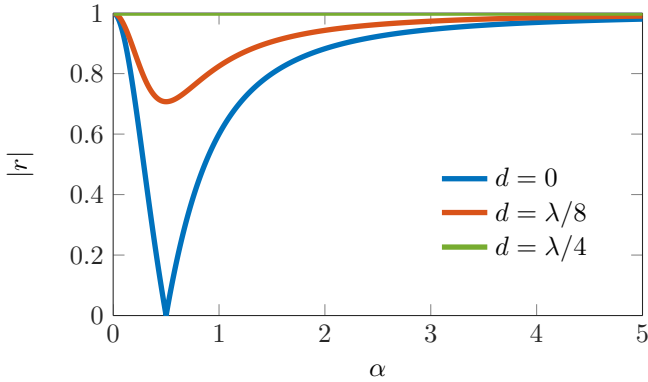


Figure 5.8: Absolute value of the reflection coefficient $|r|$ as a function of input field strength for different distances between the qubit and the mirror. The qubit is on resonance with the incoming field and the coupling rate $\gamma = 1$.

which gives the master equation

$$\dot{\rho} = -i[H_{\text{tot}}, \rho] + \mathcal{D} \left[e^{i\phi} \alpha + (1 + e^{i\phi}) L \right] \rho, \quad (5.45)$$

where the Hamiltonian $H_{\text{tot}} = -(\Delta/2)\sigma_z + \sin \phi L^\dagger L + \frac{1}{2i} (\alpha L^\dagger (e^{i\phi} + 1) - h.c.)$. The Hamiltonian is in the rotating frame of the incoming field with $\Delta = \omega_0 - \omega_d$. We can expand the dissipator and simplify the master equation to get

$$\dot{\rho} = -i[H_{\text{eff}}, \rho] + 2(1 + \cos \phi) \mathcal{D} [L] \rho, \quad (5.46)$$

where the effective Hamiltonian now is

$$H_{\text{eff}} = -(\Delta/2)\sigma_z + \sin \phi L^\dagger L - i \left(\alpha L^\dagger (e^{i\phi} + 1) - h.c. \right). \quad (5.47)$$

For $\phi = 0$, we see that the master equation can be rewritten as

$$\dot{\rho} = -i[H_{\text{tr}} - i(\alpha L'^\dagger - L' \alpha^*)] + \mathcal{D} [L'] \rho \quad (5.48)$$

by defining $L' = 2L = \sqrt{2\gamma}\sigma_- \equiv \sqrt{\Gamma}\sigma_-$. Here we have defined a renormalized coupling rate Γ that is twice the original relaxation rate γ . This is the coupling rate that is used in the previous sections and also in paper II. As an example, let us look at the scattering property of this setup by calculating the reflection coefficients r for different distances between the mirror and the qubit. The absolute value of $r = \langle \alpha_{\text{out}} \rangle / \alpha$, where $\alpha_{\text{out}} = e^{i\phi} \alpha + (1 + e^{i\phi}) L$, is plotted in Fig. 5.8. Note that the

phase ϕ is gained by the field over the entire trip between the qubit and the mirror (i.e. back and forth). We can convert this into distance in terms of wavelength of the field as $d = \phi \frac{\lambda}{4\pi}$. As we have an open end, the field is maximum at the mirror and the qubit couples maximally to the field at this point. At $d = \lambda/4$, the field goes to zero and we do not see any effect of the qubit on the reflected field, as expected. We get intermediate results for $d = \lambda/8$. Such an setup has also been tested experimentally recently (but with a slightly different boundary condition) and the results are presented in [76].

"You probably think this paper's about you: narcissists' perceptions of their personality and reputation."
Carlson, E. N., Vazire, S. and Oltmanns, T. F.,
Journal of Personality and Social Psychology 101, 185–201 (2011).

Listed in Scientists' Silly, Dark, and Sometimes Inappropriate Humor,
Slate.com

6

Overview of the articles

In this chapter, we provide a brief summary of the appended papers on which the thesis is based on. In particular, we will highlight the salient points of the articles and show how the framework developed in the previous chapters is connected to the work presented.

6.1 Cross-Kerr Effect for propagating microwaves

In paper I, we look at inducing photon-photon interaction at microwave frequencies for propagating photons. As discussed in the introduction, photons rarely interact with each other in vacuum and such interactions are usually engineered using a nonlinear material. In this experimental work, an effective photon-photon interaction is mediated using the lowest three levels of an artificial atom, the superconducting transmon. Two coherent fields, control and probe, close to resonance with these two transition frequencies, are scattered off of the transmon. The interaction effectively induces a phase change in the probe field due to the presence of the control field *à la* the cross-Kerr effect.

In the article, two setups are investigated. In one, the transmon is coupled to an

open transmission line and in another it is placed at the end of a semi-infinite transmission line. The second setup corresponds to having an atom in front of a mirror and has only one input-output port, thus reducing the loss of signal in the reflected field. The output fields scattered from the transmons are measured using a homodyne detector.

The input-output relations are different for the two setups as we already saw in Chapter 3. In the case of the transmon connected to an open transmission line, only the transmitted field is measured. Combining these two cases we can write the average output in the steady-state for both the fields as [141]

$$\alpha_{\text{out}}^{(c)} = \alpha_{\text{in}}^{(c)} + \sqrt{\frac{\Gamma_{01}}{k_n}} \langle \sigma_-^{01} \rangle_{ss}, \quad (6.1)$$

$$\alpha_{\text{out}}^{(p)} = \alpha_{\text{in}}^{(p)} + \sqrt{\frac{\Gamma_{12}}{k_n}} \langle \sigma_-^{12} \rangle_{ss}, \quad (6.2)$$

where k_n is the number of output channels i.e. $k_n = 1$ for atom in front of a mirror and $k_n = 2$ for an atom in an open transmission line. The lowering operators are given by $\sigma_-^{01} = |0\rangle \langle 1|$ and $\sigma_-^{12} = |1\rangle \langle 2|$. The expectation values are calculated by solving the master equation of the system as discussed in Chapter 3. The Hamiltonian of the three level system in the rotating frame of the two drives can be written as $H_{\text{tr}} = -\Delta_c |0\rangle \langle 0| + \Delta_p |2\rangle \langle 2|$, where the detuning between the transition frequencies and the drive frequencies are given as $\Delta_c = \omega_{10} - \omega_c$ and $\Delta_p = \omega_{21} - \omega_p$. The coherent drives can be included in the Hamiltonian as $H_{\text{drive}} = -i\sqrt{\Gamma_{01}/k_n}(\alpha_c \sigma_-^{01\dagger} - \text{h.c.}) - i\sqrt{\Gamma_{12}/k_n}(\alpha_p \sigma_-^{12\dagger} - \text{h.c.})$. With these, the master equation without including dephasing can be written as

$$\dot{\rho} = -i[H_{\text{tr}} + H_{\text{drive}}, \rho] + \Gamma_{01} \mathcal{D}[\sigma_-^{01}] \rho + \Gamma_{12} \mathcal{D}[\sigma_-^{12}] \rho. \quad (6.3)$$

The setup in the experiment is slightly different, where the probe was close to the resonance of the 0 – 1 transition and the control was close to the resonance of the 1 – 2 transition. The above model however gives a more intuitive picture. In this case, starting with a transmon in the ground state, the probe is scattered from the transmon only when the control field is on. Thus the phase shift in the absence of control field is 0. As it is more straightforward to interpret, we will use this model in the next section as well, where we look at photon detection using a three level atom.

From the measurement results, we see that an average conditional phase change of 10 and 20 degrees is induced in the probe field using setup 1 and 2 respectively. The input signals are in the single photon range, i.e the average number of

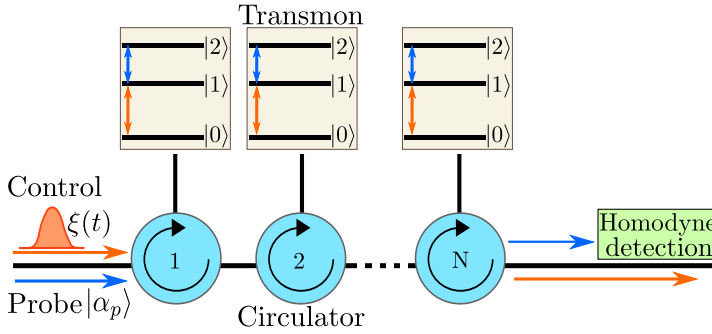


Figure 6.1: Schematic of setup proposed in paper II for microwave photon detection.

photons per interaction time is around one for both control and probe fields. The observed phase shifts are much larger than what is realized in traditional Kerr medium without cavities [39, 142] and hence the title giant cross-Kerr effect.

6.2 Quantum nondemolition detection of a propagating microwave photon

Using the cross-Kerr effect for quantum nondemolition (QND) measurements have been discussed for some time in literature [37, 48–50]. Given that a single transmon can induce a large conditional phase shift, the setup discussed in paper I naturally lends itself to the problem of QND detection of a single photon. Such a setup was theoretically analyzed for photon detection in reference [143]. It was shown there that the effect induced on the probe field by a single photon using a single transmon is not sufficient to overcome the fundamental vacuum noise. Intuitively, this can be understood as follows. A single atom can process only one excitation at a time. This means that even with a perfect absorption of the single photon by a transmon, it can at most scatter one photon from the coherent probe field. The coherent field in itself has half a photon of noise in the quadratures. Also, the presence of probe field in the $1 - 2$ transition reduces the probability of absorption of the control photon by the transmon as shown in paper IV. Thus, a single transmon without a cavity does not lead to distinguishable outputs with and without a photon and so does not help for the purpose of photon detection. It was also found that coupling many transmons close to each other or separated across wavelengths didn't improve the signal-to-noise ratio to rise above 1.

In paper II, we propose a setup that is able to overcome these limitations. The

key ingredient is to couple the transmons unidirectionally i.e. to cascade them using circulators as shown in Fig. 6.1. In such a setup, we can show that using two coherent drives, similar to the previous section, the conditional phase change in the probe accumulates over several transmons [40]. In the article, we check the performance of the setup for photon detection.

We take two different approaches to model the input single photon that is eventually needed to be detected by our setup. In one, we consider a tunable cavity as the source as in section 5.2. In the other approach, we use the Fock state formalism discussed in section 3.4. The control field that will contain the single photon is on resonance with the $0 - 1$ transition of all the transmons. This control field and a coherent probe field (on resonance with the $1 - 2$ transition) are scattered on the chain of cascaded transmons. The output probe field is then measured using a homodyne detector as in the previous section. If the control field has a photon at some time t , the effect on the probe field is seen from the measured homodyne current. We integrate the homodyne current over a time period T and this integrated current becomes our signal. The single photon itself survives this measurement process, making the scheme non-destructive.

To evaluate the performance of the setup, we take two approaches. In one, we solve the unconditional master equations and from the average dynamics calculate the signal-to-noise ratio (SNR). In another approach, we simulate quantum trajectories using the stochastic master equation for homodyne detection, similar to the ones shown in section 4.2. From these, we get the histograms of the signal measured with and without a single photon in the control field. From the mean and variance of the histogram, we calculate the signal-to-noise ratio (SNR) of the proposed detector. From the simulation results, we also see that as we increase the number of transmons, the signal distribution (histogram) does not remain Gaussian in the case of having a single photon in the control field. To take this into account we define a better measure, detection fidelity. As shown in the article, we can overcome the noise (i.e. get a SNR above 1) and detect the presence of a single photon with a 90% fidelity in certain parameter regimes.

Furthermore, we also consider imperfections such as dephasing of the transmons, power loss in circulators and imperfect homodyne detection. We conclude that for small imperfections the signal survives and we can still detect the photon. Comparing with experimentally available performance of these devices, it should be possible (probably with some effort) to build such a device with currently available resources. The major difficulty comes from circulators which are bulky devices that are off-chip. Apart from cooling down these bulky devices, we also have to worry about impedance matching the lines when we go on and off chips.

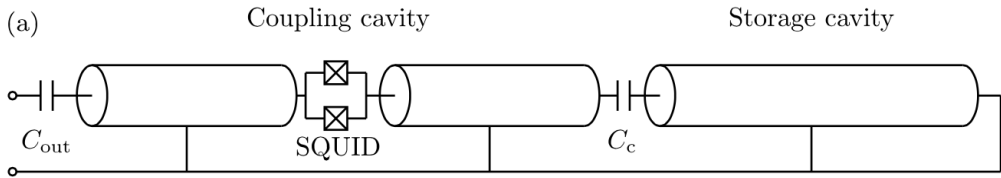


Figure 6.2: Schematic setup for coupled cavities considered in papers III and VI.

Our proposed scheme looks more attractive with the development of on-chip circulators [144]. Chiral quantum optics might also be a solution for realizing the proposed setup [145]. Further to this work, reference [55] shows how to improve the maximum signal that one can get from a single transmon by using a cavity for the probe field and by using more sophisticated filtering techniques. The signal can be further improved by once again cascading these individual units (transmon+cavity).

The proposal in paper II is one of the many proposals [52–61, 146, 147] for solving the long standing problem of detecting single itinerant microwave photon. In paper IV, we review some of the above proposals, which can be broadly classified as destructive or nondestructive type of detectors. The destructive microwave photon detectors are predominantly mapped as a Λ system. Such a Λ system can be realized using a current biased Josephson junction with a suitable bias current. It was shown theoretically in reference [53] that a photon detection of 100% is possible by one of these current biased junctions at the end of a transmission line. A more recent proposal for photon detection uses impedance matched Λ systems implemented by driving a qubit coupled to a resonator [146, 147]. Such a setup was also experimentally realized recently [62]. As these results were published quite close to the submission of paper IV, they are not reviewed in the same. Apart from these destructive schemes, in paper IV, we mainly present a pedagogical review of the nondestructive photon detector proposals based on Paper II and [55].

6.3 Coupled superconducting resonators

In one of the approaches of paper II, we consider a cavity with tunable coupling as a source of single photons. By tuning the coupling of the cavity, photon wave packets of desirable shapes (a gaussian, for example) can be created [28, 29, 114]. In paper III, we consider one such implementation of a tunable cavity that could

lead to the shaping of photon wave packets in the future. The tunable cavity in this case is made up of two cavities - a $\lambda/4$ resonator that acts as the storage cavity and a $\lambda/2$ resonator that acts as a coupling cavity. We have a SQUID at the current anti-node of the coupling cavity i.e. at its middle (see Fig. 6.2). By threading flux through the SQUID loop, we can modify the total inductance of the resonator and hence its mode frequencies.

The device can be analyzed following the circuit model presented in chapter 2. For the coupling cavity alone, we can write down the Lagrangian and from it the Euler-Lagrange equation of motion for the flux. From an approximate solution of this equation, we can find the resonant frequency of the coupling cavity as a function of the flux through the SQUID [148, 149]. The analysis can be extended by including the storage cavity and the coupling to the transmission line. By considering only the two lowest modes of the coupling and storage cavities, we end up with two normal modes. As is well known in any such coupled oscillator systems, we can have either an under, over or critically damped system. This is characterized by the ratio of the coupling to the transmission line κ to the coupling between the the cavities g .

The results presented in paper III can be understood as follows. The effective coupling of the storage cavity is via the coupling cavity, which acts like a barrier between the transmission line and the storage cavity. By bringing the coupling cavity on and off resonance with the storage cavity (similar to lowering and raising of a potential barrier), we can effectively tune the coupling of the storage cavity to the transmission line. In the sample discussed in the paper III, the coupling can be tuned by three orders of magnitude. This is seen from the lifetime of the field stored in the cavity which is shown to vary from 14ns to 18 μ s. Also by varying the detuning of the coupling cavity, it is shown that we can release the field in exponentially decaying wave packets of different widths. The above experiments were done when the cavity was filled with a coherent state that has on average 80 photons. However, the results suggests that by loading the cavity with a single photon and by modulating the coupling, we should be able to get single photon wave packets of different shapes. As mentioned in the introduction, such sources of single photons are of importance not only for quantum optics but also for quantum computing and communication.

In paper VI, a similar device but operating at a different parameter regime is presented. In the device presented in paper III, the energy relaxation rate set by κ was larger than the energy exchange rate between the cavities. Thus, we could understand the results as in the above paragraph. In paper VI however, the damping to the transmission line is much smaller than the energy exchange

rate between the cavities, which means there is significant energy oscillation between the cavities while there is also decay to the transmission line. This parameter scheme however allows us to demonstrate a different scheme for catching and releasing microwave photons. In this case, we can start with the coupling cavity completely decoupled from the storage cavity. The incoming signal is then captured in the coupling cavity and then swapped into the storage cavity by bringing them both on resonance. The excitation can then be stored in the resonator cavity and released either directly by tuning the coupling as in paper III or by doing a swap back into the coupling cavity. This protocol thus allows us to catch and release photons at a wide range of frequencies (corresponding to that of the tunable coupling cavity) and we are no longer restricted to the frequency range of the storage cavity. We hope that such devices can play the role of photonic memories in the microwave domain. We once again note that this initial demonstration is with coherent fields and further work is needed to show that the setup works for non-classical fields as well.

6.4 Generating single photons on demand

As the final topic, we look at generating single photons on demand. As mentioned in the introduction, several cavity based schemes for generating single microwave photons exist [25–29]. However, the use of cavities limit the bandwidth of operation and requires full control of both the qubit and the cavity. A cavity free approach was theoretically studied in [30] and experimentally demonstrated in [31]. In this setup, an atom is asymmetrically coupled to two transmission lines. The coupling of the atom to the control line is much weaker compared to the emission line. A π pulse from the weakly coupled control line excites the qubit which then preferably emits in the emission line. However, as noted in [31], there is also a direct coupling between the transmission line which might lead to leakage of photons from the incoming π pulse into the emission line and one needs to separate these from the emission of the atom. Also, it might be difficult in such a setup to get the photons in desired wave packet shapes.

In paper V, we propose two different setups to generate single photons on demand. Both of these use atom in front a mirror, which is crucial for getting high efficiency. As we already discussed in chapter 3, an excited atom in an open transmission line emits a photon in the left and right moving modes with equal probability. By placing the atom in front of a mirror, we collect all the emission from the atom. However, the coherent pulse used to excite the atom also comes out through the same port. Thus, we have to separate it from the

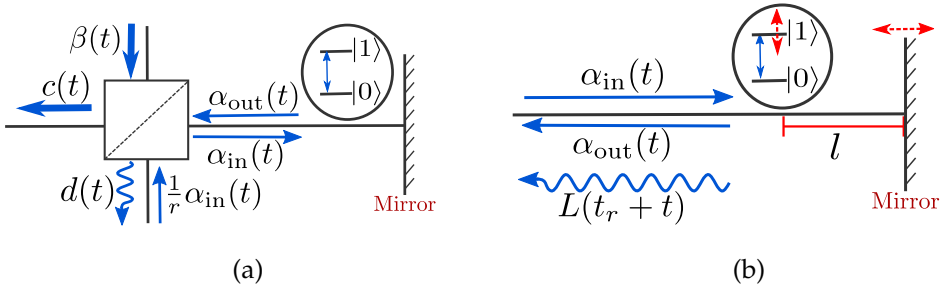


Figure 6.3: Schematic setups to generate single photons (a) Using a beam splitter (b) Using tunable coupling.

atomic decay. We can see this from the input-output relation which is given as $\alpha_{\text{out}}(t) = \alpha_{\text{in}}(t) + \sqrt{\Gamma}\sigma_{-}(t)$, where Γ is the effective coupling rate of the qubit to the transmission line. $\alpha_{\text{in}}(t)$ is the input π -pulse. We propose two different methods to separate the atomic decay from $\alpha_{\text{in}}(t)$.

In the first method (Fig. 6.3a), we use an unbalanced beam splitter with reflection coefficient $r \rightarrow 1$. It can be shown that such a beam splitter can be used to implement a displacement operator by using a strong coherent beam [150]. We use this to "undisplace" the coherent part of the output field and separate the atomic decay in one of the output channels. This can also be seen from the beam splitter input-output relations as shown in the article.

To characterize the efficiency of this method, we calculate P_n , the probability of having n photons in the output field ($d(t)$ in Fig. 6.3a). This is done by calculating the m^{th} order coherence function of the output (Eq. (3.64)). From the correlation function, we can calculate the photon m -tuples and the probabilities P_n [30]. The probability of having exactly one photon in the output becomes the measure of efficiency of our setup. We show that using experimentally realizable values for the beam splitter, a photon generation efficiency of 97% is straightforward to achieve.

In method two (Fig. 6.3b), we take advantage of the on-chip tunability of superconducting circuits as follows. The coupling between a transmon and the transmission line depends on the value of voltage at the coupling point. An open boundary condition at the end of the transmission line ($d = 0$), imposes the condition that the voltage is maximum at this point for all the allowed modes. A qubit at $d = 0$ thus has a maximum coupling to the transmission line. The mode structure due to the boundary condition imposes a node at a distance $d = \lambda/4$ for each of the mode. A qubit at this distance with the corresponding frequency

is completely decoupled from the transmission line. By changing the boundary condition i.e. by moving the mirror, we can go from a qubit that is maximally coupled to completely decoupled from the transmission line. A tunable boundary condition with a SQUID at the end of the transmission line, thus leads to a tunable coupling [151]. An alternative is to place the qubit at a finite distance from the mirror and tune the frequency of the qubit, which also leads to tunable coupling [76]. As we discussed in the previous section, the advantage of such a tunable system is to shape the output photon in desirable wave packets.

The photon generation in the second method is as follows. We start with the qubit coupled to the transmission and tune the coupling to be very close to 0. We send a strong π -pulse and excite the qubit. At the end of the pulse, we tune the coupling to 0. This can be done fast as we started at a very low coupling before the pulse. Now, a single excitation is trapped in the qubit which can be then released as needed in a desirable wave packet by tuning the coupling accordingly. In this case, we once again calculate the photon generation efficiency as before and find that with current technologies it can reach above 97%.

Given that the above setups are quite simple, one can imagine extending it to generate either correlated or entangled photons. As all of the ingredients required to test the proposals are readily available, we hope to see experimental realizations of the schemes presented in the near future.

Cuius rei demonstrationem mirabilem sane detexi hanc marginis exiguitas non caperet.

(I have discovered a truly remarkable proof of this theorem which this margin is too small to contain.)

Pierre de Fermat

7

Summary

Linear optical quantum computing (LOQC) is an approach to develop a quantum computer primarily using linear elements such as beam splitters along with single photon sources and detectors. However, to perform universal quantum computing, some nonlinearity is required [15, 17]. Superconducting circuits have the advantage of possessing a strong low loss nonlinearity that comes from the Josephson junction, which can enable development of all-optical quantum computing at microwave frequencies [17]. This however requires efficient single photon devices in the microwave regime, especially a single microwave photon detector, a first implementation of which has only been recently realized. In this thesis, we look at our proposals for microwave single photon devices based on the appended papers.

One of the main results of the thesis, is the proposal for a nondestructive detector for propagating single microwave photons as presented in paper II. The detector is based on the large photon-photon interaction mediated by a three level superconducting transmon, as shown in paper I. We also show how to efficiently generate single microwave photons on demand by using an atom in front of a mirror in paper V. In paper III and VI, we present experimental results on coupled cavities which could serve the purpose of a photonic quantum memory. While

the proposals are primarily aimed at circuit QED setups, we believe they could be extended to other systems where atoms are strongly coupled to one-dimensional waveguides. These include superconducting qubits coupled to surface acoustic waves [152], quantum dots coupled to photonic waveguides [153] or surface plasmons [154].

References

- [1] J. P. Dowling and G. J. Milburn. “Quantum technology: the second quantum revolution.” *Philosophical transactions. Series A, Mathematical, physical, and engineering sciences* **361**, 1655–1674 (2003) [cit. on p. 1].
- [2] *Measuring and manipulating individual quantum systems - Scientific Background on the Nobel Prize in Physics 2012*. eprint: http://www.nobelprize.org/nobel_prizes/physics/laureates/2012/advanced-physicsprize2012.pdf. Last visited on 13 May 2017 [cit. on p. 2].
- [3] S. Haroche and D. Kleppner. “Cavity Quantum Electrodynamics”. *Physics Today* **42**, 24 (1989) [cit. on p. 2].
- [4] H. Walther, B. T. H. Varcoe, B.-G. Englert, and T. Becker. “Cavity quantum electrodynamics”. *Reports on Progress in Physics* **69**, 1325 (2006) [cit. on pp. 2, 22].
- [5] S. Debnath, N. M. Linke, C. Figgatt, K. A. Landsman, K. Wright, and C. Monroe. “Demonstration of a small programmable quantum computer with atomic qubits”. *Nature* **536**, 63–66 (2016) [cit. on p. 2].
- [6] T. D. Ladd, F. Jelezko, R. Laflamme, Y. Nakamura, C. Monroe, and J. L. O’Brien. “Quantum computers.” *Nature* **464**, 45–53 (2010) [cit. on p. 2].
- [7] M. H. Devoret and R. J. Schoelkopf. “Superconducting Circuits for Quantum Information: An Outlook”. *Science* **339**, 1169–1174 (2013) [cit. on pp. 2, 24, 57].
- [8] G. Wendin. “Quantum information processing with superconducting circuits: a review” (2016). arXiv: 1610.02208 [cit. on pp. 2, 18, 24, 57].

- [9] A. Wallraff, D. I. Schuster, A. Blais, L. Frunzio, R.-S. Huang, J. Majer, S. Kumar, S. M. Girvin, and R. J. Schoelkopf. “Strong coupling of a single photon to a superconducting qubit using circuit quantum electrodynamics”. *Nature* **431**, 162–167 (2004) [cit. on pp. 2, 23].
- [10] J. Q. You and F. Nori. “Atomic physics and quantum optics using superconducting circuits”. *Nature* **474**, 589–597 (2011) [cit. on p. 2].
- [11] J. Clarke and F. K. Wilhelm. “Superconducting quantum bits”. *Nature* **453**, 1031–1042 (2008) [cit. on p. 2].
- [12] R. J. Schoelkopf and S. M. Girvin. “Wiring up quantum systems”. *Nature* **451**, 664–669 (2008) [cit. on p. 2].
- [13] C. M. Wilson, G. Johansson, A. Pourkabirian, M. Simoen, J. R. Johansson, T. Duty, F. Nori, and P. Delsing. “Observation of the dynamical Casimir effect in a superconducting circuit”. *Nature* **479**, 376–379 (2011) [cit. on pp. 2, 16, 24].
- [14] E. Knill, R. Laflamme, and G. J. Milburn. “A scheme for efficient quantum computation with linear optics”. *Nature* **409**, 46–52 (2001) [cit. on p. 2].
- [15] P. Kok, W. J. Munro, K. Nemoto, T. C. Ralph, J. P. Dowling, and G. J. Milburn. “Linear optical quantum computing with photonic qubits”. *Reviews of Modern Physics* **79**, 135–174 (2007) [cit. on pp. 2, 83].
- [16] S. Barz. “Quantum computing with photons: introduction to the circuit model, the one-way quantum computer, and the fundamental principles of photonic experiments”. *Journal of Physics B: Atomic, Molecular and Optical Physics* **48**, 083001 (2015) [cit. on p. 2].
- [17] P. Adhikari, M. Hafezi, and J. M. Taylor. “Nonlinear optics quantum computing with circuit QED”. *Physical Review Letters* **110**, 060503 (2013) [cit. on pp. 2, 83].
- [18] R. J. Kokkonen, T. Ollikainen, R. E. Lake, S. Saarenpää, J. Kokkala, C. B. Dag, and M. Möttönen. “Quantum Gates for Propagating Microwave Photons” (2017). arXiv: 1703.02241 [cit. on p. 2].

- [19] M. Planck. "On the Theory of the Energy Distribution Law of the Normal Spectrum". *Verhandlungen der Deutschen Physikalischen Gessellschaft* **2**, 237–245 (1900) [cit. on p. 3].
- [20] A. B. Arons and A. Einstein. "Concerning an Heuristic Point of View Towards the Emission and Transformation of Light; Einstein's Proposal of the Photon Concept—a Translation of the *Annalen der Physik* Paper of 1905". *American Journal of Physics* **33**, 367 (1965) [cit. on p. 3].
- [21] A. Aspect and P. Grangier. "Chapter 10 - The First Single-Photon Sources". *Single-Photon Generation and Detection: Physics and Applications*. Ed. by A. Migdall, S. V. Polyakov, J. Fan, and J. C. Bienfang. Vol. 45. Experimental Methods in the Physical Sciences. Academic Press, 2013, pp. 315–350 [cit. on p. 3].
- [22] M. D. Eisaman, J. Fan, A. Migdall, and S. V. Polyakov. "Invited Review Article: Single-photon sources and detectors". *Review of Scientific Instruments* **82**, 071101 (2011) [cit. on pp. 3, 4, 6, 7].
- [23] N. Sangouard and H. Zbinden. "What are single photons good for?" *Journal of Modern Optics* **59**, 1458–1464 (2012) [cit. on p. 3].
- [24] J. Bienfang, J. Fan, A. Migdall, and S. Polyakov. "Chapter 1 - Introduction". *Single-Photon Generation and Detection: Physics and Applications*. Ed. by A. Migdall, S. V. Polyakov, J. Fan, and J. C. Bienfang. Vol. 45. 2013, pp. 1–24 [cit. on pp. 3, 7].
- [25] A. A. Houck, D. I. Schuster, J. M. Gambetta, J. A. Schreier, B. R. Johnson, J. M. Chow, L. Frunzio, J. Majer, M. H. Devoret, S. M. Girvin, and R. J. Schoelkopf. "Generating single microwave photons in a circuit". *Nature* **449**, 328–331 (2007) [cit. on pp. 3, 79].
- [26] M. Hofheinz, E. M. Weig, M. Ansmann, R. C. Bialczak, E. Lucero, M. Neeley, A. D. O'Connell, H. Wang, J. M. Martinis, and A. N. Cleland. "Generation of Fock states in a superconducting quantum circuit". *Nature* **454**, 310–314 (2008) [cit. on pp. 3, 79].

- [27] D. Bozyigit, C. Lang, L. Steffen, J. M. Fink, C. Eichler, M. Baur, R. Bianchetti, P. J. Leek, S. Filipp, M. P. da Silva, A. Blais, and A. Wallraff. “Antibunching of microwave-frequency photons observed in correlation measurements using linear detectors”. *Nature Physics* **7**, 154–158 (2011) [cit. on pp. 3, 79].
- [28] Y. Yin, Y. Chen, D. Sank, P. J. J. O’Malley, T. C. White, R. Barends, J. Kelly, E. Lucero, M. Mariantoni, A. Megrant, C. Neill, A. Vainsencher, J. Wenner, A. N. Korotkov, A. N. Cleland, and J. M. Martinis. “Catch and Release of Microwave Photon States”. *Physical Review Letters* **110**, 107001 (2013) [cit. on pp. 3, 5, 23, 77, 79].
- [29] M. Pechal, L. Huthmacher, C. Eichler, S. Zeytinoglu, A. A. Abdumalikov, S. Berger, A. Wallraff, and S. Filipp. “Microwave-Controlled Generation of Shaped Single Photons in Circuit Quantum Electrodynamics”. *Physical Review X* **4**, 041010 (2014) [cit. on pp. 3, 5, 23, 77, 79].
- [30] J. Lindkvist and G. Johansson. “Scattering of coherent pulses on a two-level system—single-photon generation”. *New Journal of Physics* **16**, 055018 (2014) [cit. on pp. 4, 36–38, 79, 80].
- [31] Z. H. Peng, S. E. de Graaf, J. S. Tsai, and O. V. Astafiev. “Tuneable on-demand single-photon source in the microwave range”. *Nature Communications* **7**, 12588 (2016) [cit. on pp. 4, 79].
- [32] H. J. Kimble. “The quantum internet”. *Nature* **453**, 1023–1030 (2008) [cit. on p. 4].
- [33] A. Browaeys. “Catch and Release of Photons”. *Physics* **6**, 25 (2013) [cit. on p. 5].
- [34] D. Maxwell, D. J. Szwer, D. Paredes-Barato, H. Busche, J. D. Pritchard, A. Gauguet, K. J. Weatherill, M. P. A. Jones, and C. S. Adams. “Storage and Control of Optical Photons Using Rydberg Polaritons”. *Physical Review Letters* **110**, 103001 (2013) [cit. on p. 5].
- [35] J. Wenner, Y. Yin, Y. Chen, R. Barends, B. Chiaro, E. Jeffrey, J. Kelly, A. Megrant, J. Y. Mutus, C. Neill, P. J. J. O’Malley, P. Roushan, D. Sank, A. Vainsencher, T. C. White, A. N. Korotkov, A. N. Cleland, and J. M. Martinis.

- “Catching Time-Reversed Microwave Coherent State Photons with 99.4% Absorption Efficiency”. *Physical Review Letters* **112**, 210501 (2014) [cit. on pp. 5, 23].
- [36] R. W. Boyd. *Nonlinear Optics*. Third Edition. Academic Press, 2008 [cit. on pp. 5, 6].
- [37] P. Grangier, J. A. Levenson, and J.-P. Poizat. “Quantum non-demolition measurements in optics”. *Nature* **396**, 537–542 (1998) [cit. on pp. 6–8, 75].
- [38] H. Kang and Y. Zhu. “Observation of large Kerr nonlinearity at low light intensities.” *Physical review letters* **91**, 093601 (2003) [cit. on p. 6].
- [39] V. Venkataraman, K. Saha, and A. L. Gaeta. “Phase modulation at the few-photon level for weak-nonlinearity-based quantum computing”. *Nature Photonics* **7**, 138–141 (2013) [cit. on pp. 6, 75].
- [40] S. R. Sathyamoorthy. “Quantum non-demolition detection of propagating microwave photons”. Master’s thesis. Chalmers University of Technology, 2012 [cit. on pp. 6, 76].
- [41] G. J. Milburn. “Quantum optical Fredkin gate”. *Physical Review Letters* **62**, 2124–2127 (1989) [cit. on p. 6].
- [42] I. L. Chuang and Y. Yamamoto. “Simple quantum computer”. *Physical Review A* **52**, 3489–3496 (1995) [cit. on p. 6].
- [43] G. D. Hutchinson and G. J. Milburn. “Nonlinear quantum optical computing via measurement”. *Journal of Modern Optics* **51**, 1211–1222 (2004) [cit. on p. 6].
- [44] T. C. Ralph, K. J. Resch, and A. Gilchrist. “Efficient Toffoli gates using qudits”. *Physical Review A* **75**, 022313 (2007) [cit. on p. 6].
- [45] J. H. Shapiro. “Single-photon Kerr nonlinearities do not help quantum computation”. *Physical Review A* **73**, 062305 (2006) [cit. on p. 6].

- [46] J. Gea-Banacloche. “Impossibility of large phase shifts via the giant Kerr effect with single-photon wave packets”. *Physical Review A* **81**, 043823 (2010) [cit. on p. 6].
- [47] D. J. Brod and J. Combes. “Passive CPHASE Gate via Cross-Kerr Nonlinearities”. *Physical Review Letters* **117**, 080502 (2016) [cit. on p. 6].
- [48] N. Imoto, H. H. A. Haus, and Y. Yamamoto. “Quantum nondemolition measurement of the photon number via the optical Kerr effect”. *Physical Review A* **32**, 2287–2292 (1985) [cit. on pp. 6, 8, 75].
- [49] V. B. Braginsky and F. Y. Khalili. “Quantum nondemolition measurements: the route from toys to tools”. *Reviews of Modern Physics* **68**, 1–11 (1996) [cit. on pp. 6, 8, 55, 75].
- [50] W. J. Munro, K. Nemoto, R. G. Beausoleil, and T. P. Spiller. “High-efficiency quantum-nondemolition single-photon-number-resolving detector”. *Physical Review A* **71**, 033819 (2005) [cit. on pp. 6, 8, 75].
- [51] R. H. Hadfield. “Single-photon detectors for optical quantum information applications”. *Nature Photonics* **3**, 696–705 (2009) [cit. on p. 6].
- [52] G. Romero, J. J. García-Ripoll, and E. Solano. “Microwave Photon Detector in Circuit QED”. *Physical Review Letters* **102**, 173602 (2009) [cit. on pp. 7, 77].
- [53] B. Peropadre, G. Romero, G. Johansson, C. M. Wilson, E. Solano, and J. J. Garcia-Ripoll. “Approaching perfect microwave photodetection in circuit QED”. *Physical Review A* **84**, 063834 (2011) [cit. on pp. 7, 77].
- [54] L. Neumeier, M. Leib, and M. J. Hartmann. “Single-Photon Transistor in Circuit Quantum Electrodynamics”. *Physical Review Letters* **111**, 063601 (2013) [cit. on pp. 7, 77].
- [55] B. Fan, G. Johansson, J. Combes, G. J. Milburn, and T. M. Stace. “Nonabsorbing high-efficiency counter for itinerant microwave photons”. *Physical Review B* **90**, 035132 (2014) [cit. on pp. 7, 77].

- [56] O. Kyriienko and A. S. Sørensen. “Continuous-Wave Single-Photon Transistor Based on a Superconducting Circuit”. *Physical Review Letters* **117**, 140503 (2016) [cit. on pp. 7, 77].
- [57] A. Cridland, J. Lacy, J. Pinder, and J. Verdú. “Single Microwave Photon Detection with a Trapped Electron”. *Photonics* **3**, 59 (2016) [cit. on pp. 7, 77].
- [58] J. Leppäkangas, M. Marthaler, D. Hazra, S. Jebari, G. Johansson, and M. Hofheinz. “Multiplying microwave photons by inelastic Cooper-pair tunneling” (2016). arXiv: 1612.07098 [cit. on pp. 7, 77].
- [59] B. R. Johnson, M. D. Reed, A. A. Houck, D. I. Schuster, L. S. Bishop, E. Ginossar, J. M. Gambetta, L. DiCarlo, L. Frunzio, S. M. Girvin, and R. J. Schoelkopf. “Quantum non-demolition detection of single microwave photons in a circuit”. *Nature Physics* **6**, 663–667 (2010) [cit. on pp. 7, 8, 77].
- [60] Y.-F. Chen, D. Hover, S. Sendelbach, L. Maurer, S. T. Merkel, E. J. Pritchett, F. K. Wilhelm, and R. McDermott. “Microwave Photon Counter Based on Josephson Junctions”. *Physical Review Letters* **107**, 217401 (2011) [cit. on pp. 7, 77].
- [61] A. Narla, S. Shankar, M. Hatridge, Z. Leghtas, K. M. Sliwa, E. Zalys-Geller, S. O. Mundhada, W. Pfaff, L. Frunzio, R. J. Schoelkopf, and M. H. Devoret. “Robust concurrent remote entanglement between two superconducting qubits”. *Physical Review X* **6**, 031036 (2016) [cit. on pp. 7, 77].
- [62] K. Inomata, Z. Lin, K. Koshino, W. D. Oliver, J.-S. Tsai, T. Yamamoto, and Y. Nakamura. “Single microwave-photon detector using an artificial Λ -type three-level system”. *Nature Communications* **7**, 12303 (2016) [cit. on pp. 7, 77].
- [63] S. K. Lamoreaux, K. A. van Bibber, K. W. Lehnert, and G. Carosi. “Analysis of single-photon and linear amplifier detectors for microwave cavity dark matter axion searches”. *Physical Review D* **88**, 035020 (3 2013) [cit. on p. 7].

- [64] H. Zheng, M. Silveri, R. T. Brierley, S. M. Girvin, and K. W. Lehnert. “Accelerating dark-matter axion searches with quantum measurement technology” (2016). arXiv: 1607.02529 [cit. on p. 7].
- [65] V. B. Braginsky, Y. I. Vorontsov, and K. S. Thorne. “Quantum nondemolition measurements.” *Science* **209**, 547–557 (1980) [cit. on pp. 7, 8].
- [66] V. B. Braginskii and Y. I. Vorontsov. “Quantum-mechanical limitations in macroscopic experiments and modern experimental technique”. *Soviet Physics Uspekhi* **17**, 644 (1975) [cit. on p. 8].
- [67] V. Braginskii, Y. I. Vorontsov, and F. Y. Khalili. “Quantum singularities of a ponderomotive meter of electromagnetic energy”. *Journal of Experimental and Theoretical Physics* **46**, 705–706 (1977) [cit. on p. 8].
- [68] K. S. Thorne, R. W. P. Drever, C. M. Caves, M. Zimmermann, and V. D. Sandberg. “Quantum nondemolition measurements of harmonic oscillators.” *Physical Review Letters* **40**, 667–671 (1978) [cit. on p. 8].
- [69] W. G. Unruh. “Quantum nondemolition and gravity-wave detection.” *Physical Review D* **19**, 2888–2896 (1979) [cit. on p. 8].
- [70] C. M. Caves, K. S. Thorne, R. W. P. Drever, V. D. Sandberg, and M. Zimmermann. “On the measurement of a weak classical force coupled to a quantum-mechanical oscillator. I. Issues of principles.” *Reviews of Modern Physics* **52**, 341–392 (1980) [cit. on p. 8].
- [71] C. Guerlin, J. Bernu, S. Deléglise, C. Sayrin, S. Gleyzes, S. Kuhr, M. Brune, J.-M. Raimond, and S. Haroche. “Progressive field-state collapse and quantum non-demolition photon counting”. *Nature* **448**, 889–893 (2007) [cit. on p. 8].
- [72] F. Helmer, M. Mariani, E. Solano, and F. Marquardt. “Quantum nondemolition photon detection in circuit QED and the quantum Zeno effect”. *Physical Review A* **79**, 052115 (2009) [cit. on p. 8].

- [73] L. Chirolli and G. Burkard. “Quantum nondemolition measurements of a qubit coupled to a harmonic oscillator”. *Physical Review B* **80**, 184509 (2009) [cit. on p. 8].
- [74] I. Diniz, E. Dumur, O. Buisson, and A. Auffèves. “Ultrafast quantum nondemolition measurements based on a diamond-shaped artificial atom”. *Physical Review A* **87**, 033837 (2013) [cit. on p. 8].
- [75] L. Sun, A. Petrenko, Z. Leghtas, B. Vlastakis, G. Kirchmair, K. M. Sliwa, A. Narla, M. Hatridge, S. Shankar, J. Blumoff, L. Frunzio, M. Mirrahimi, M. H. Devoret, and R. J. Schoelkopf. “Tracking photon jumps with repeated quantum non-demolition parity measurements”. *Nature* **511**, 444–448 (2014) [cit. on p. 8].
- [76] I.-C. Hoi, A. F. Kockum, L. Tornberg, A. Pourkabirian, G. Johansson, P. Delsing, and C. M. Wilson. “Probing the quantum vacuum with an artificial atom in front of a mirror”. *Nature Physics* **11**, 1045–1049 (2015) [cit. on pp. 9, 16, 69, 71, 81].
- [77] A. A. Houck, H. E. Türeci, and J. Koch. “On-chip quantum simulation with superconducting circuits”. *Nature Physics* **8**, 292–299 (2012) [cit. on p. 12].
- [78] D. A. Wells. “Application of the Lagrangian Equations to Electrical Circuits”. *Journal of Applied Physics* **9**, 312–320 (1938) [cit. on p. 11].
- [79] B. Yurke and J. Denker. “Quantum network theory”. *Physical Review A* **29**, 1419 (1984) [cit. on pp. 11, 21].
- [80] M. H. Devoret. “Quantum Fluctuations in Electrical Circuits”. *Les Houches, Session LXIII* (1995) [cit. on p. 11].
- [81] U. Vool and M. H. Devoret. “Introduction to Quantum Electromagnetic Circuits” (2016). arXiv: 1610.03438 [cit. on p. 11].
- [82] B. D. Josephson. “Possible new effects in superconductive tunnelling”. *Physics Letters* **1**, 251–253 (1962) [cit. on p. 14].

- [83] M. Tinkham. *Introduction to Superconductivity*. Second edition. Dover Publications, 2004 [cit. on pp. 14, 15].
- [84] J. R. Johansson. “Quantum mechanics in superconducting circuits and nanomechanical devices”. PhD thesis. Chalmers University of Technology, 2009 [cit. on p. 16].
- [85] J. Lindkvist. “Quantum optics and relativistic motion with superconducting circuits”. PhD thesis. Chalmers University of Technology, 2015 [cit. on pp. 16, 21].
- [86] J. Koch, T. M. Yu, J. Gambetta, A. A. Houck, D. I. Schuster, J. Majer, A. Blais, M. H. Devoret, S. M. Girvin, and R. J. Schoelkopf. “Charge-insensitive qubit design derived from the Cooper pair box”. *Physical Review A* **76**, 042319 (2007) [cit. on pp. 17, 18].
- [87] V. Bouchiat, D. Vion, P. Joyez, D. Esteve, and M. H. Devoret. “Quantum coherence with a single Cooper pair”. *Physica Scripta* **1998**, 165 (1998) [cit. on p. 17].
- [88] Y. Makhlin, G. Schoen, and A. Shnirman. “Josephson-junction qubits with controlled couplings”. *Nature* **398**, 305–307 (1999) [cit. on pp. 17, 19].
- [89] Y. Nakamura, Y. A. Pashkin, and J. S. Tsai. “Coherent control of macroscopic quantum states in a single-Cooper-pair box”. *Nature* **398**, 786 (1999) [cit. on p. 17].
- [90] L. S. Bishop. “Circuit Quantum Electrodynamics”. PhD thesis. Yale University, 2010 [cit. on p. 18].
- [91] J. M. Martinis, M. H. Devoret, and J. Clarke. “Energy-Level Quantization in the Zero-Voltage State of a Current-Biased Josephson Junction”. *Physical Review Letters* **55**, 1543–1546 (1985) [cit. on p. 19].
- [92] J. E. Mooij, T. P. Orlando, L. Levitov, L. Tian, C. H. der Wal, and S. Lloyd. “Josephson persistent-current qubit”. *Science* **285**, 1036–1039 (1999) [cit. on p. 19].

- [93] D. Vion, A. Aassime, A. Cottet, P. Joyez, H. Pothier, C. Urbina, D. Esteve, and M. H. Devoret. "Manipulating the Quantum State of an Electrical Circuit". *Science* **296**, 886–889 (2002) [cit. on p. 19].
- [94] A. Zazunov, V. S. Shumeiko, E. N. Bratus', J. Lantz, and G. Wendin. "Andreev Level Qubit". *Physical Review Letters* **90**, 087003 (2003) [cit. on p. 19].
- [95] A. Kitaev. "Protected qubit based on a superconducting current mirror" (2006). arXiv: cond-mat/0609441 [cit. on p. 19].
- [96] V. E. Manucharyan, J. Koch, L. I. Glazman, and M. H. Devoret. "Fluxonium: Single Cooper-Pair Circuit Free of Charge Offsets". *Science* **326**, 113–116 (2009) [cit. on p. 19].
- [97] B. Peropadre, J. Lindkvist, I.-C. Hoi, C. M. Wilson, J. J. Garcia-Ripoll, P. Delsing, and G. Johansson. "Scattering of coherent states on a single artificial atom". *New Journal of Physics* **15**, 035009 (2013) [cit. on p. 21].
- [98] M. E. Peskin and D. V. Schroeder. *An Introduction to Quantum Field Theory*. Westview Press, 1995 [cit. on p. 21].
- [99] M. Sandberg, C. M. Wilson, F. Persson, T. Bauch, G. Johansson, V. Shumeiko, T. Duty, and P. Delsing. "Tuning the field in a microwave resonator faster than the photon lifetime". *Applied Physics Letters* **92**, 203501 (2008) [cit. on p. 22].
- [100] A. Palacios-Laloy, F. Nguyen, F. Mallet, P. Bertet, D. Vion, and D. Esteve. "Tunable Resonators for Quantum Circuits". *Journal of Low Temperature Physics* **151**, 1034–1042 (2008) [cit. on p. 22].
- [101] O. V. Astafiev, A. A. Abdumalikov Jr., A. M. Zagoskin, Y. A. Pashkin, Y. Nakamura, and J. S. Tsai. "Ultimate On-Chip Quantum Amplifier". *Physical Review Letters* **104**, 183603 (2010) [cit. on p. 23].
- [102] I.-C. Hoi, C. M. Wilson, G. Johansson, T. Palomaki, B. Peropadre, and P. Delsing. "Demonstration of a Single-Photon Router in the Microwave Regime". *Physical Review Letters* **107**, 073601 (2011) [cit. on p. 23].

- [103] E. Schrödinger. “An Undulatory Theory of the Mechanics of Atoms and Molecules”. *Physical Review* **28**, 1049–1070 (1926) [cit. on p. 25].
- [104] H.-P. Breuer and F. Petruccione. *The theory of open quantum systems*. Oxford University Press, 2006 [cit. on pp. 26, 28, 29, 44, 45, 47, 48, 54].
- [105] C. W. Gardiner and P. Zoller. *Quantum Noise*. Springer, 2004 [cit. on pp. 26, 29, 36, 37, 57, 59].
- [106] I. Rau, G. Johansson, and A. Shnirman. “Cavity quantum electrodynamics in superconducting circuits: Susceptibility at elevated temperatures”. *Physical Review B* **70**, 054521 (2004) [cit. on p. 29].
- [107] A. A. Clerk, M. H. Devoret, S. M. Girvin, F. Marquardt, and R. J. Schoelkopf. “Introduction to quantum noise, measurement, and amplification”. *Reviews of Modern Physics* **82**, 1155–1208 (2010) [cit. on p. 30].
- [108] C. Gardiner and M. Collett. “Input and output in damped quantum systems: Quantum stochastic differential equations and the master equation”. *Physical Review A* **31**, 3761–3774 (1985) [cit. on p. 33].
- [109] R. Loudon. *The Quantum Theory of Light*. Oxford University Press, 2000 [cit. on pp. 36–38].
- [110] M. J. Stevens. “Photon Statistics, Measurements, and Measurements Tools”. *Single-Photon Generation and Detection: Physics and Applications*. Ed. by A. Migdall, S. V. Polyakov, J. Fan, and J. C. Bienfang. Vol. 45. Elsevier Inc., 2013, pp. 25–68 [cit. on p. 37].
- [111] B. Q. Baragiola. “Open systems dynamics for propagating quantum fields”. PhD thesis. The University of New Mexico, 2014 [cit. on p. 38].
- [112] K. M. Gheri, K. Ellinger, T. Pellizzari, and P. Zoller. “Photon-Wavepackets as Flying Quantum Bits”. *Fortschritte der Physik* **46**, 401–415 (1998) [cit. on p. 39].
- [113] J. E. Gough, M. R. James, and H. I. Nurdin. “Quantum master equation and filter for systems driven by fields in a single photon state”. *Decision*

- and Control and European Control Conference (CDC-ECC), 2011 50th IEEE Conference on. 2011, pp. 5570–5576 [cit. on p. 39].
- [114] J. E. Gough, M. R. James, H. I. Nurdin, and J. Combes. “Quantum filtering for systems driven by fields in single-photon states or superposition of coherent states”. *Physical Review A* **86**, 043819 (2012) [cit. on pp. 39, 64, 77].
- [115] B. Q. Baragiola, R. L. Cook, A. M. Brańczyk, and J. Combes. “N-photon wave packets interacting with an arbitrary quantum system”. *Physical Review A* **86**, 013811 (2012) [cit. on p. 39].
- [116] *Tirukkural on Wikipedia*. <https://en.wikipedia.org/wiki/Tirukkural>. Accessed: 2017-04-28 [cit. on p. 43].
- [117] *Tirukural translation*. <https://www.himalayanacademy.com/view/tirukural>. Accessed: 2017-04-28 [cit. on p. 43].
- [118] H. M. Wiseman and G. J. Milburn. *Quantum Measurement and Control*. Cambridge University Press, 2010 [cit. on pp. 44, 46, 48, 49, 51].
- [119] T. A. Brun. “A simple model of quantum trajectories”. *American Journal of Physics* **70**, 719–737 (2002) [cit. on pp. 44, 45].
- [120] L. Tornberg. “Superconducting qubits - measurement , entanglement , and noise”. PhD thesis. Chalmers University of Technology, 2009 [cit. on pp. 45, 47, 48, 51].
- [121] J. R. Johansson, P. D. Nation, and F. Nori. “QuTiP 2: A Python framework for the dynamics of open quantum systems”. *Computer Physics Communications* **184**, 1234–1240 (2013) [cit. on pp. 49, 52].
- [122] H. Carmichael. *An Open Systems Approach to Quantum Optics*. Springer Berlin Heidelberg, 2001 [cit. on p. 49].
- [123] H. M. Wiseman and G. J. Milburn. “Interpretation of quantum jump and diffusion processes illustrated on the Bloch sphere”. *Physical Review A* **47**, 1652–1666 (1993) [cit. on p. 52].

- [124] M. Mariani, M. J. Storz, F. K. Wilhelm, W. D. Oliver, A. Emmert, A. Marx, R. Gross, H. Christ, and E. Solano. “On-Chip Microwave Fock States and Quantum Homodyne Measurements” (2005). arXiv: cond-mat/0509737 [cit. on p. 53].
- [125] M. P. da Silva, D. Bozyigit, A. Wallraff, and A. Blais. “Schemes for the observation of photon correlation functions in circuit QED with linear detectors”. *Physical Review A* **82**, 043804 (2010) [cit. on p. 53].
- [126] C. C. Gerry and P. L. Knight. *Introductory Quantum Optics*. Cambridge University Press, 2008 [cit. on p. 54].
- [127] A. D. Córcoles, E. Magesan, S. J. Srinivasan, A. W. Cross, M. Steffen, J. M. Gambetta, and J. M. Chow. “Demonstration of a quantum error detection code using a square lattice of four superconducting qubits”. *Nature Communications* **6**, 6979 (2015) [cit. on p. 57].
- [128] R. Barends, J. Kelly, A. Megrant, A. Veitia, D. Sank, E. Jeffrey, T. C. White, J. Mutus, A. G. Fowler, B. Campbell, Y. Chen, Z. Chen, B. Chiaro, A. Dunsworth, C. Neill, P. O’Malley, P. Roushan, A. Vainsencher, J. Wenner, A. N. Korotkov, A. N. Cleland, and J. M. Martinis. “Superconducting quantum circuits at the surface code threshold for fault tolerance”. *Nature* **508**, 500–503 (2014) [cit. on p. 57].
- [129] D. Ristè, S. Poletto, M.-Z. Huang, A. Bruno, V. Vesterinen, O.-P. Saira, and L. DiCarlo. “Detecting bit-flip errors in a logical qubit using stabilizer measurements”. *Nature Communications* **6**, 6983 (2015) [cit. on p. 57].
- [130] J. Kelly, R. Barends, A. G. Fowler, A. Megrant, E. Jeffrey, T. C. White, D. Sank, J. Y. Mutus, B. Campbell, Y. Chen, Z. Chen, B. Chiaro, A. Dunsworth, I.-C. Hoi, C. Neill, P. J. J. O’Malley, C. Quintana, P. Roushan, A. Vainsencher, J. Wenner, A. N. Cleland, and J. M. Martinis. “State preservation by repetitive error detection in a superconducting quantum circuit”. *Nature* **519**, 66–69 (2015) [cit. on p. 57].
- [131] R. Barends, A. Shabani, L. Lamata, J. Kelly, A. Mezzacapo, U. L. Heras, R. Babbush, A. G. Fowler, B. Campbell, Y. Chen, Z. Chen, B. Chiaro, A. Dunsworth, E. Jeffrey, E. Lucero, A. Megrant, J. Y. Mutus, M. Neeley, C.

- Neill, P. J. J. O'Malley, C. Quintana, P. Roushan, D. Sank, A. Vainsencher, J. Wenner, T. C. White, E. Solano, H. Neven, and J. M. Martinis. "Digitized adiabatic quantum computing with a superconducting circuit". *Nature* **534**, 222–226 (2016) [cit. on p. 57].
- [132] C. Gardiner. "Driving a quantum system with the output field from another driven quantum system". *Physical Review Letters* **70**, 2269–2272 (1993) [cit. on pp. 57, 60].
- [133] H. Carmichael. "Quantum trajectory theory for cascaded open systems". *Physical Review Letters* **70**, 2273–2276 (1993) [cit. on p. 57].
- [134] J. Combes, J. Kerckhoff, and M. Sarovar. "The SLH framework for modeling quantum input-output networks" (2016). arXiv: 1611.00375 [cit. on pp. 59, 60, 62].
- [135] J. Gough and M. R. James. "Quantum Feedback Networks: Hamiltonian Formulation". *Communications in Mathematical Physics* **287**, 1109–1132 (2009) [cit. on p. 60].
- [136] J. Gough and M. R. James. "The Series Product and Its Application to Quantum Feedforward and Feedback Networks". *IEEE Transactions on Automatic Control* **54**, 2530–2544 (2009) [cit. on p. 60].
- [137] N. Tezak, A. Niederberger, D. S. Pavlichin, G. Sarma, and H. Mabuchi. "Specification of photonic circuits using quantum hardware description language". *Philosophical Transactions of the Royal Society of London A: Mathematical, Physical and Engineering Sciences* **370**, 5270–5290 (2012) [cit. on p. 61].
- [138] A. L. Grimsmo. "Time-Delayed Quantum Feedback Control". *Physical Review Letters* **115**, 060402 (2015) [cit. on p. 62].
- [139] H. Pichler and P. Zoller. "Photonic Circuits with Time Delays and Quantum Feedback". *Physical Review Letters* **116**, 093601 (2016) [cit. on p. 62].
- [140] K. Lalumière, B. C. Sanders, A. F. van Loo, A. Fedorov, A. Wallraff, and A. Blais. "Input-output theory for waveguide QED with an ensemble

- of inhomogeneous atoms". *Physical Review A* **88**, 043806 (2013) [cit. on pp. 66–68].
- [141] I.-C. Hoi. "Quantum Optics with Propagating Microwaves in Superconducting Circuits". PhD thesis. Chalmers University of Technology, 2009 [cit. on p. 74].
- [142] C. Perrella, P. Light, J. Anstie, F. Benabid, T. Stace, A. White, and A. Luiten. "High-efficiency cross-phase modulation in a gas-filled waveguide". *Physical Review A* **88**, 013819 (2013) [cit. on p. 75].
- [143] B. Fan, A. Kockum, J. Combes, G. Johansson, I.-c. Hoi, C. Wilson, P. Delsing, G. Milburn, and T. Stace. "Breakdown of the Cross-Kerr Scheme for Photon Counting". *Physical Review Letters* **110**, 053601 (2013) [cit. on p. 75].
- [144] A. C. Mahoney, J. I. Colless, S. J. Pauka, J. M. Hornibrook, J. D. Watson, G. C. Gardner, M. J. Manfra, A. C. Doherty, and D. J. Reilly. "On-Chip Microwave Quantum Hall Circulator". *Physical Review X* **7**, 011007 (2017) [cit. on p. 77].
- [145] P. Lodahl, S. Mahmoodian, S. Stobbe, A. Rauschenbeutel, P. Schneeweiss, J. Volz, H. Pichler, and P. Zoller. "Chiral quantum optics". *Nature* **541**, 473–480 (2017) [cit. on p. 77].
- [146] K. Koshino, K. Inomata, Z. Lin, Y. Nakamura, and T. Yamamoto. "Theory of microwave single-photon detection using an impedance-matched Λ system". *Physical Review A* **91**, 043805 (2015) [cit. on p. 77].
- [147] K. Koshino, Z. Lin, K. Inomata, T. Yamamoto, and Y. Nakamura. "Dressed-state engineering for continuous detection of itinerant microwave photons". *Physical Review A* **93**, 023824 (2016) [cit. on p. 77].
- [148] M. Wallquist, V. S. Shumeiko, and G. Wendin. "Selective coupling of superconducting charge qubits mediated by a tunable stripline cavity". *Physical Review B* **74**, 224506 (2006) [cit. on p. 78].

- [149] J. Bourassa, F. Beaudoin, J. M. Gambetta, and A. Blais. “Josephson junction-embedded transmission-line resonators: from Kerr medium to in-line transmon”. *Physical Review A* **86**, 013814 (2012) [cit. on p. 78].
- [150] M. G. A. Paris. “Displacement operator by beam splitter”. *Physics Letters, Section A: General, Atomic and Solid State Physics* **217**, 78–80 (1996) [cit. on p. 80].
- [151] K. Koshino and Y. Nakamura. “Control of the radiative level shift and linewidth of a superconducting artificial atom through a variable boundary condition”. *New Journal of Physics* **14**, 043005 (2012) [cit. on p. 81].
- [152] M. V. Gustafsson, T. Aref, A. F. Kockum, M. K. Ekström, G. Johansson, and P. Delsing. “Propagating phonons coupled to an artificial atom”. *Science* **346**, 207–211 (2014) [cit. on p. 84].
- [153] P. Lodahl, S. Mahmoodian, and S. Stobbe. “Interfacing single photons and single quantum dots with photonic nanostructures”. *Reviews of Modern Physics* **87**, 347–400 (2015) [cit. on p. 84].
- [154] M. S. Tame, K. R. McEnery, Ş. K. Özdemir, J. Lee, S. A. Maier, and M. S. Kim. “Quantum plasmonics”. *Nature Physics* **9**, 329–340 (2013) [cit. on p. 84].

